PAPER MACHINE CROSS-DIRECTIONAL CONTROL NEAR SPATIAL DOMAIN BOUNDARIES

By

Stevo Mijanovic

Dipl. Ing. (Electrical Engineering) University of Montenegro, Serbia and Montenegro

A THESIS SUBMITTED IN PARTIAL FULFILLMENT OF

THE REQUIREMENTS FOR THE DEGREE OF

DOCTOR OF PHILOSOPHY

in

THE FACULTY OF GRADUATE STUDIES

DEPARTMENT OF ELECTRICAL AND COMPUTER ENGINEERING

We accept this thesis as conforming

to the required standard

THE UNIVERSITY OF BRITISH COLUMBIA

March 2004

Abstract

This work is concerned with the modification of an existing industrial paper machine cross-directional (CD) control law near spatial domain boundaries (paper sheet edges), taking into account relevant control engineering criteria: closed-loop stability, performance, and robustness.

Paper machine CD control systems belong to a set of large, multivariable, spatially-distributed control systems, having 30–300 control inputs and 200–2000 process outputs. The objective of CD control is to reduce the variations of a particular paper sheet property (basis weight - weight per unit area, moisture content, or thickness) in the cross-direction (the direction perpendicular to the sheet travel direction) as much as possible. CD control systems can properly be described as two-dimensional systems, with one time dimension and one spatial dimension (cross-direction). The state-of-the-art industrial CD controllers of interest in this work are designed assuming spatially-invariant CD processes. Indeed, a lot of recently developed techniques for the design of spatially-distributed control laws make use of the spatial-invariance assumption. However, very many of the real-life systems (including paper machine CD processes) are not spatially-invariant.

Paper machine edges represent a clear disruption of the assumed spatial-invariance. As a result, initially designed spatially-invariant control laws must be modified before implementation on the real (spatially-variant) paper machines. The current industrial techniques for modifying CD control laws near spatial domain boundaries are based on techniques for extending finite-width signals, borrowed from the field of signal processing. As these techniques do not take into account relevant control engineering criteria, they can lead to very poor control near the edges, and potentially even destabilize the overall CD control system.

The main contributions of this work are the three novel approaches to modifying the existing industrial CD control law that directly take into account important control engineering criteria. In addition, the newly developed closed-loop approach has also been successfully tested on a paper machine in a working paper mill.

A developed closed-loop stability transfer approach is a straightforward perturbation technique for the spatially-invariant CD controller, that is guaranteed to stabilize a closed-loop system with the actual (spatially-variant) CD plant.

Next, the similarities between effects observed near spatial domain boundaries of the industrial CD control systems and the well-known Gibbs effect are illustrated. Subsequently, based on the techniques for mitigating the Gibbs effect, the so-called open-loop approach to modifying the existing CD control law is developed and illustrated with a closed-loop simulation example.

Finally, in a closed-loop approach to modifying the existing industrial CD controller, the objective is restated in terms of a block-decentralized static output feedback design problem. Static modifications of the existing controller's two constant matrix components are then sequentially computed by the use of a novel low-bandwidth static output feedback controller design algorithm. The relevant control engineering criteria (closed-loop stability, performance, and robustness) are all systematically taken into account with this approach. Since the resulting closed-loop system robustness margins near the sheet edges are directly considered, the possibility of CD control instability originating from the edges and 'creeping' into the rest of the system is eliminated with the new approach. The new approach has a clear economic benefit for the papermakers, since with a stable, robust, and performance improving control law near the sheet edges, the quality of the paper sheet near the edges can be significantly improved, thus resulting in less paper being trimmed off and more on-spec paper being produced from which the papermaker can extract his orders.

The newly developed closed-loop approach to modifying the existing industrial CD control law near spatial domain boundaries is tested and verified on a paper machine in a working paper mill. The obtained closed-loop control results are presented.

Table of Contents

List of Tables

List of Figures

Acknowledgments

This project has been carried out as a collaboration between the University of British Columbia and the industrial partner Honeywell Process Solutions - North Vancouver. I would like to thank my research supervisors Dr. Greg Stewart from Honeywell Process Solutions, and Profs. Guy Dumont and Michael Davies from the University of British Columbia (UBC) for their advice and guidance throughout the course of my graduate studies. Prof. Michael Davies admitted me into UBC graduate school and Prof. Guy Dumont encouraged me to do a PhD thesis. Over the past few years, I have greatly benefited from the regular (weekly) meetings with my industrial supervisor Dr. Greg Stewart. Valuable discussions during these meetings have left an indelible impact on this work.

This project would not have been possible without the technical and financial assistance of the industrial partner Honeywell Process Solutions - North Vancouver. I consider this industrial collaboration a particularly useful experience for myself. Numerous people from Honeywell have in or the other way contributed to this project. In particular, I would like to acknowledge the help of the following people: Cristian Gheorghe, Joyce Choi, Bijan Nazem, Paul Baker, Stephen Chu, Chuck Chung, Roger Chen, Amor Lahouaoula, Max Kean, Pengling He, Dan Stevens, Scott Morgan, Johan Backstrom, Rhonda Kieper, and Bob Vyse.

The financial support of my research work, over the past few years, by the Natural Sciences and Engineering Research Council of Canada (NSERC) and the Science Council of British Columbia is also gratefully acknowledged.

During my graduate studies at UBC, I have benefited from the technical discussions/talks with a large number of people. Particularly useful have been the discussions with the past and present members of the UBC Pulp and Paper Centre: Junqiang Fan, Shiro Ogawa, Michael Chong Ping, Kayvan Najarian, Leonardo Kammer, Zoran Nesic, Mihai Huzmezan, Ahmed Ismail, Manpreet Sidhu, Stephan Bibian, Tatjana Zikov, Setareh Aslani, and David Yang. Also I would like to gratefully acknowledge the help of the Pulp and Paper Centre staff (past and present), in particular: Brenda Dutka, Brian MacMillan, Lisa Brandly, and Ken Wong.

I would have never reached graduate school if there had not been a steady and continuous support of my parents, Savo and Slavojka Mijanovic, during my earlier education years. I owe a great deal to their love and support. In addition, the encouragement of my father and other immediate family from my native land, over the course of the last few years, has made my graduate school years much easier.

Finally, I would like to specially acknowledge the help and support of my wife Mila

Mijanovic. Her love and patience have tremendously helped me during my graduate studies over the last five years, as well as with all my endeavours since 1996. She provides a constant inspiration and feedback in my life, and helps me lead a good life. (*The good life is one inspired by love and guided by knowledge* - Bertrand Russell.)

Dedicated to the
everlasting memory
of my mother

Chapter 1

Introduction

1.1 Industrial Paper Making - The Paper Machine

Although the ancient Egyptians produced the world's first writing material, real paper making began in China about 1900 years ago. In the following centuries, it spread to Europe and North America through the Middle East. Paper continued to be made by hand until the beginning of the 19th century when the first paper machine was built in England. In the past two centuries, paper machines have been developed, making it possible to increase production, and to establish rigorous standards of quality. Today, paper making is a multi-billion dollar industry employing hundreds of thousands of people worldwide.

The fibrous raw material for paper making is called pulp. Pulp fibers are usually of vegetable origin, but other types (mineral, animal, or synthetic fibres) have been used in some special applications as well [61]. The task of the paper machine is to transform a slurry of water and pulp fibres into a sheet of paper conforming to the required standards of quality. A typical fourdrinier-type paper machine is illustrated in Figure 1.1. After numerous stages of pulp pre-processing (not shown in Figure 1.1), a very dilute mixture of water and pulp fibres (approximately 99.5% water and 0.5% fibres) enters the headbox at the left of the figure. The dry paper is wound up on the reel (100–200 metres downstream from the headbox) at the right of the figure by which stage the composition has become about 95% fibre and 5% moisture. Today's paper machines are typically between 3–10m wide. The following is a very brief description of the modern paper making process; detailed descriptions can be found in [25, 61].

The overall machine is divided into four sections (Figure 1.1) [61]:

- **Sheet-forming section** in the Wet end of the paper machine. The mixture of water and pulp fibres (with only ~0.5% fibres concentration) is delivered onto the moving forming fabric (in today's modern machines, almost exclusively, made of plastic web materials). The forming fabric is moving at speeds that could possibly be in excess of 100km/h, in the so-called machine direction (MD). By the use of various drainage elements (forming board, hydrofoil assemblies, table rolls, vacuum boxes, etc.), a significant amount of water is removed, resulting in formation of a paper sheet with ~20% fibres concentration leaving the machine's Wet end.

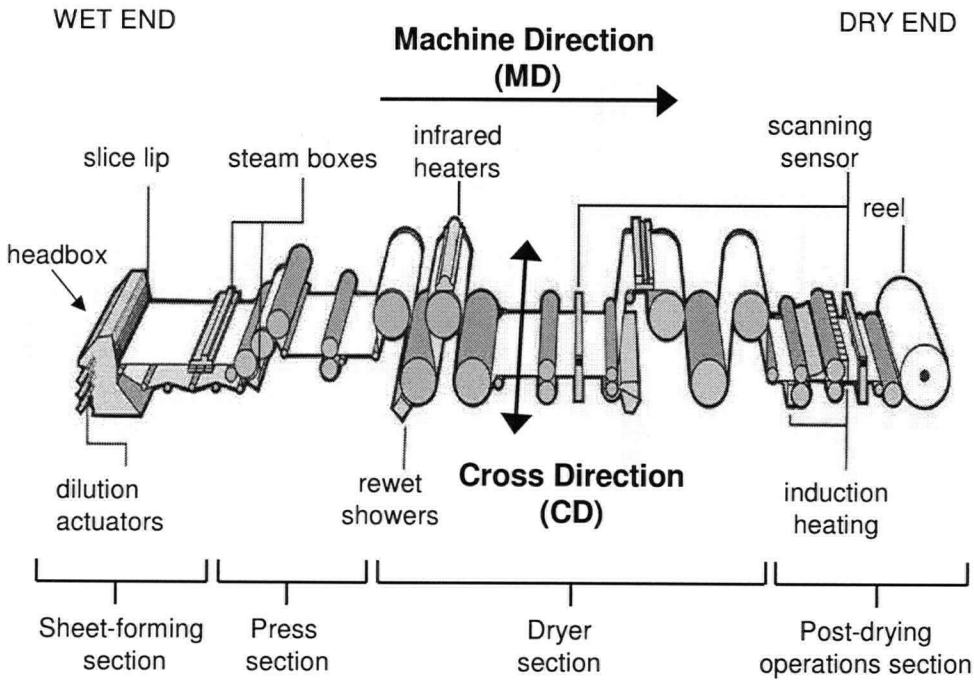

Figure 1.1: Schematic view of the paper machine showing typical positions of the scanner(s) and various CD actuator arrays, as well as illustrating machine and cross directions (Figure courtesy of Honeywell Process Solutions - North Vancouver).

- **Press section** of the paper machine. In this section, the sheet is heated by steam boxes, before being pressed and further dewatered by the counter-rotating rolls, resulting in a sheet with approximately 40% fiber concentration just before the Dryer section.

- In the **Dryer section**, the sheet's water content is further reduced through evaporation, by the use of a series of large-diameter, rotating, steam filled cans. The sheet leaving the Dryer section contains only 5–9% water content by weight (91–95% fiber concentration).

- **Post-drying operations section** is the final section of the paper machine, where the paper sheet thickness (caliper) and surface properties (e.g. gloss) are being controlled. At the end of the paper machine, which is, as pointed out earlier, located 100–200m away from the headbox, the sheet is finally wound up onto the reel.

The direction of sheet travel is known in the paper making industry as the machine-direction (MD). The direction perpendicular to machine-direction is called cross-direction (CD). The machine and cross directions are illustrated in Figure 1.1.

It is also important to note that paper machines usually have high-pressure water jets,

located very near the end of the Sheet-forming section (in the machine-direction) and not far from the machine edges (in the cross-direction). These jets are called 'trim squirts' as they trim off narrow strips of the paper sheet, on both sides of the machine, before it enters Press section [61], as illustrated in Figure 1.2.

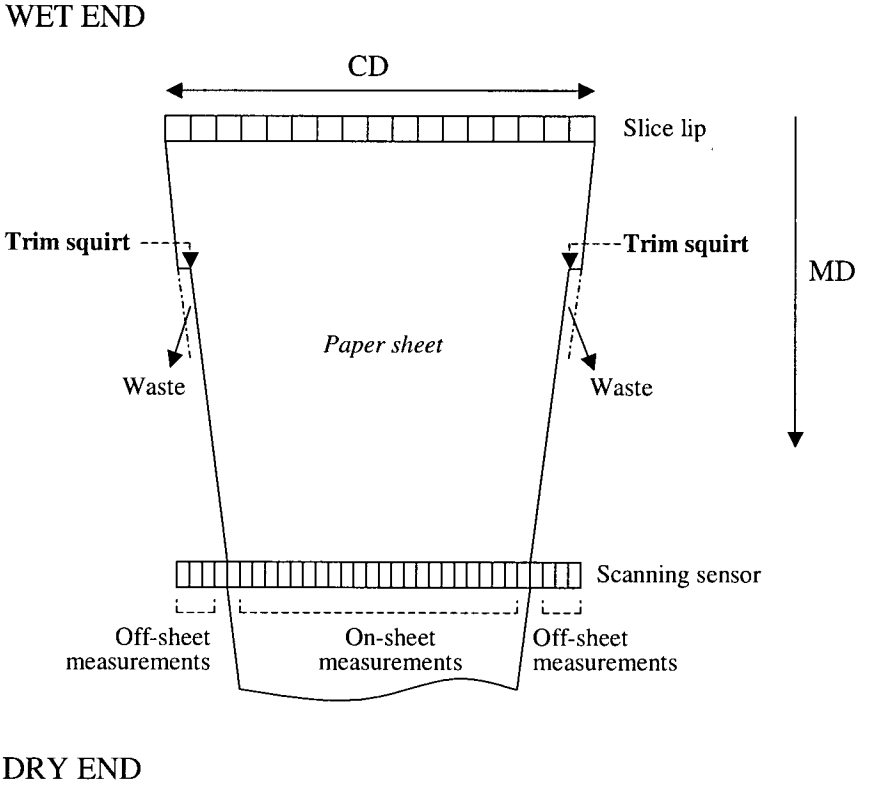

Figure 1.2: Illustration of trim squirts, used for trimming-off of narrow paper sheet strips, in the sheet-forming section.

The most important paper sheet properties are: (1) the sheet weight per unit area (usually given in terms of grams per square meter - gsm), (2) the sheet moisture content (given in terms of a percentage of the sheet weight - %), and (3) the thickness (caliper) of the finished sheet (given in μm). These properties are measured by a scanning sensor, located near the end of the machine (in the Dry end), that traverses the moving sheet back and forth in the cross-direction (CD), measuring these properties at 200-2000 points (see Figure 1.3). The quality of the paper sheet is defined in terms of weight, moisture content, and caliper variations [1]. The smaller the variations are about the target values, the better the paper sheet.

The scan time (the time required for the scanner to traverse the sheet once in cross-direction) depends on the width of the sheet and the scanner's speed, and is usually

between $15 - 45 seconds$. If a roll of paper consists of m scans and the sheet properties are measured at n locations across the sheet, the sheet measurements are given by $y(i,j)$, where $i = 1, 2, ..., n$ and $j = 1, 2, ..., m$, and the average value is:

$$\overline{y} = \sum_{i=1}^{n} \sum_{j=1}^{m} \frac{y(i,j)}{m \cdot n} \tag{1.1}$$

An important sheet quality factor is the variance of the measured property, known as 'two sigma' within the industry, defined by [1],

$$2\sigma = 2 \cdot \sqrt{\sum_{i=1}^{n} \sum_{j=1}^{m} \frac{(y(i,j) - \overline{y})^2}{m \cdot n - 1}}, \tag{1.2}$$

where $\overline{y}$ is given by (1.1).

Since the scanning sensor traverses the moving sheet, it traces a diagonal path along the sheet (as illustrated in Figure 1.3), resulting in the measurement sheet profiles containing both MD and CD sheet variations. As a result of process design and the nature of the actuators, the industrial approach to paper machine control is to consider the MD and CD control problems separately.

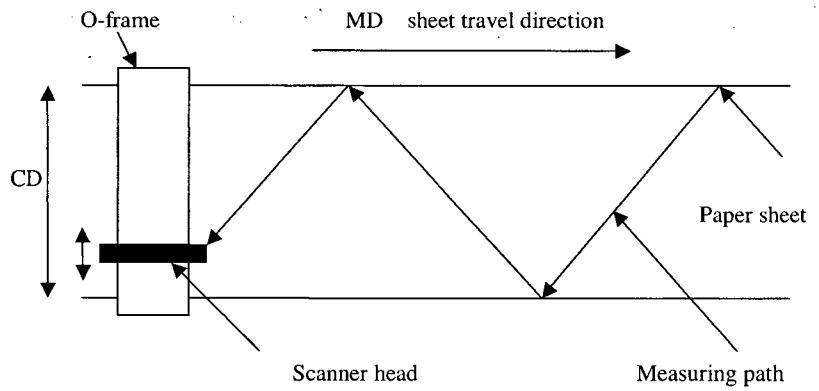

Figure 1.3: Illustration of the scanning sensor's measuring path (Figure courtesy of J. Fan [20]).

Machine-direction (MD) control deals with controlling the average value of each measurement scan, and the resulting MD control loops are relatively simple Single-Input-Single-Output (SISO) loops. Paper machine MD basis weight control is usually realized by controlling the concentration of pulp fibres being delivered to the machine headbox. MD moisture control, on the other hand, is typically achieved by controlling the overall

steam flow into the machine's dryer section. Machine-direction (MD) control is outside the scope of this work, and no MD actuators are illustrated in Figure 1.1.

1.2 Paper Machine Cross-Directional (CD) Control Systems

Cross-direction (CD) control is concerned with controlling dynamically varying, but zero-mean measurement profiles, and is performed by an array of actuators distributed across the machine (in cross-direction). In most cases, paper machines have at least one actuator array for controlling each of the important sheet properties (weight, moisture, and caliper). Except for some of the most recent approaches to CD control [6, 7, 20], different sheet properties are controlled by separate and independent control systems. The most common ways of realizing industrial paper machine CD control are detailed in Sections 1.2.1–1.2.3 below.

1.2.1 Basis Weight Control

Basis weight (weight per unit area), expressed in grams per square meter (gsm) or pounds per ream ($lbs/ream$)[1], is a fundamental property of the paper sheet, and its variations cause variations in most other sheet properties [12]. The desired target values for basis weight vary from about $35gsm$ for a light weight 'telephone directory grade' paper sheet, $45gsm$ - newsprint, $300gsm$ - book cover, to $450gsm$ for a cardboard sheet [65].

The role of CD basis weight actuators is to distribute pulp fibers evenly across the machine width (in the cross-direction) so that variability of the basis weight CD profile is minimized. Weight actuators are located at the headbox (at the far left in Figure 1.1), furthest upstream from the scanning sensor. As a result, a significant delay (dead time) is a dominant characteristic of industrial CD weight control systems.

Two main types of actuators are used for controlling CD weight profiles: slice lip actuators and dilution actuators. The traditional way of achieving CD weight control is by the use of slice lip actuators. A mixture of water and pulp fibres exits the headbox through a gap (slice), which is between 1–$6cm$ tall depending on the type of paper being produced, and as wide as the paper machine. The slice has an adjustable top lip and a fixed apron or bottom lip. The upper lip, in addition to being adjustable up or down as a unit, can also be locally bent (moved up or down) by the use of CD actuators. The larger the actuator opening, the more fibres are delivered, thus resulting in a heavier sheet in the localized area around that actuator. As an illustration, a possible steady-state response

[1] $1\ [ream] = 3000\ [square\ feet] \Longrightarrow 1\ [lbs/ream] = 1.6289\ [gr/m^2]$

of the basis weight profile to slice lip actuators is shown in Figure 1.4. The actuator

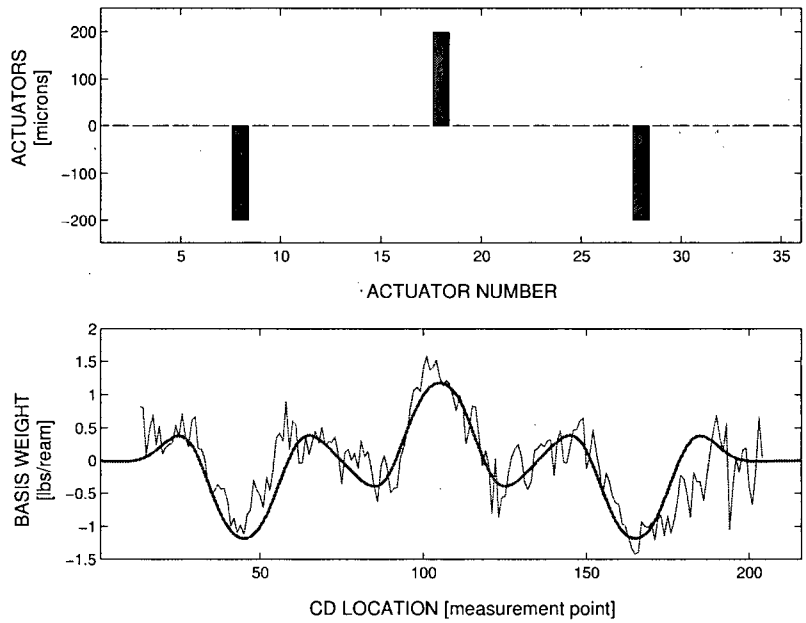

Figure 1.4: Slice lip basis weight control: measured (thin line) and modelled (thick line) steady-state bump response shapes (lower figure) in the case of deflection of 3 out of 36 slice lip actuators (upper figure). Data obtained during the industrial trial described in Chapter 6.

spacing (x_a) and a total number of actuators (n) can vary significantly, depending on the installation, and can be anywhere between x_a =70–200mm and n =30–118 or more actuators [65].

A more recent approach to CD basis weight control is by the use of dilution actuators [74], located across the back of the paper machine headbox (see Figure 1.1). These actuators locally alter the concentration of pulp fibres in the headbox by injecting a stream of low consistency white water. Obviously, an increase in the low consistency stream locally reduces the concentration of fibres, thus resulting in a local decrease of basis weight. The most important advantage of dilution actuators, in comparison to slice lip actuators, is a significantly smaller actuator spacing (x_a = 35mm) and a narrower spatial response, which translates into better CD controllability characteristics.

1.2.2 Moisture Control

The three main types of CD moisture actuators are: steam boxes, rewet showers, and infrared heaters [12]. Steam box arrays, in two possible locations, and one array of rewet

showers as well as an array of infrared heaters, are illustrated in Figure 1.1.

Steam showers improve water removal (through the principle of hot pressing) by locally increasing the sheet temperature [12, 61]. In the hot pressing procedure, steam is applied to the sheet structure, where it condenses, giving up its heat, and thus resulting in an increase of the sheet temperature. The higher sheet temperature increases water fluidity, thus making the water removal by the presses easier and more efficient. An important economic benefit resulting from the use of steam showers before or in the press section (see Figure 1.1), is a subsequent dryer load reduction. It has been found that improved water removal before the dryer section leads to overall net energy (steam) savings [12]. The location of steam shower actuators mainly depends on the type of paper being produced. In case of heavier grade papers, steam showers located on the fourdrinier forming table tend to work better, while steam showers located in the press section give better results in the case of light grade papers [12]. The number of steam box actuators can be as high as $n = 171$, and the actuator spacing is usually between x_a =75–150mm. Steam boxes are generally slow actuators with a time constant of approximately 200-250sec [62].

In the case of the appearance of (over)dry streaks in the paper sheet, these are re-moisturized by the use of rewet showers (water sprays). Rewet shower actuators apply an atomized water spray directly to the sheet, thus increasing the moisture content in the localized area. The spacing between these actuators is usually in the range x_a =70–150mm, and the number can be as high as $n = 120$ in some wider machine applications. In contrast to steam boxes, rewet showers are very fast actuators with the time constant comparable to scan time ($T_s = 15 - 45sec$) and the dynamics is mainly dominated by the transport delay (dead time) [62].

1.2.3 Caliper Control

In the final section of the paper machine (Dry end), the paper sheet is fed to a vertical stack of rotating rollers, known as a calender stack. The rollers exert pressure onto the sheet with the objective of smoothing and evening the sheet thickness (caliper). Cross-directional caliper variations are modified by the use of CD caliper actuators which locally change the pressure exerted onto the paper sheet.

While early CD caliper control was done mainly by the use of hot and cold air showers, modern CD caliper control systems almost exclusively use induction heaters. High frequency electric current induces eddy currents in a calender roll made of ferrous materials. Such induced eddy currents cause a local heat build up, resulting in a temperature increase which also causes the roll diameter to increase. This, in turn increases the pressure locally exerted onto the sheet causing the caliper (thickness) to be reduced. A decrease of the roll's diameter, achieved through temperature reduction, has clearly the opposite

effect, i.e. the sheet's caliper will increase. The number of induction heaters, on a typical paper machine can be as high as $n = 150$, and the usual actuator spacing is $x_a = 75mm$ [62].

Of all the actuators considered in this chapter, induction heaters are by far the slowest. The response time generally varies from very slow to almost an integrating processes. Considering the location of inductions heaters (in the Dry end, near the scanning sensor), the delay of these systems, in contrast to weight and moisture control systems, is usually quite negligible. It is interesting to note, from a historical point of view, that the first computer controlled paper machine CD control systems were actually CD caliper control systems, bought and installed in 1973 (see graphs in Figure 612 in [12]).

1.3 CD Process Attributes

As demonstrated in Sections 1.1–1.2, paper machine CD processes are large, multivariable, spatially-distributed processes with 30–300 inputs (actuators) and 200-2000 outputs (measurement points). In the CD control literature, CD processes are most often considered to have separable dynamic and spatial responses [18, 20, 23, 45, 62, 65],

$$y(z) = G(z) \cdot u(z), \qquad G(z) = g(z) \cdot G_0 \tag{1.3}$$

where $y(z) \in \mathcal{C}^m$, $u(z) \in \mathcal{C}^n$ are the $\mathcal{Z}$-transforms of the output (measurement) profile and the input (actuator) profile respectively ($200 \leq m \leq 2000$ and $30 \leq n \leq 300$), $g(z)$ is a $\mathcal{Z}$-transform of the process time response, and $G_0 \in \mathcal{R}^{m \times n}$ is a constant, process spatial response matrix.

The temporal response $g(z)$ is usually modelled as a stable, first-order-plus-deadtime (FOPDT) scalar transfer function,

$$g(z) = \frac{z^{-d}}{1 - a_0 z^{-1}} \tag{1.4}$$

where d is the process delay in samples and a_0 is a process pole (determined by the process time constant and control system's sampling time). Depending on the property being controlled and the type of actuators being used, process time constant and delay can vary significantly. As pointed out in Section 1.2, some actuators have a very fast, almost instantaneous, response (e.g. rewet showers modifying moisture profiles), while some others are extremely slow, almost integrating processes (e.g. induction heaters affect on caliper profiles). On the other hand, the process delay (dead time) d is mainly determined by the distance between the actuators and a scanning sensor and machine speed. As a result, it can vary from less than one scan (caliper control by the use of induction heating

actuators) to up to 9 scans (basis weight control by the means of slice lip or dilution actuators). In terms of their spatial responses, modelled by the matrix G_0 in (1.3), CD processes can also vary significantly. Spatial response to a single actuator can be as narrow as a few centimetres (basis weight control by the use of dilution actuators) or as wide as a few metres (slice lip basis weight control on a heavy grade paper) [62].

As an illustration of the spatiotemporal nature of CD processes, a typical CD process model response, in the case of a spatial impulse and temporal step input signal (i.e. one actuator 'bumped' to a predetermined value and kept at that value), is illustrated in Figure 1.5. It is a model of basis weight response to a slice lip actuator.

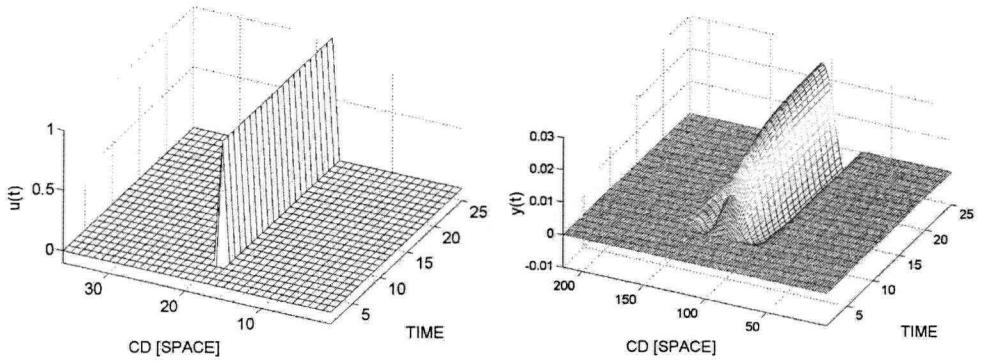

Figure 1.5: Illustration of the two-dimensional characteristics of the CD processes: CD process model basis weight response to a slice lip actuator.

Another very important characteristic of CD process models is their inherent severe ill-conditioning [23, 33, 45, 62]. In other words, the singular values of the matrix G_0 in (1.3) vary significantly. The ratio between the largest and the smallest singular value (condition number γ):

$$\gamma(G_0) = \frac{\overline{\sigma}(G_0)}{\underline{\sigma}(G_0)} \gg 1, \tag{1.5}$$

and can reach into thousands. As an example, the singular values of a basis weight control process model with 36 slice lip actuators, at steady-state ($\omega = 0$), are given in Figure 1.6. The maximum singular value, for this particular model, is $1.674 \cdot 10^{-2}$, and the minimum $5.101 \cdot 10^{-6}$, resulting in a condition number $\gamma(G(z)_{z=1}) = 3281.71$. As a result of the process model separability (1.3)–(1.4), ill-conditioning is present across all dynamic frequencies since the condition number remains unchanged (and very large) with frequency ω: $\gamma(G(e^{j\omega})) = \gamma(G_0)$, $0 \leq \omega \leq \pi$.

Significant process model uncertainty is another important attribute of industrial CD control systems. CD process models are usually identified from noisy input/output data, and there are numerous sources of model uncertainty. Uncertainty can arise, for example,

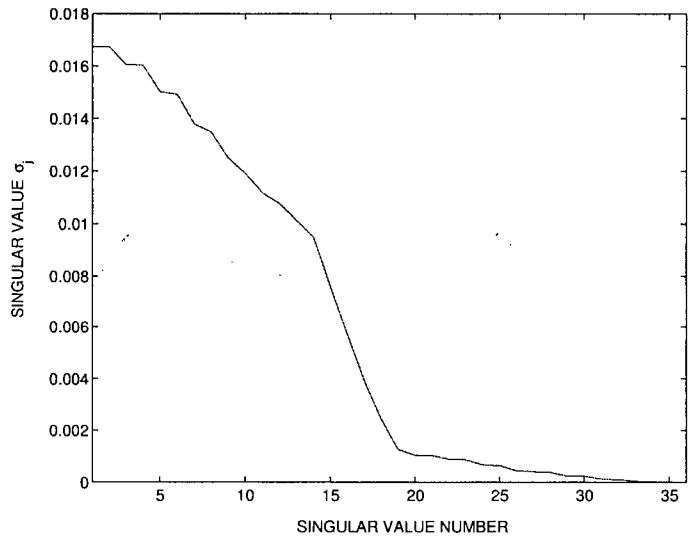

Figure 1.6: Steady-state singular values of a typical CD process model.

from (1) wandering of the paper web, (2) paper shrinkage characteristics, (3) flow pattern of extruded liquid paper stock in the initial stage of the paper making process (on the forming wire) [32]. All of these factors generally change with time, depend on the paper grade being made, machine speed, etc. As a result, it has become recognized, that industrial CD control systems must deal systematically with the inherent process model uncertainty [9, 10, 18, 19, 45, 62, 65, 73].

To summarize, some of the most important characteristics of the CD control systems are: large-scale (30–300 inputs and 200–2000 outputs), ill-conditioning (condition number potentially in the order of thousands across all dynamical frequencies), and a significant process model uncertainty. Some of the approaches developed for addressing these characteristics are outlined in Section 1.3.1 below.

1.3.1 Approaches to CD Control

Major advances in the cross-directional control of web forming processes were achieved in [18]. Therein, controllability of the cross-directional processes, in terms of the spatial Fourier components of the process output $y(t)$, was analyzed, and it was shown that, for control purposes, it is enough to identify only those spatial frequency components of the CD profile that are controllable. After this, the parametrization of CD process received a lot of attention [20, 21, 22, 38, 42, 45, 62]. Parametrization describes the compact representation of the system input, output, and the resulting interaction matrix with a certain set of basis functions. The Fourier transform [18, 20, 62], Gram polynomials [38, 42],

and singular value decomposition (SVD) [18] represent different ways of parameterizing the CD control system. The main objective of parametrization is to identify compactly those components that can be controlled. System parametrization leads to problem size reduction, which in turn leads to a substantial computational load reduction [21, 22, 42].

In [18] for the first time, the robustness of CD control systems was thoroughly analyzed. In that thesis, the author gave some very important insight about the robust stability of CD control systems for web forming processes with the controller $C(z) = c(z)[G_0^T G_0]^{-1} G_0^T = c(z)C$, where $G_0 \in \Re^{m \times n}$ is the plant model from (1.3), the scalar transfer function $c(z)$ contains dynamical response of the controller, and the constant matrix $C \in \Re^{n \times m}$ contains the spatial response of the controller. Results were compared using analysis in an artificial case of infinite width web with infinite actuator array. In both cases robustness was analyzed in cases of additive uncertainty in the process plant. In the analysis of the actual control system with controller $C(z) = c(z)C$, robustness in case of the process spatial response (G_0) additive uncertainty Δ, with limited maximum singular value ($\overline{\sigma}(\Delta) < \Omega$), was investigated. The analysis considered closed-loop singular values, in which case the analysis of the MIMO system with a given stabilizing controller can be carried out as the analysis of a set of n (n – is the number of actuators) SISO loops. It was found that robust stability can be guaranteed through detuning either the dynamic response or the spatial response of the controller. However, these methods have the drawback that all controllable modes will be detuned and not only the poorly controllable ones.

Further advances in the analysis and design of robust controllers were made in [19, 45]. In [45], the paper machine CD control problem was analyzed from the robust performance point of view. The analysis was done for the case of a square interaction matrix. A continuous time model was used, separability of dynamic and spatial responses assumed, and model uncertainty G_Π was expressed in terms of ranges on the elements of interaction matrix G and the parameters of the common dynamic part $g(s)$. Two design techniques were presented, one with decentralized controller structure with $C(s) = c(s)S$, where S is a diagonal matrix and the other with model-inverse-based controller $C(s) = c(s)G^{-1}$. The former technique can be applied only in the case of a positive definite spatial response process interaction matrix G. If G is not positive definite then the model-inverse-based controller has to be used. In case of decentralized controller design, circulant symmetric matrix theory was used to obtain bounds on the plant within which robust performance is guaranteed. Closed-loop robustness was achieved through detuning of the controller dynamics $c(s)$. This would usually lead to a conservative control design since all the controllable modes are detuned. Main drawback of these techniques is that neither the decentralized nor model-inverse control is suitable for ill-conditioned plants.

In [19], a robust design procedure was developed for separable controllers, given with $C(s) = c(s)C$. Singular value decomposition of the system was performed and the set of n SISO systems was analyzed. Analysis was done both for the case of simultaneous uncertainties in the spatial response part of the interaction matrix (limited maximum singular value uncertainty) and for the dynamical part (parameter uncertainty). Detuning of the controller in order to achieve robustness can be done either by detuning its dynamics $c(s)$ or by detuning the pre-compensator matrix $C = [G^TG + \Omega I]^{-1}G^T$. In both cases there is a degradation of the performance of well-controllable modes of the system but this occurs to a lesser extent in the case of detuning the pre-compensator matrix C. The problems can also arise if, due to uncertainty, the sign of the process gain at high spatial frequencies changes. In that case, the closed-loop system might be destabilized.

In [9] a larger class of uncertainty structures was allowed which included: additive, multiplicative input, multiplicative output, inverse multiplicative input and inverse multiplicative output uncertainties. The analysis in case of controller structure $C(s) = V\Sigma(s)_cU^T$, with process matrix $G(s) = g(s)U\Sigma V^T = U\Sigma(s)V^T$ where $\Sigma(s)$ is a matrix with *pseudo singular values* $\sigma_i(s)$ was performed. A modification of the DK-iteration (μ synthesis) algorithm was presented where K-step of the design procedure was reduced to the design of n independent robust SISO controllers, where n is the number of actuators. The major advancement of this approach is its ability to handle a larger set of model uncertainties, but the controller design technique remains fairly complex. However, further refinements of this approach were presented in [73].

Robustness of CD control systems with respect to different basis functions used for system representation was analyzed in [10]. The comparison was made between minimum variance controllers designed using representation based on orthogonal polynomials, Fourier methods, singular value decomposition, splines and wavelets. The comparison was performed by analyzing the condition number (ratio of maximum and minimum singular value) of the system models obtained using different methods. It was found that in all of these cases robustness is practically the same except in the case of representation with splines. For spline representation, the system was found to be significantly less robust with respect to uncertainties in actuator response shape. Therefore, the choice of system representation (except in case of representation with splines) can be left to considerations other than robustness.

1.4 Spatially-Distributed Control Systems

As illustrated in previous sections, paper machine CD control systems clearly belong to a broader class of spatially-distributed control systems that, in turn, form an important

subset of large, multivariable, coupled industrial control systems. In addition to flat sheet forming industries (including paper, steel, and plastics making processes), spatially-distributed control systems arise in various other applications. For example: flow control, control of vehicular platoons, microelectromechanical systems (MEMS), space telescopes, systems described by partial differential equations with constant coefficients and spatially-distributed actuation and measurements, all belong to a set of spatially-distributed control systems. As a result of an increasing interest of the control engineering community in these systems, there have been many new tools developed recently for the analysis and controller synthesis of spatially distributed control systems [8, 15, 31, 34, 35, 46, 62, 66], some of which are discussed below.

First, it should be noted that an important assumption, usually necessary for the application of the above mentioned techniques, is *spatial invariance. Spatial invariance* means that process dynamics are (assumed) invariant with respect to translation in some spatial coordinates(s). As a result of this assumption, the subsequent controller synthesis procedure can be significantly simplified [8]. The systems analyzed in [8] are infinite-dimensional. The analysis and controller synthesis for such systems (see for example [11]), in general, is significantly more complex than for finite-dimensional systems. However, with the spatial invariance assumption, it was shown [8] that quadratically optimal controllers can be synthesized by solving a parameterized (over spatial frequency) family of finite-dimensional problems. It was also shown in [8] that controllers computed via quadratic optimal techniques, including LQR, $\mathcal{H}_2$, and $\mathcal{H}_\infty$ optimization, preserve the spatially invariant characteristics of the process. In addition, it was demonstrated that such optimal controllers have a degree of localization similar to that of the plant, justifying implementation of localized controllers in the case of localized processes (plants).

Distributed control of spatially-invariant systems, by the use of linear matrix inequalities (LMIs), was investigated in [13, 15]. Therein, a state-space approach is used on continuous-time and spatially-discrete systems with spatial coordinates $s_i \in D_i$, where D_i is a set of integers $\mathbb{Z}$ or some finite set $\{1, 2, ..., N_i\}$. As a performance criterion, the l_2-induced norm is used, with the space l_2 being a set of functions mapping $D_1 \times \cdots \times D_L$ to $\mathbb{R}^\bullet$, where L is a number of spatial coordinates and $\mathbb{R}^\bullet$ is a set of real valued finite vectors. Applications of the proposed approach, based on LMIs, were presented in [14, 24]. It was demonstrated in [24], that a distributed control approach yields far superior results in comparison to the decentralized control techniques, and results comparable to centralized control techniques at a fraction of required computational time.

However, very often, practical control systems (including CD control systems) are not spatially-invariant, and the above techniques can not be implemented without further modifications. Even more, because of the idealized boundary conditions (spatial invari-

ance) assumed in the design process, there is no guarantee of performance (not even stability) around the boundaries. In other words, there exist destabilizing boundary conditions. A class of bounded, spatially distributed systems with associated boundary conditions, for which stability and performance are guaranteed after implementing a controller designed under process spatial invariance assumption is presented in [44].

The importance of boundary conditions is also very well known in the theory of partial differential equations (PDE) [68]. The class of PDEs in which boundary conditions are specifically taken into account are the so called boundary value problems (BVP). In PDE theory, there are three types of boundary conditions that are most often implemented: Dirichlet, Neumann, and Robin boundary conditions. In the case of Dirichlet boundary conditions (BC), the finite-width signals are extended with a constant (predefined) value. In the case of Neumann BC, the signal extension is defined such that its first derivative (with respect to the spatial coordinate in question) remains constant, and in the case of Robin boundary conditions such that a linear combination of the signal extension and its first derivative has a predefined value.

In addition to the theory of PDEs, the importance of boundaries has also long been recognized in the field of signal processing, where the boundaries of a signal typically require modification to the filtering. Temporal (causal) filters require initial conditions to be specified, and noncausal filters (e.g. image processing) may require both initial and final conditions to be specified [16].

As illustrated in Section 1.3 above, paper machine CD processes belong to an important class of filters that are causal in one direction (time), but noncausal in space. It is illustrated in Section 2.2 below, that industrial CD controllers, of particular interest in this work, belong to the same class of spatio-temporal filters. These filters (systems) carry the additional risk of instability due to incorrect design of boundary conditions. These boundaries may be interpreted as points of discontinuity in the signal. The effect of the boundaries on the filtered signal is clearly influenced by the way the filtering is modified to handle these.

1.5 Industrial Paper Machine CD Control Systems

This work is concerned with modifying a particular realization of the industrial paper machine CD control law - a Honeywell CD controller - around spatial domain boundaries. The controller structure, tuning technique, and implementation are presented in [62, 64, 65, 66]. Industrial CD control systems with the specific controller structure under consideration in this work are currently installed on more than 4200 paper machines worldwide.

A simplified diagram of the industrial CD control system relevant to this work is illustrated in Figure 1.7. Industrial CD controller software resides on a PC that is connected by network to the paper machine's actuator array and scanning sensor (the scanner is sometimes connected to the PC via serial connection). Based on the measurements $y(t)$ obtained from the scanning system and the desired target value $r(t)$, the controller algorithm generates a control signal $u(t)$, that is subsequently sent to the actuator array.

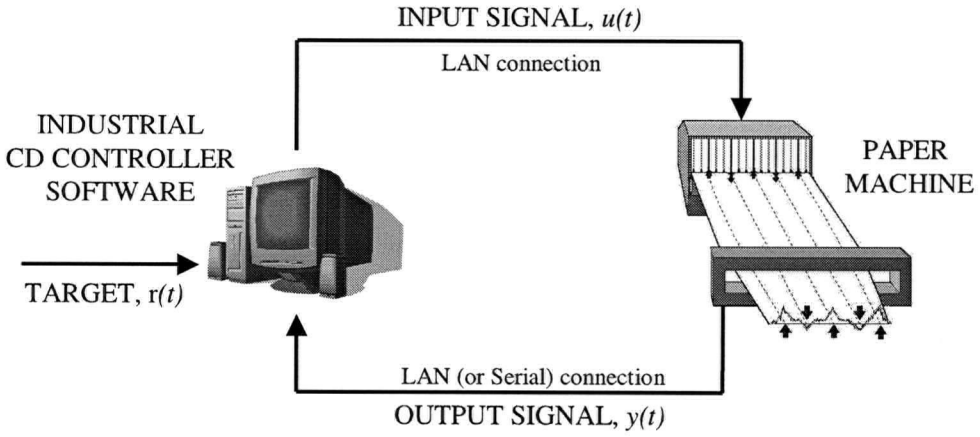

Figure 1.7: Simplified diagram of an industrial CD control system.

A more detailed block diagram, indicating data flow in this industrial CD control system, is given in Figure 1.8. The scanning sensor measures the sheet properties at 200-2000 points, thus generating the so called high-resolution (scanner's spatial resolution) vector profile $y_{HR}(t)$. After the each scan, this vector of measurements is delivered to the industrial controller's *measurement processing* section. The measured signal is then dynamically filtered in order to separate machine-direction (MD) and cross-direction (CD) components of the profile. As pointed out earlier, the MD component is controlled by a separate control loop, not illustrated in Figures 1.7–1.8. Since the MD/CD separation involves the use of a dynamic filter, it clearly introduces additional dynamics into the CD control loop.

As the number of CD actuators (30–300) is usually ~3–10 times smaller than the number of measurement points, the high-resolution CD profile is spatially low-pass filtered (spatial anti-alias filtering), before being downsampled to the actuator resolution (spatial low-resolution) $y_{LR}(t)$. Finally, the error between the measurement profile and the desired profile is passed to the *linear time-invariant CD controller* algorithm.

The industrial linear time-invariant CD controllers are essentially 2D (spatio-temporal)

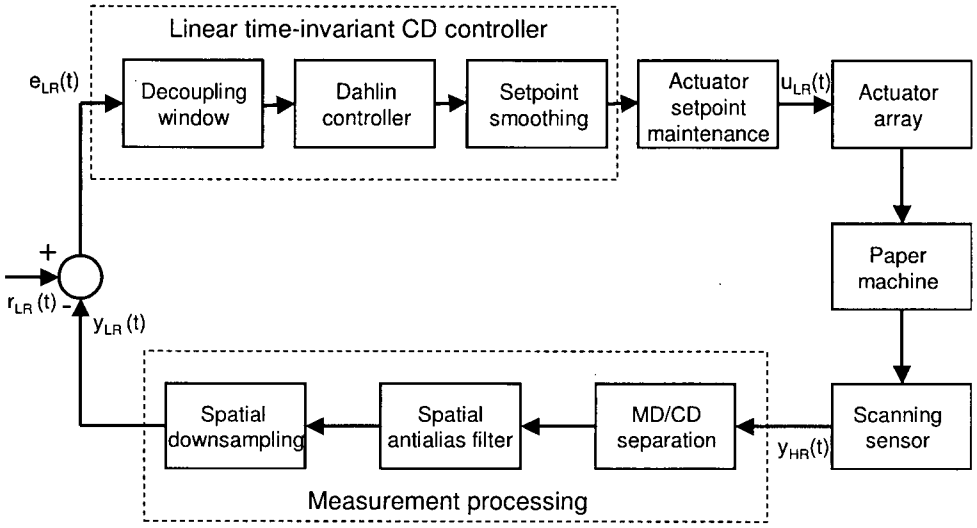

Figure 1.8: Data flow in an industrial CD control system; HR: High-Resolution (Scanner spatial resolution) LR: Low-Resolution (Actuator spatial resolution).

filters, causal in time and noncausal in the spatial domain [31, 50, 66]. They consist of three blocks (1) a spatial decoupling algorithm, (2) a Dahlin controller, and (3) a setpoint smoothing algorithm, connected in cascade as illustrated in Figure 1.8. In current industrial practice, these blocks (i.e. CD controller) are most often tuned using a two-dimensional loop shaping technique [62, 65, 66]. A spatial invariance approximation is central to this technique, which is an extension of traditional loop shaping and addresses the closed-loop performance and robust stability criteria in terms of the spatial and temporal frequency domains.

The output of the linear time-invariant CD controller passes through the *Actuator setpoint maintenance* section, a nonlinear block that does constant checking/verification to ensure the setpoints do not violate physical constraints, before the setpoints are finally delivered to the actuator array.

1.5.1 Problems Near the Sheet Edges (Spatial Domain Boundaries)

The two-dimensional loop shaping technique has been successfully implemented on more than 100 paper machines worldwide to date. However, as the process characteristics near the sheet edges are clearly different from those in the centre of the sheet, the spatially-invariant CD controllers (spatio-temporal filters) are modified at the edges on a real paper machine [50]. The current industry practice uses methods (that extend the signal beyond

the sheet edges) based on the techniques in the field of signal processing. These will be described in detail in Section 2.1 and include: zero padding, signal average padding, and reflection padding [67]. Unfortunately, often these approximations then lead to unsatisfactory control at the edges, and control systems can even be destabilized [50, 63]. One such example is illustrated in Figure 1.9.

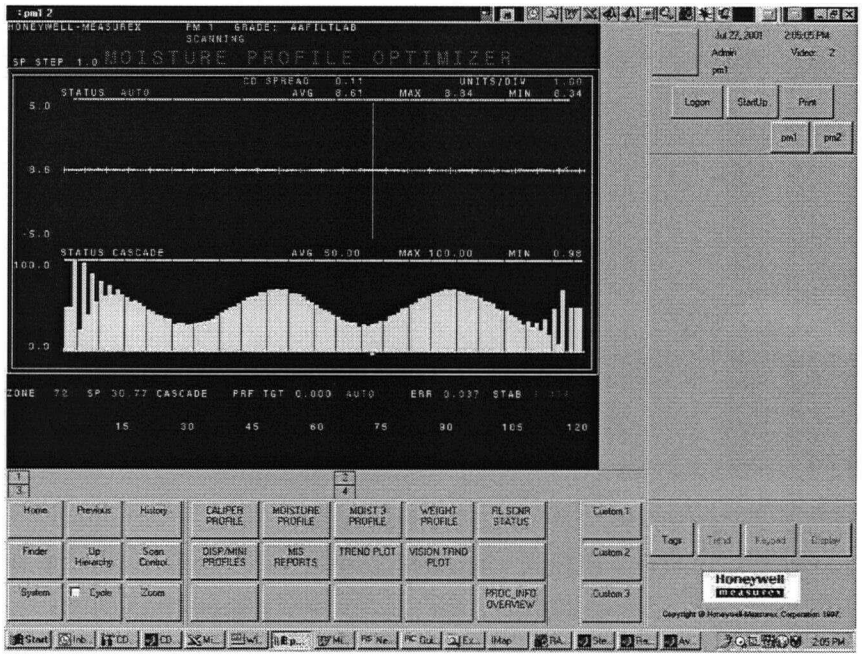

Figure 1.9: Illustration of the problems ('actuator picketing' in the lower portion of the screenshot) that often occur when implementing current CD control techniques near the sheet edges.

Figure 1.9 is a screenshot of the Honeywell hardware-in-the-loop paper machine simulator. It illustrates the behavior of a simulated CD moisture control system, with process output (CD moisture) and actuator array profiles shown. It can be seen that the process output profile is very good (flat). However, the actuator array, while being very-well behaved (smooth) away from the edges, shows clear signs of instability near the edges. The edge actuators are moving in the opposite directions, developing a well-known mode of instability referred to as 'actuator picketing' by paper makers, because of the picket fence appearance of the actuator profile. Such a control signal is most likely not reducing paper sheet profile variations as CD processes are essentially spatial low-pass filters [17, 18], but it is also indicative of a low stability margin on $\overline{\sigma}(T_{ud})$ - the maximum singular value of the closed-loop transfer matrix gain from the process output disturbance d to the control signal u.

'Actuator picketing', originating from the edges, often 'creeps' into the rest of the system, finally destabilizing the whole control system. In order to prevent instability, in practice the edge actuators of the paper machine CD control systems very often are placed in open-loop [63].

1.6 Aims and Contributions of the Work

The spatial invariance assumption is central to the two-dimensional loop shaping technique, used for tuning the industrial paper machine cross-directional control systems. As a result of the assumed periodic (idealized) boundary conditions, the control laws are modified near the spatial domain boundaries (paper sheet edges) before implementation on a real paper machine. The current industrial techniques for extending the finite-width signals are borrowed from the field of signal processing, and do not take into account relevant control engineering criteria or physical reality. As a result CD controller performance near the edges can be very poor.

The **objective** of this work is to modify the existing industrial CD control law, initially designed with the process spatial-invariance assumption, so that important control engineering criteria, such as: closed-loop stability, performance, and robustness are taken into account. At the same time, the structure and complexity of the existing control law are to be unchanged.

The main **contributions** of this work are:

1. The introduction of a straightforward technique for achieving a stabilizing controller for a known plant by modifying a controller that is known to stabilize a second, related plant. The technique can be applied to a broad class of systems with multivariable linear time-invariant transfer matrix models and controllers, including industrial paper machine cross-directional control systems. Although the main objective of this technique is closed-loop stability transfer, in certain circumstances, a successful controller design in terms of closed-loop performance can also be achieved.

2. The development of a novel stability-preserving method for modifying boundary conditions (BCs) of a spatially-distributed controller, initially computed assuming idealized spatially-invariant BCs. An analogy between the effects observed when implementing such controllers, with various boundary conditions, on the actual (i.e. finite, non-periodic) processes and the well-known Gibbs phenomenon is observed. Stability-preserving modifications, based on a method for reducing the Gibbs effect, are developed. The technique is demonstrated in the case of the industrial paper machine CD controller.

3. A new approach to the redesign of industrial paper machine cross-directional (CD) controllers near spatial domain boundaries is presented. The method directly takes into account relevant control engineering criteria, such as closed-loop stability, performance, and robustness. The new approach modifies the CD control law near the paper sheet edges (spatial domain boundaries) by sequentially applying a novel low-bandwidth static output feedback design algorithm on two matrix components of the existing industrial controller. The existing industrial CD controller structure or complexity are not changed with the new approach.

4. A successful implementation of the above approach has been tested on an industrial paper machine. It is demonstrated that with the new approach a trade-off between the final product quality (paper sheet smoothness) and controller aggressiveness can be achieved. When compared against the existing industrial practice, the implementation of the new technique resulted in improved paper sheet quality and lower actuator usage (i.e. smaller control signal magnitudes).

1.7 Thesis Overview

The remainder of the thesis is organized as follows. The concept of explicit and implicit boundary conditions (BCs), in terms of spatio-temporal filters of interest in this work, is introduced in Chapter 2. The spatio-temporal filters under consideration are the key element in defining paper machine cross-directional (CD) process and controller models. The main characteristics of industrial paper machine CD control systems and the two-dimensional loop shaping technique (tuning tool for the industrial CD controllers) are also presented in Chapter 2. The objective of this work is specified at the end of this chapter.

In Chapter 3, a novel and straightforward closed-loop stability preserving perturbation technique, for CD controllers initially designed under the idealized process spatial-invariance assumption, is presented. The technique is simple and requires no additional computation on the part of the designer, and, as illustrated in Chapter 3, can be implemented on a broad class of linear time-invariant systems with known plant perturbations. However, in terms of the objectives of this work, performance requirements other than closed-loop stability are not addressed with this approach.

The similarities between the effects observed in the industrial paper machine CD control systems and the well-known Gibbs phenomenon in Fourier analysis are summarized in Chapter 4. Next, CD controller modification technique, inspired by a method for reducing the Gibbs effect is presented. The proposed technique guarantees the stability of the resulting CD controller. A closed-loop simulation example of this controller modification technique is also presented in Chapter 4.

In Chapter 5, the objective of modifying paper machine CD control law is stated in terms of a block-decentralized static output feedback (SOF) design problem via appropriately defined linear fractional transformation (LFT). The subsequent design approach is based on a novel low-bandwidth static output feedback design algorithm, sequentially implemented on two constant matrix components of the existing industrial CD controller. This approach systematically takes into account all objectives of this work, and important control engineering criteria: closed-loop stability, performance, and robustness. At the end of this chapter, a closed-loop simulation example with the Honeywell hardware-in-the-loop paper machine simulator is presented.

The new approach to CD control near the paper sheet edges, presented in Chapter 5, has been tested on a paper machine in a working paper mill. The industrial trial procedure and results are given in Chapter 6. Three different sets of the CD control law modifications (conservative, balanced, and aggressive) were computed and implemented. The results are then compared with the results achieved by current industrial practice.

Finally, conclusions and suggestions for future research are given in Chapter 7.

Chapter 2

Problem Statement

Considering the two-dimensional nature of CD control systems, CD controllers (of interest in this work) and CD processes can be viewed as 2-D (spatiotemporal) filters. Further taking into account the main focus of the thesis (CD control near spatial domain boundaries), boundary conditions (BC) of such filters are clearly of particular importance here.

Section 2.1 introduces the concept of explicit and implicit boundary conditions in terms of the class of spatiotemporal filters that are the basic building block for the paper machine cross-directional process and controller models of interest in this work. Industrial CD process and controller models under consideration are detailed in Section 2.2. The main characteristics and tasks of the industrial cross-directional control systems, including an overview of the CD controller tuning method (two-dimensional loop shaping technique [65, 66]), are also presented in Section 2.2. Finally, the objective of this work is specified in Section 2.3.

2.1 Explicit and Implicit Boundary Conditions

A well known problem in engineering is the filtering of signals with discontinuities. We can find examples of this problem related to temporal as well as spatial filters. In the temporal domain, it is well known that it is of particular importance to handle sudden changes of the variables that define the state of such systems. The transients that occur as a consequence of those abrupt changes (i.e. discontinuities) can pose significant problems, and engineering systems have to be able to withstand such transients. An analogous effect occurs with spatial filters. The unwanted consequences of such filtering are spatial ripples (equivalent to temporal transients), for example edge blurring in image processing [28]. The importance of spatial filters' ability to handle input signal discontinuities is even greater in cases where spatial filters are placed in a feedback loop (see Figure 2.4). In such cases, the unwanted effects of signals' discontinuities can be magnified as the filtered discontinuous signal is being brought back to the filter's input.

In order to place our problem in a familiar context, we will consider the issue of spatial boundary conditions as appearing in partial differential equations and image processing.

Consider the update equation of a two-dimensional signal,

$$y(i,k+1) = \sum_{j=-l_h}^{l_h} h_j \cdot y(i+j,k), i \in \Omega = \{i : 1 \leq i \leq n\} \tag{2.1}$$

where $y \in \mathcal{R}$ ($\mathcal{R}$ - set of real numbers), and (2.1) represents the implementation of a non-causal FIR filter in the first index (spatial dimension), and a causal, first-order IIR filter in the second index (temporal dimension), with scalar filter coefficients $h_j \in \mathcal{R}$, and $j = -l_h, \ldots, l_h$. We will consider filtering of a signal $y(i,k)$ that is defined on a finite spatial domain consisting of n discrete locations $i = 1, \ldots, n$. Immediately it can be seen that the relation (2.1) is incomplete as it requires information from $y(i,k)$ on a boundary layer

$$\delta\Omega = \{i : 1 - l_h \leq i \leq 0 \quad \cup \quad n+1 \leq i \leq n+l_h\} \tag{2.2}$$

as illustrated in Figure 2.1.

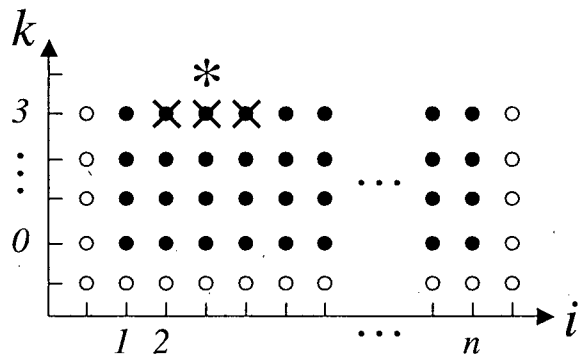

Figure 2.1: The template structure and explicit boundary layer $\delta\Omega$ (denoted by ○ for $i = 0$ and $i = n + 1$) of a spatiotemporal filter with $l_h = 1$ in (2.1)-(2.3). (The row of ○ at k = -1 indicates the initial conditions of the causal filter and are not important for the case being considered.)

The need for such auxiliary conditions arises in numerical solutions to partial differential equations [68] and image processing [16]. The three most important kinds of boundary conditions in PDEs are Dirichlet, Neumann, and Robin conditions [68]. In the case of Dirichlet boundary conditions (BC), the finite-width signals are extended with a constant (predefined) value, while in the case of Neumann BC, the signal extension is defined such that its first derivative (with respect to the spatial coordinate in question) remains constant. Finally, in the case of Robin boundary conditions a linear combination of the signal extension and its first derivative has a predefined value. Image processing [67] provides another set of filter modifications for boundary conditions, often referred

to as edge padding. Common padding techniques include reflection, zero, average, and periodic padding. Each of the above boundary conditions may be represented by creating an explicit boundary layer on $\delta\Omega$ by executing:

$$y(i,k+1) = \sum_{j=1}^{n} g_{ij} \cdot y(j,k+1) + w(i,k+1), \quad i \in \delta\Omega \tag{2.3}$$

with corresponding scalar constants g_{ij}, exogenous signal $w(i,k)$, and $\delta\Omega$ as defined in (2.2), following the update in (2.1). However, as we are concerned only with the values of $y(i,k)$ within the spatial domain for $i \in \Omega$ we can eliminate the explicit boundary layer by solving (2.1) and (2.3) obtaining[1] the implicit form

$$y(i,k+1) = \sum_{j=1}^{n} h_{ij} \cdot y(j,k), \quad i \in \Omega \tag{2.4}$$

As a result, the relation (2.1) along with any one of the boundary conditions is implementable with the matrix equation,

$$Y(k+1) = H \cdot Y(k), \quad Y(k) = [y(1,k), \ldots, y(n,k)]^T \tag{2.5}$$

where $H \in \mathcal{R}^{n \times n}$ is a constant matrix whose elements are given by

$$h_{ij} = \begin{cases} h_{j-i}, & \mid j-i \mid \leq l_h \quad \text{and} \quad l_h+1 \leq i \leq n-l_h \\ 0, & \mid j-i \mid > l_h \quad \text{and} \quad l_h+1 \leq i \leq n-l_h \\ \delta h_{ij}, & 1 \leq i \leq l_h \quad \text{and} \quad n-l_h+1 \leq i \leq n \end{cases} \tag{2.6}$$

where $j = 1, \cdots, n$, and the coefficients δh_{ij} determine the implicit boundary conditions. Examples are presented in Table 2.1 obtained by solving h_{ij} in (2.4) for the common BCs (assuming a spatially symmetric filter in (2.1) with $l_h = 1$, i.e., $h_1 = h_{-1}$).[2] It is illustrated in Section 2.2 that both CD process and industrial CD controller represent a slight generalization of the system given by (2.5).

Since two cases of BCs will be used often throughout the thesis, we introduce a shorthand notation. The matrix H in (2.5) defining a spatial filter with Dirichlet BCs, corre-

[1]We are considering the homogeneous form of each, as it is general enough to include all the cases of interest in CD control.

[2]The parameter b that appears in Table 2.1 in case of Robin boundary conditions is a predefined function of spatial and temporal domains.

Boundary Cond.	Coefficients δh_{ij} in (2.6)		
1. Dirichlet	$\delta h_{11} = h_0$	$\delta h_{12} = h_1$	
2. Neumann	$\delta h_{11} = h_0 + h_1$	$\delta h_{12} = h_1$	
3. Robin	$\delta h_{11} = h_0 + b \cdot h_1$	$\delta h_{12} = h_1$	
4. Reflection	$\delta h_{11} = h_0$		
5. Zero	$\delta h_{11} = h_0$	$\delta h_{12} = h_1$	
6. Average	$\delta h_{11} = h_0 + \frac{h_1}{n}$	$\delta h_{12} = h_1 + \frac{h_1}{n}$	$\delta h_{1j} = \frac{h_1}{n}$
7. Periodic	$\delta h_{11} = h_0$	$\delta h_{12} = h_1$	$\delta h_{1n} = h_1$

Table 2.1: Matrix coefficients in (2.6) resulting from the representation of spatial filters (order $l_h = 1$) with various boundary conditions.

sponding to a Toeplitz matrix H_t, given by

$$\mathcal{T}(\overline{h}, n) = H_d := \begin{cases} h_{j-i}, & -l_h \leq j - i \leq l_h \\ 0, & \text{otherwise} \end{cases} \tag{2.7}$$

with $\overline{h} = [h_{-l_h}, \cdots, h_{l_h}]$. The matrix arising from the imposition of periodic BCs on a spatial filter, corresponding to a circulant matrix H_c, given by

$$\mathcal{C}(\overline{h}, n) = H_c := \begin{cases} h_{j-i}, & -l_h \leq j - i \leq l_h \\ h_{j-i-n}, & n - l_h \leq j - i \\ h_{j-i+n}, & j - i \leq -(n - l_h) \\ 0, & \text{otherwise} \end{cases} \tag{2.8}$$

The non-zero elements of the Toeplitz and circulant matrices H_t and H_c, as well as the difference between the two $\Delta H = H_c - H_t$, in case $n = 36$ and $l_h = 4$ are illustrated in Figure 2.2.

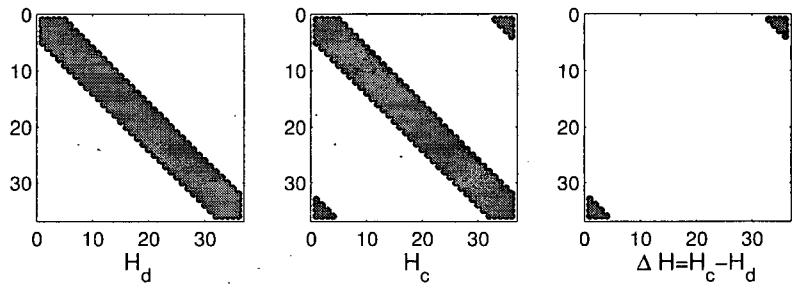

Figure 2.2: The non-zero elements of the matrix H_d in (2.7) (a); matrix H_c in (2.8) (b); and the difference $\Delta H = H_c - H_d$ (c).

Boundary Conditions	Stability
1. Dirichlet	Stable
2. Neumann	Marginally stable
3. Robin (with $b = 1.1$)	Unstable
4. Reflection	Stable
5. Zero	Stable
6. Average	Marginally stable
7. Periodic	Marginally stable

Table 2.2: Stability of the system in (2.5) with $l_h = 1$, $n = 20$, and filter coefficients $h_0 = 0.8$, $h_1 = 0.1$, in case of various boundary conditions in Table 2.1.

The stability of the system given in (2.5) is completely determined by the eigenvalues of the matrix H. The system in (2.5) is stable (marginally stable) if and only if all the eigenvalues of H are in the open (closed) unit circle. The implementation of the various boundary conditions in (2.6) requires modification of the first and last l_h rows of H in (2.5). As such, it affects the locations of the eigenvalues and possibly the stability of the system. An illustrative example, in case of filter in (2.1) with $l_h = 1$, $n = 20$, and filter coefficients $h_0 = 0.8$, $h_1 = 0.1$, is presented in Table 2.2, demonstrating that the BCs of the filter can influence the stability of the system given in (2.5).

2.2 Paper Machine CD Control System

Paper machine CD control systems usually have a significantly greater number of measurements (200–2000) than the number of actuators (30–300). In industrial systems the measurement array is typically low-pass filtered and downsampled to the number of actuators (see Figure 1.8 in Section 1.5) thus permitting the use of square transfer matrix models. The standard model of a paper machine CD control system shown in Figure 2.3, subject to process output disturbances, is given by:

$$y(z) = G(z) \cdot u(z) + d(z), \quad u(z) = K(z) \cdot y(z) \tag{2.9}$$

where $y(z), u(z) \in \mathcal{C}^n$ ($\mathcal{C}$ - set of complex numbers) are the $\mathcal{Z}$-transforms of the output (measurement) profile and the input (actuator) profile respectively, and $d(z) \in \mathcal{C}^n$ is the $\mathcal{Z}$-transform of the process output disturbance. The objective of the CD controller $K(z) \in \mathcal{C}^{n \times n}$ is rejection of disturbances $d(z)$.

The transfer matrix $G(z) \in \mathcal{C}^{n \times n}$ can be written as:

$$G(z) = [I - Az^{-1}]^{-1} B z^{-d} \tag{2.10}$$

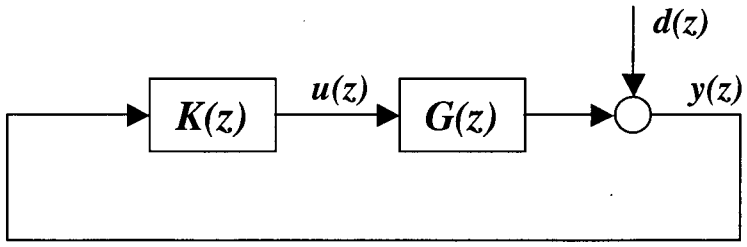

Figure 2.3: The industrial CD control system.

where the constant matrices A and $B \in \mathcal{R}^{n\times n}$ represent spatial filters with Dirichlet BCs (2.7):

$$\begin{aligned} A_d &= \mathcal{T}(\overline{a}, n) \qquad & B_d &= \mathcal{T}(\overline{b}, n) \\ \overline{a} &= a_0 & \overline{b} &= [b_{-l_b}, \cdots, b_{l_b}] \end{aligned} \tag{2.11}$$

where the coefficients modelling the spatial response $[b_{-l_b}, \cdots, b_{l_b}]$, the discrete time pole a_0, and the process model delay d are identified from input-output data, e.g. using commercial software described in [32]. Typically the paper sheet response to an actuator is symmetric with $b_{-j} = b_j$ in (2.11) and much narrower than the paper sheet so that $l_b \ll n$. This structure and the use of a band-diagonal Toeplitz matrix B_d in (2.10) is standard in the modelling of CD processes [23].

The structure of the industrial CD controller of interest in this work (illustrated in Figure 2.4) has been obtained through the years of theoretical analysis and industrial testing. Presently, there are more than 4200 installations of this particular controller performing CD control on paper machines worldwide. The controller structure, detailed below, represents a specific realization of the *Linear time-invariant CD controller*, illustrated in Figure 1.8 in Section 1.5, with its three distinctive sections (Decoupling window, Dahlin controller, and the Setpoint smoothing section) connected in cascade. Decoupling window is represented with a static matrix, Dahlin controller with a scalar transfer function, and a Setpoint smoothing section with a static matrix in a local dynamic feedback loop.

The industrial controller $K(z)$ in (2.9) of interest in this work (and illustrated in Figure 2.4) is given by [49, 50, 52, 53, 62, 63, 64, 65]:

$$K(z) = [I - Dz^{-1}]^{-1} D \cdot C \cdot c(z) \tag{2.12}$$

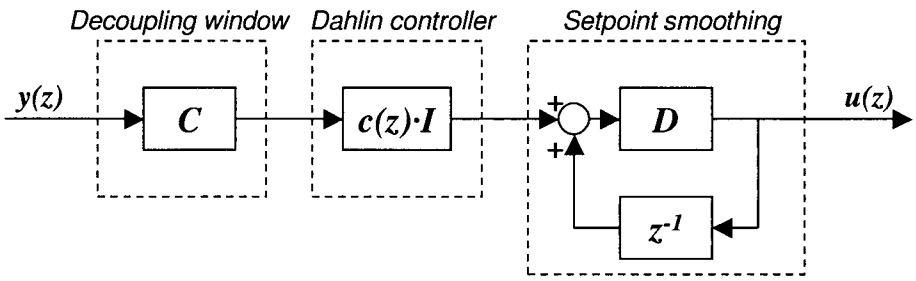

Figure 2.4: The industrial CD controller structure. (Compare with *Linear time-invariant CD controller* in Figure 1.8)

where the matrices (spatial filters) C and $D \in \mathcal{R}^{n\times n}$ are defined as

$$c_{ij} = \begin{cases} c_{j-i}, & |\, j-i \,| \leq l_c \quad \text{and} \quad l_c+1 \leq i \leq n-n_{C1} \\ 0, & |\, j-i \,| > l_c \quad \text{and} \quad n_{C1}+1 \leq i \leq n-n_{C1} \\ \delta c_{ij}, & 1 \leq i \leq n_{C1} \quad \text{and} \quad n-n_{C1}+1 \leq i \leq n \end{cases} \tag{2.13}$$

$$d_{ij} = \begin{cases} d_{j-i}, & |\, j-i \,| \leq l_d \quad \text{and} \quad n_{D1}+1 \leq i \leq n-n_{D1} \\ 0, & |\, j-i \,| > l_d \quad \text{and} \quad n_{D1}+1 \leq i \leq n-n_{D1} \\ \delta d_{ij}, & 1 \leq i \leq n_{D1} \quad \text{and} \quad n-n_{D1}+1 \leq i \leq n \end{cases} \tag{2.14}$$

and $j = 1, \cdots, n$. The coefficients collected in:

$$\overline{c} = [c_{-l_c}, \ldots, c_{l_c}] \qquad \overline{d} = [d_{-l_c}, \ldots, d_{l_d}] \tag{2.15}$$

with $c_{-k} = c_k$ for $k = 1, \cdots, l_c$ and $d_{-j} = d_j$ for $j = 1, \cdots, l_d$ are determined by controller tuning. Typically, the elements d_j are greater than zero, i.e. $\overline{d} > 0$. The size of the implicit boundary layer must be at least as large as the corresponding filter order ($n_{C1} \geq l_c$ and $n_{D1} \geq l_d$). The scalar transfer function $c(z)$ in (2.12) is a standard deadtime compensator known as the Dahlin controller in the process industries [62], given by:

$$c(z) = \frac{(1-\alpha)(1-a_0 z^{-1})}{(1-a_0)[1+(1-\alpha)\sum_{i=1}^{d-1} z^{-i}]}, \tag{2.16}$$

where a_0 and d are process dynamic parameters, defined in (2.10)–(2.11), and $\alpha \in [0,1]$ is a closed-loop control system tuning variable.

2.2.1 Industrial CD Controller Tuning Technique: Two-Dimensional Loop Shaping

State-of-the-art method for tuning the above industrial CD controller (i.e. determining the values for $\bar{c}$, $\bar{d}$, and α in (2.15)–(2.16)) is the two-dimensional loop shaping technique [62, 65, 66]. *Spatial invariance* assumption is central to this technique, as detailed below.

The two-dimensional loop shaping approach to CD controller tuning is as follows. First, the boundary conditions of the process model are changed from Dirichlet to periodic by substituting $B = B_c$ in (2.10), where

$$B_c = \mathcal{C}(\bar{b}, n) \tag{2.17}$$

is a symmetric circulant matrix in (2.8). This imposes spatial shift invariance on the plant model $G(z)$ in (2.9). A CD controller is then synthesized based on the spatially invariant plant model using the two-dimensional loop shaping technique described in [62, 66]. This generates the coefficients $\bar{c}$ and $\bar{d}$ in (2.15) for the matrices C and D in (2.12) with periodic BCs,

$$C_c = \mathcal{C}(\bar{c}, n), \quad D_c = \mathcal{C}(\bar{d}, n) \tag{2.18}$$

This design technique results in a stable controller, stable closed-loop, and desired closed-loop performance assuming all boundary conditions are periodic. Such an idealized cross-directional system is illustrated in Figure 2.5.

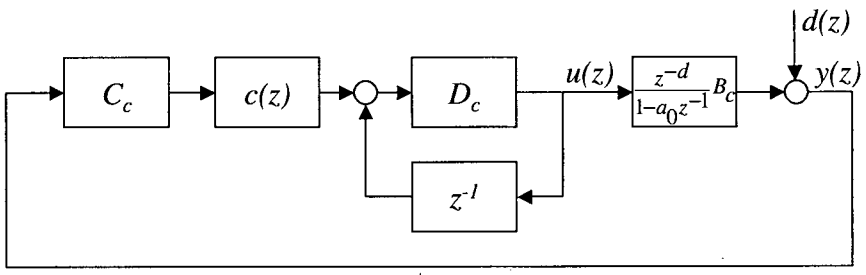

Figure 2.5: Idealized cross-directional control system with periodic boundary conditions.

However, the controller must be implemented on the system modeled with Dirichlet BCs given by $B = B_d$ in (2.11). From (2.10)–(2.11) and (2.17), it can easily be seen that the difference between the true (Toeplitz symmetric) and idealized (circulant symmetric) CD process models is given by:

$$\Delta G(z) = \frac{z^{-d}}{1 - a_0 z^{-1}} [\mathcal{C}(\bar{b}, n) - \mathcal{T}(\bar{b}, n)] = G_c(z) - G_d(z), \tag{2.19}$$

and contains the 'ears' of the circulant symmetric transfer matrix $G_c(z)$. (Figure 2.2 illustrates the location of non-zero entries of the corresponding Toeplitz and circulant matrices as well as the difference between the two.)

Similarly, the difference between the controller resulting from periodic and Toeplitz symmetric matrices is given by,

$$\Delta C = \mathcal{C}(\bar{c}, n) - \mathcal{T}(\bar{c}, n), \qquad \Delta D = \mathcal{C}(\bar{d}, n) - \mathcal{T}(\bar{d}, n), \tag{2.20}$$

and contains the 'ears' of the controller circulant symmetric matrices C_c and D_c.

Current industrial practice for modifying idealized CD control law, given with (2.12) and (2.18), before implementation on a real paper machine, consists of replacing controller's idealized (periodic) BCs with the corresponding Dirichlet, Average, or Reflection boundary conditions. As these techniques do not take into account relevant closed-loop control engineering criteria, they can lead to poor control (even instability) near spatial domain boundaries (paper sheet edges). One such example was illustrated in Figure 1.9 in Section 1.5.1.

2.3 Objective of the Work

Briefly stated, the objective of this work is to modify the existing CD control law - initially computed assuming process spatial invariance using a two-dimensional loop shaping tool - near spatial domain boundaries in a way that satisfies controller performance requirements.

Let us define the modifications to existing controller matrices in (2.12) in terms of additive matrix perturbations $\delta C, \delta D \in \mathcal{R}^{n\times n}$ in Figure 2.6. The elements of δC and δD are given by,

$$[\delta C]_{ij} = \begin{cases} \delta c_{ij}, & 1 \le i \le n_{C1} \quad \text{and} \quad n - n_{C1} + 1 \le i \le n \\ & 1 \le j \le n_{C2} \quad \text{and} \quad n - n_{C2} + 1 \le j \le n \\ 0, & \text{otherwise} \end{cases} \tag{2.21}$$

$$[\delta D]_{ij} = \begin{cases} \delta d_{ij}, & 1 \le i \le n_{D1} \quad \text{and} \quad n - n_{D1} + 1 \le i \le n \\ & 1 \le j \le n_{D2} \quad \text{and} \quad n - n_{D2} + 1 \le j \le n \\ 0, & \text{otherwise} \end{cases} \tag{2.22}$$

with $l_c \le n_{C1} \le n/2$, $l_d \le n_{D1} \le n/2$, and $1 \le n_{C2}, n_{D2} \le n$. However, normally $n_{C1}, n_{C2}, n_{D1}, n_{D2} \ll n$, resulting in only upper-left and lower-right corners of the matrices δC and δD being different from zero. The parameters l_c and l_d are the respective widths of the matrix bands of C and D in (2.13)–(2.14). Also, n_{C1} and n_{D1} represent the length of the implicit boundary layers of the spatial filters C and D respectively. It should be noted

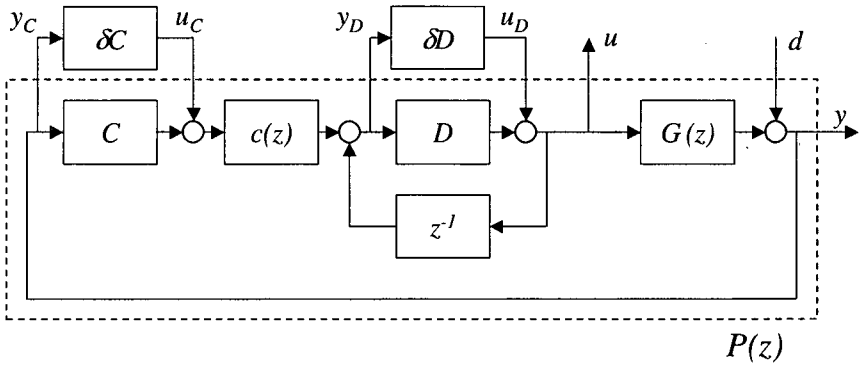

Figure 2.6: CD control system with control law modifications, δC and δD, near spatial domain boundaries.

that the existing industrial controller modifications near paper sheet edges (based on zero, average, and reflection padding) can be represented with the perturbation matrices δC and δD in (2.21)-(2.22), with $n_{C1} = l_c$, $n_{D1} = l_d$, $1 \leq n_{C2}, n_{D2} \leq n$.

By factoring out controller perturbations δC and δD as shown in Figure 2.6, a lower linear fractional transformation (LFT) as illustrated in Figure 2.7, can be defined. The generalized plant $P(z)$ in Figure 2.7 consists of the closed-loop transfer functions that can be obtained, after some straightforward algebra, from the system shown in Figure 2.6.

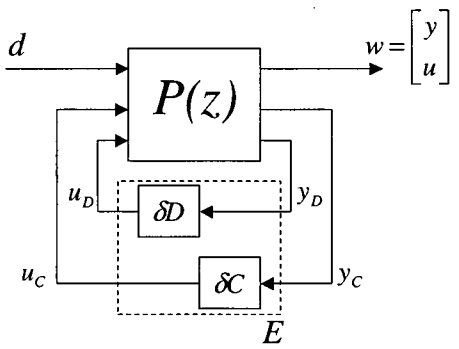

Figure 2.7: Problem reformulated in terms of linear fractional transformation (LFT).

As pointed out in Section 2.2, the modifications δC and δD currently used in industrial CD control systems do not take into account relevant control engineering criteria and can lead to very poor control near spatial domain boundaries. The objective of this work is to find a compensator E in Figure 2.7, such that:

1. $\delta D, \delta C \in \mathcal{R}^{n \times n}$ are static matrices with $n_{C1}, n_{C2}, n_{D1}, n_{D2} \ll n$ in (2.21) and (2.22).

2. The resulting closed-loop system in Figure 2.7 is stable.

3. The closed-loop performance of the system, as measured by the 2-norm of the process output vector at low frequencies, is improved:

$$\|y(e^{j\omega}, E)\|_2 < \|y(e^{j\omega}, 0)\|_2, \qquad \forall\, |\omega| < \omega_b, \tag{2.23}$$

   for some $\omega_b > 0$.

4. The gain $M(e^{j\omega}, E) : d \rightarrow u$ is limited across all the frequencies, i.e. for a given weight $W(e^{j\omega})$:

$$\overline{\sigma}(M(e^{j\omega}, E)) < W(e^{j\omega}), \qquad \forall\, \omega, \tag{2.24}$$

   where $\overline{\sigma}(\cdot)$ denotes the maximum singular value.

The first requirement above is a consequence of the main objective of this work: designing a localized modification of the existing industrial control law near the paper sheet edges without changing the controller structure. The need for the second requirement is obvious. The third requirement is in accordance with the main objective of CD control: the reduction of process output variations as measured by their 2-norm [1]. The fourth requirement is a result of the desired limit on control action, so that robustness characteristics of the system (as measured by $\|K[I - GK]^{-1}\|_\infty$) are preserved. In the two-dimensional loop shaping procedure, the process model uncertainty is modelled as additive uncertainty, and consequently $\|K[I - GK]^{-1}\|_\infty$ is a measure of system robustness.

Chapter 3

A Closed-Loop Stability Transfer Between Systems

In this chapter, a novel and straightforward perturbation technique is developed for modifying the spatially-invariant CD controller, in a manner that is guaranteed to stabilize a closed-loop control system with the true (spatially-variant) CD process model. The technique is based on the known difference between the idealized (spatially-invariant) and the true (spatially-variant) paper machine cross-directional process models and requires no further computation on the part of the designer. Closed-loop stability (requirement 2 in Section 2.3) is maintained in an efficient and straightforward manner with this technique, however, the other requirements from Section 2.3 are not considered at this stage.

It was demonstrated in [51] that this technique can also be implemented on a broad class of linear control systems with known plant perturbations. In Section 3.2, the set of transfer matrix models under consideration in this chapter is presented. A straightforward controller perturbation technique, guaranteeing closed-loop stability for the class of systems in question, is given in Section 3.3. The application of the technique to industrial paper machine cross-directional control systems is illustrated in Section 3.4. Another three examples of the use of the presented technique, taken from very different applications, are demonstrated in Section 3.5. In that regard, Section 3.5 strays from the main object of this work - paper machine CD control near the sheet edges - but examines some familiar controller design techniques in terms of the controller perturbation technique from Section 3.3.

3.1 Control Systems with Known Plant Deviations

A control engineer is often faced with implementing a controller for a plant G_P that is different from the plant G_0 for which a feedback controller K_0 has been designed. The deviation of the true plant from its mathematical model can be separated into two categories - unknown and known. While a practical control system will often contain both types of deviations, this chapter focuses on the known deviations.

It is not uncommon in control engineering for the plant model used for controller synthesis to differ from the true plant by a known amount. In many cases, the use of *all* knowledge of a plant model may overly complicate the synthesis of the feedback controller.

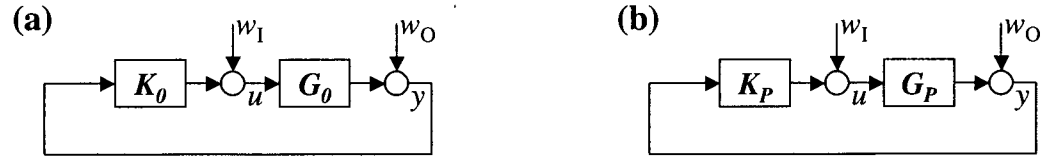

Figure 3.1: (a) Original and (b) modified closed-loop control systems.

Deliberate model simplifications, prior to controller design occur, for example:

- to replace spatially-distributed plant models with more convenient spatially-invariant models [8, 15, 17, 34, 45, 49, 65, 66],
- to eliminate time delay from plant models [58, 59, 60],
- to eliminate the recycle dynamics in certain chemical processes [57, 70],
- to remove complicated high-order dynamics [58],
- to replace a multivariable process model with a diagonal process model in order to facilitate the design of a decentralized controller [54, 58, 75].

Deliberate model approximation is not the only source of known faults in a plant model. Factors whose influence is *potentially* known include:

- failure of actuators or sensors [37, 40, 58, 77],
- multiple models for various operating points [29, 56],
- model changes resulting from re-identification of all or part of the transfer matrix.

While there already exist various control strategies for many of the examples listed above (see, for example, references in [51]), the contribution of this work is a straightforward perturbation technique for the modification of a controller K_0, originally designed for G_0, such that closed-loop stability is guaranteed for the known plant G_P.

3.2 Relationships Between Plant Models

In this section we present the class of transfer matrix models under consideration. We consider relationships between transfer matrix models in six standard configurations taken from [58].

Let the original or nominal plant model be the linear, time-invariant transfer matrix $G_0 \in \mathcal{C}^{m\times n}$. Consider a linear, time-invariant transfer matrix $K_0 \in \mathcal{C}^{n\times m}$ representing

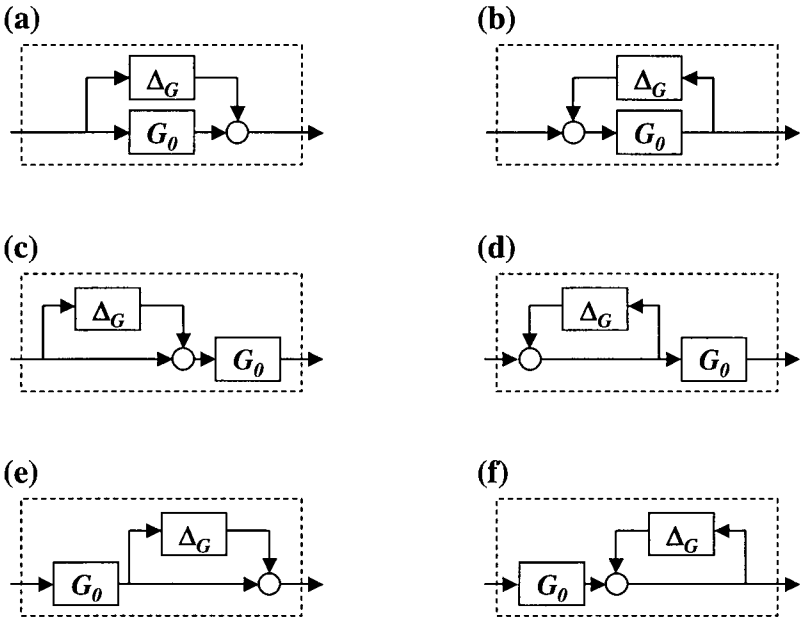

Figure 3.2: Block diagrams for various G_P in terms of G_0 and Δ_G. (a) Additive perturbation, (b) Inverse additive perturbation, (c) Multiplicative input perturbation, (d) Inverse multiplicative input perturbation, (e) Multiplicative output perturbation, (f) Inverse multiplicative output perturbation (compare Figure 8.5 in [58]).

a feedback controller such that the closed-loop system in the configuration illustrated in Figure 3.1a is internally stable.

Now denote a second linear, time-invariant transfer matrix plant model by $G_P \in \mathcal{C}^{m\times n}$ where $G_P \neq G_0$. In general, there are many ways to represent the difference between two matrices, but here we will restrict the study to six standard configurations, illustrated in Figure 3.2:

$$\begin{aligned}
&(a) \quad G_P = G_0 + \Delta_G \\
&(b) \quad G_P = (I - G_0\Delta_G)^{-1}G_0 \\
&(c) \quad G_P = G_0(I + \Delta_G) \\
&(d) \quad G_P = G_0(I - \Delta_G)^{-1} \\
&(e) \quad G_P = (I + \Delta_G)G_0 \\
&(f) \quad G_P = (I - \Delta_G)^{-1}G_0
\end{aligned} \tag{3.1}$$

Although the presentation of Figure 3.2 is reminiscent of the representation of model uncertainty (see for example [58, 76]), for the purposes of this work we will assume full knowledge of the perturbation Δ_G.

The problem at hand is to replace the original feedback controller K_0 with a feedback

controller K_P, resulting in the closed-loop control system illustrated in Figure 3.1b, such that:

1. Internal stability is guaranteed for the closed-loop system defined by K_P and G_P.
2. Modifications to the existing controller K_0 are straightforward and require less work than would a full redesign of K_P for G_P.

Section 3.3 presents results that may be used for modifying the original feedback controller K_0 to achieve a new controller K_P such that the closed-loop system in Figure 3.1b is internally stable.

3.3 Augmentation of Feedback Controllers

In this section we present a controller perturbation technique that allows the straightforward generation of a stabilizing controller K_P for G_P in Figure 3.1b, given a known stabilizing controller K_0 for the plant G_0 in Figure 3.1a.

Theorem 1 (Stability Transfer) *If the system in Figure 3.1a with (G_0, K_0) is internally stable, then the system in Figure 3.1b with (G_P, K_P) is internally stable if Δ_G is stable, $\Delta_K = -\Delta_G$, and*

(a)	$K_P = (I - K_0\Delta_K)^{-1}K_0;$	$G_P = G_0 + \Delta_G$	
(b)	$K_P = K_0 + \Delta_K;$	$G_P = (I - G_0\Delta_G)^{-1}G_0$	
(c)	$K_P = (I - \Delta_K)^{-1}K_0;$	$G_P = G_0(I + \Delta_G)$	*with stable* $(I + \Delta_G)^{-1}$
(d)	$K_P = (I + \Delta_K)K_0;$	$G_P = G_0(I - \Delta_G)^{-1}$	*with stable* $(I - \Delta_G)^{-1}$
(e)	$K_P = K_0(I - \Delta_K)^{-1};$	$G_P = (I + \Delta_G)G_0$	*with stable* $(I + \Delta_G)^{-1}$
(f)	$K_P = K_0(I + \Delta_K);$	$G_P = (I - \Delta_G)^{-1}G_0$	*with stable* $(I - \Delta_G)^{-1}$

Proof: Given in Appendix A.

Remark 1: The only restriction placed on the design of the controller K_0 is that it stabilizes G_0 in Figure 3.1a. Theorem 1 then transfers *only* the stability to the perturbed system in Figure 3.1b. The issue of closed-loop *performance* in either system is not addressed by Theorem 1.

Remark 2: In [71, 72], the nominal plant-controller pair has been written in terms of stable coprime factors as $G_0 = ND^{-1}$ and $K_0 = XY^{-1}$. Subsequently, it has been shown that the family of controllers $K_P = [X + DQ][Y - NQ]^{-1}$ stabilizes the set of perturbed plants $G_P = [N + YS][D - XS]^{-1}$ if and only if the perturbations (S, Q) form a closed-loop stable pair. In light of this result, Theorem 1 is equivalent to providing -

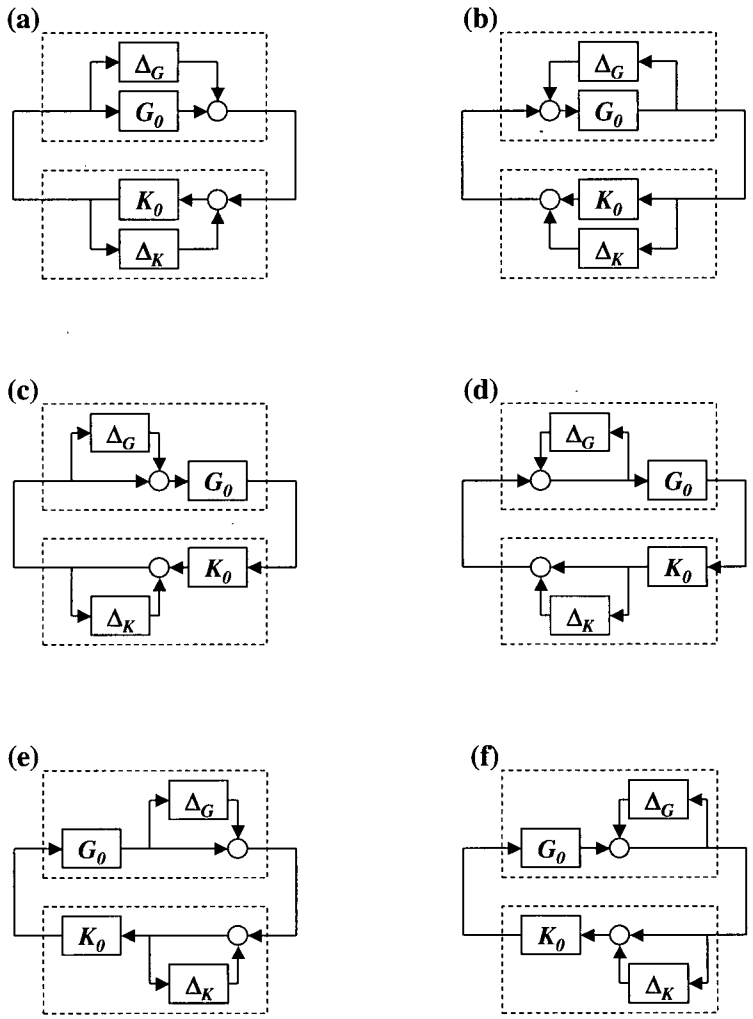

Figure 3.3: Block diagrams indicating the various configurations of G_P and K_P described in Theorem 1.

without any additional computation - a controller perturbation Q that stabilizes the given plant perturbation S for each of the cases (a)-(f). So closed-loop stability is recovered by providing a stabilizing design for the problem in [71, 72] and without the use of the restrictive assumption that (G_P, K_0) is a stable pair as in the double-Youla formulation [3]. On the other hand [3] and [71, 72] provide an additional degree of freedom to allow design for performance, while our proposed technique does not.

Remark 3: The additional requirement on stability of $(I+\Delta_G)^{-1}$ or $(I-\Delta_G)^{-1}$ in the cases (c)-(f) in Theorem 1 is necessary to avoid cancellation of unstable modes between the plant and controller.

Remark 4: Theorem 1 does not necessarily require stability of the transfer matrices G_0, G_P, K_0, or K_P. However the various restrictions on the stability of Δ_G, $(I+\Delta_G)^{-1}$,

and/or $(I - \Delta_G)^{-1}$ may indirectly place stability restrictions on K_P or G_P.

Remark 5: The closed-loop systems corresponding to each of the cases in Theorem 1 are illustrated in Figure 3.3. There is an easily-recognized pattern relating the configuration of K_P (expressed in terms of K_0 and Δ_K) to the configuration of G_P (expressed in terms of G_0 and Δ_G). This duality arises from the fact that the blocks are configured so that for $\Delta_K = -\Delta_G$, the controller perturbation will partially 'cancel' the plant perturbation. As a result, some of the closed-loop transfer functions of the perturbed systems will be identical to the corresponding closed-loop transfer functions of the original systems (see Table 3.1).

As pointed out in Remark 1 above, the issue of closed-loop performance is not addressed by Theorem 1. However, in certain circumstances this technique may also achieve a successful controller design in terms of closed-loop performance. For example, the Smith predictor [54, 59, 60] and the recycle compensator [57, 70] are shown to be special cases of this method that have been applied in industrial situations without a need for further modification. More details about various applications of Theorem 1 can be found in [51] and its references.

Table 3.1: Closed-loop transfer functions in Figure 3.1b for the various configurations of G_P and K_P in Theorem 1.

case	w_O to u $M = (I - KG)^{-1}K$	w_I to y $M = (I - GK)^{-1}G$	w_O to y $M = (I - GK)^{-1}$	w_I to u $M = (I - KG)^{-1}$
(a) $M_P =$	M_0	$[M_0 + \Delta_G(I - K_0G_0)^{-1}]\cdot(I + K_0\Delta_G)$	$(I + \Delta_G K_0)M_0$	$M_0(I + K_0\Delta_G)$
(b) $M_P =$	$[M_0 - \Delta_G(I - G_0K_0)^{-1}]\cdot(I - G_0\Delta_G)$	M_0	$M_0(I - G_0\Delta_G)$	$(I - \Delta_G G_0)M_0$
(c) $M_P =$	$(I + \Delta_G)^{-1}M_0$	$M_0(I + \Delta_G)$	M_0	$(I + \Delta_G)^{-1}M_0(I + \Delta_G)$
(d) $M_P =$	$(I - \Delta_G)M_0$	$M_0(I - \Delta_G)^{-1}$	M_0	$(I - \Delta_G)M_0(I - \Delta_G)^{-1}$
(e) $M_P =$	$M_0(I + \Delta_G)^{-1}$	$(I + \Delta_G)M_0$	$(I + \Delta_G)M_0(I + \Delta_G)^{-1}$	M_0
(f) $M_P =$	$M_0(I - \Delta_G)$	$(I - \Delta_G)^{-1}M_0$	$(I - \Delta_G)^{-1}M_0(I - \Delta_G)$	M_0

3.4 Application of Theorem 1 to CD Control

Let the nominal plant $G_0 \in \mathcal{C}^{n\times n}$ be the idealized CD process model with periodic boundary conditions,

$$G_0 = \frac{z^{-d}}{1 - a_0 z^{-1}}\mathcal{C}(\bar{b}, n) = \frac{z^{-d}}{1 - a_0 z^{-1}}B_c \tag{3.2}$$

and $K_0 \in \mathcal{C}^{n\times n}$ a corresponding spatially-invariant controller obtained by the two-dimensional loop shaping technique and defined with (2.12) and (2.18). Also, let the actual (spatially-variant) CD process model be denoted with $G_P \in \mathcal{C}^{n\times n}$,

$$G_P = \frac{z^{-d}}{1 - a_0 z^{-1}}\mathcal{T}(\bar{b}, n) = \frac{z^{-d}}{1 - a_0 z^{-1}}B_d \tag{3.3}$$

As pointed out earlier, in Section 2.2, the difference between the two plants $\Delta G(z) = G_c(z) - G_d(z) = G_0(z) - G_P(z)$ is the 'ears' of the circulant symmetric matrix $G_0(z)$, given with (2.19).

Based on Theorem 1, a stabilizing controller for the actual CD process model with Dirichlet boundary conditions G_P is given by $K_P = (I - K_0\Delta_K)^{-1}K_0$ configured as in Figure 3.3a with $\Delta_K = -\Delta_G = \Delta G(z)$ in (2.19). Such a modified controller may be represented as,

$$u = K_0\,(y + \Delta_K \cdot u) = K_0\,(y + \Delta G \cdot u) \tag{3.4}$$

Note the necessary *structure* of a stabilizing controller for G_P. In general, the controller K_P is an $n \times n$ transfer matrix with n^2 elements. However, a consequence of Theorem 1 is that, if one begins with a stabilizing spatially-invariant controller $K_0 = K_c(z)$ for a spatially-invariant process model $G_0 = G_c(z)$, then the closed-loop with the actual (spatially-variant) CD process model may be stabilized with an $n \times n$ transfer matrix Δ_K in (3.4) with only $l_b \cdot (l_b + 1)$ nonzero elements, (where $l_b \ll n$ is the process spatial response parameter in (2.11)) - independent of the large size of the original problem.

Figure 3.4 illustrates the location of non-zero entries in G_P, G_0, and $\Delta_G = \Delta G(z)$ for a typical industrial example with $n = 54$ actuators and the process spatial response parameter $l_b = 7$. The brute-force design of a multivariable controller would require the synthesis of all $n^2 = 2916$ transfer matrix elements in K_P. However if one begins with the controller K_0, then one may achieve a stabilizing controller via Δ_K in (3.4) by designing only $l \cdot (l + 1) = 56$ transfer matrix elements of Δ_K - fewer than 2% of the full design.

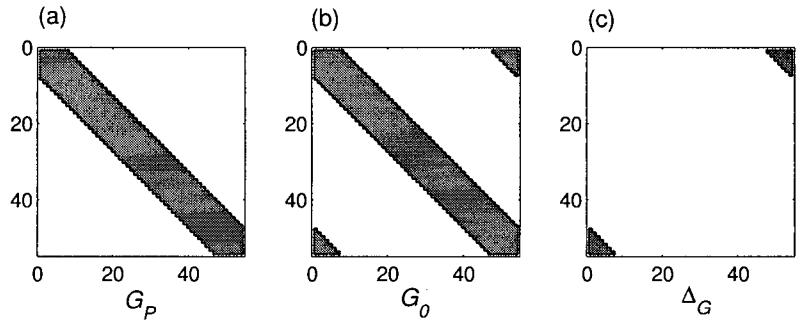

Figure 3.4: Position of the non-zero elements of: (a) the Toeplitz matrix $G_0 = G_d(z)$; (b) the circulant symmetric matrix $G_P = G_c(z)$; and (c) the difference between the two: $\Delta_G = -\Delta G(z) = G_d(z) - G_c(z)$.

Paper machine cross-directional control system with the actual (spatially-variant) pro-

cess model $G_d(z)$ in (2.10)–(2.11) and the initially designed spatially-invariant controller $K_0 = [I - D_c z^{-1}]D_c \cdot C_c \cdot c(z)$ modified based on the results of Theorem 1, is illustrated in Figure 3.5.

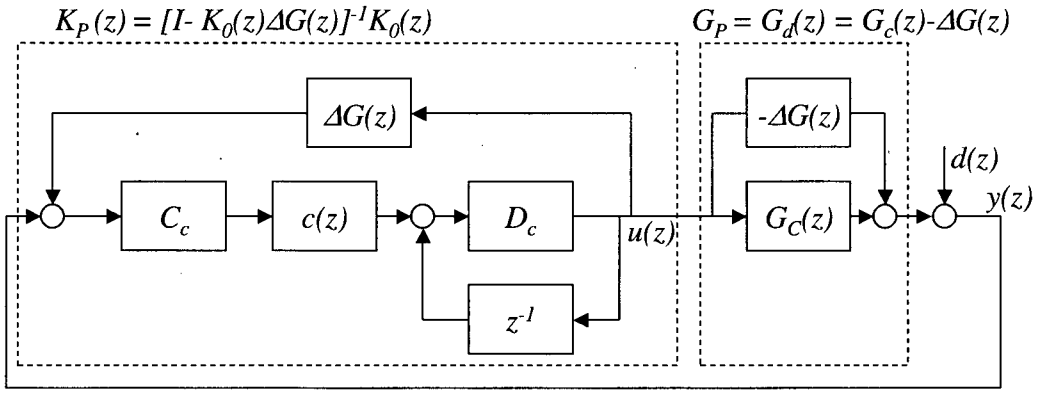

Figure 3.5: Paper machine cross-directional control system, initially computed with the two-dimensional loop shaping technique resulting in a spatially-invariant process and controller models $G_c(z), C_c, D_c$, stabilized by the use of Theorem 1.

Even as the required spatially-invariant controller perturbation is straightforward and the resulting closed-loop system stability guaranteed by Theorem 1, the other three requirements from Section 2.3 are not directly taken into account with this approach. However, the issue of performance of CD control systems based on this approach will be briefly revisited in Section 4.3.2 in Chapter 4.

3.5 Other Applications of Theorem 1

This section will stray from the main topic of this work (paper machine CD control), as three additional examples of the use of Theorem 1, drawn from very different applications, are presented. An application in the case of actuator and/or sensor failure in a multivariable control system is presented in Section 3.5.1. Finally, two familiar industrial controller design techniques - the Smith predictor and the recycle compensator - are examined in terms of Theorem 1 in Sections 3.5.2 and 3.5.3.

3.5.1 Actuator and Sensor Failures

An application in which the deviation of the true plant from the nominal plant model may potentially be known arises in the study of closed-loop control systems with actuator and/or sensor failures. If the failure is diagnosed and the effect is known, then Theorem

1 provides a simple technique that may be used to reconfigure the controller to guarantee closed-loop stability. For example, the so called fault-tolerant sensor configuration (see Figure 7b in [40]) is equivalent to the modifications illustrated in Theorem 1 (case (a)).

Consider a linear open-loop stable transfer matrix plant model G_0 and a feedback controller K_0 forming an internally stable system in Figure 3.1a. Now consider the same control system but with failed sensors and/or actuators. Let $\mathcal{I}$ denote the set of indices of failed sensors. Let $\mathcal{J}$ denote the set of indices of failed actuators. The plant with failed sensors and actuators may be modelled using an additive matrix perturbation to the original model G_0:

$$\begin{aligned} G_P &= G_0 + \Delta_G \,, \\ \Delta_G(i,j) &:= \begin{cases} -G_0(i,j), & i \in \mathcal{I} \text{ or } j \in \mathcal{J} \\ 0, & \text{otherwise} \end{cases} \end{aligned} \tag{3.5}$$

Figure 3.6 illustrates this for a plant with 20 sensors and 20 actuators where the 7^{th} sensor has failed. In other words, $\mathcal{I} = \{7\}$ and $\mathcal{J} = \emptyset$ (the empty set) in (3.5). A failed actuator would result in a column of non-zero entries in Δ_G.

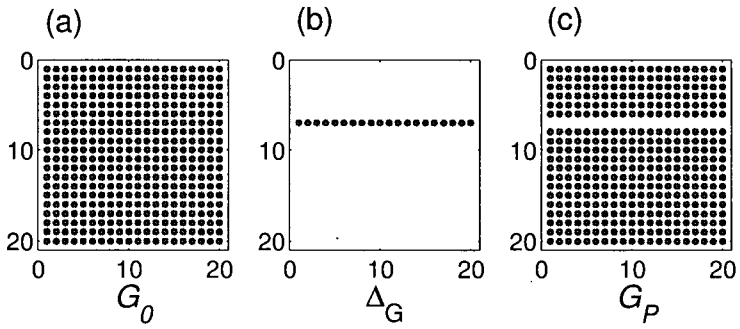

Figure 3.6: Location of the non-zero elements of (a) the nominal plant model G_0, (b) the additive perturbation Δ_G due to failure of the 7^{th} sensor, and (c) the corresponding transfer matrix model G_P.

Closed-loop stability is not guaranteed in general for the plant with actuator and/or sensor failures G_P in (3.5) and the original controller K_0. However, modification of the controller as in Figure 3.3a

$$K_P = (I - K_0\Delta_K)^{-1}K_0, \tag{3.6}$$

and setting $\Delta_K = -\Delta_G$ in (3.5) leads to an internally stable closed-loop (G_P, K_P) if Δ_G is stable according to Theorem 1. In the case of sensor failure, effectively replacing the

failed sensor signals with their modelled response, so that the control law is modified to $u = K_0(y - \Delta_G \cdot u)$.

Note that while no guarantees are provided for closed-loop performance, Theorem 1 allows the recovery of closed-loop stability without the need to perform any new controller synthesis. A fact that makes it attractive in practical fault-tolerant schemes such as in [40].

3.5.2 Smith Predictor

One of the earliest examples of the intentional simplification of the plant model for controller design is the well-known Smith predictor controller. The controller structure was proposed in 1950's by Otto Smith [59, 60] in order to improve control of the plants with dead-time dynamics,

$$g_P(s) = g_f(s)e^{-\theta s} \tag{3.7}$$

where $g_f(s)$ is a finite-dimensional transfer function.

The basic idea of the Smith predictor scheme is initially to design a controller $k_0(s)$ for the plant $g_f(s)$ in (3.7) with no delay, and afterwards modify the controller to account for the delay in $g_P(s)$ in (3.7). A detailed analysis of the Smith predictor controller characteristics, as well as a modern interpretation of this design technique (via the internal model control principle), can be found in [29, 54]. The results in Section 3.3 can be interpreted from an IMC standpoint, and used with $g_P(s)$ in (3.7) present an alternative derivation of the Smith predictor.

First, the transfer function $g_P(s)$ in (3.7) may be factored into an additive perturbation as $g_P(s) = g_0(s) + \Delta_g(s)$ with

$$g_0(s) = g_f(s), \quad \text{and} \quad \Delta_g(s) = g_f(s)(e^{-\theta s} - 1) \tag{3.8}$$

where $g_0(s)$ is a finite-dimensional transfer function and $\Delta_g(s)$ contains the deadtime of the original transfer function $g_P(s)$ in (3.7). Then using a typically low-order stabilizing controller $k_0(s)$ for the stable transfer function $g_0(s)$ in (3.8), applying Theorem 1 for the configuration in Figure 3.3a yields the controller,

$$k_P(s) = \frac{k_0(s)}{1 - k_0(s)\Delta_k(s)}, \quad \Delta_k(s) = g_0(s)(e^{-\theta s} - 1) \tag{3.9}$$

and is equivalent to the Smith predictor illustrated in Figure 3.7. (The difference in sign where $\Delta_K(s) = \Delta_G$ in (3.9) is due to negative feedback in Figure 3.7, but $\Delta_K = -\Delta_G$ in Theorem 1, due to the positive feedback.)

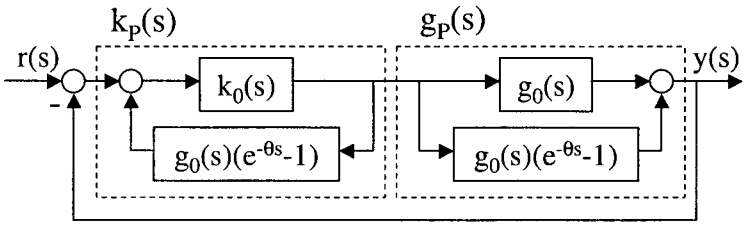

Figure 3.7: Smith-predictor design for plants with pure time delay (compare with Figure 3.3a).

A word regarding closed-loop performance is needed here. While Theorem 1 was not necessarily developed for use as a controller design technique, it is well known that the Smith predictor can be designed to provide acceptable closed-loop performance as a dead-time compensator. In general, the modification of $k_0(s)$ to $k_P(s)$ with the configuration in Figure 3.3a or Figure 3.7 will move the poles of the controller and potentially alter the closed-loop performance. For example, if $k_0(s)$ is designed with integral action, then the perturbation configuration $k_P(s)$ in Figure 3.3a could potentially eliminate it. However, the Smith predictor in Figure 3.7 is a special case since the perturbation $|\Delta_G(j\omega)| \to 0$ as $\omega \to 0$ in (3.8) meaning that $g_P(j\omega) \to g_0(j\omega)$ and $k_P(j\omega) \to k_0(j\omega)$ as $\omega \to 0$. Thus the behaviour of the perturbed loop approaches that of the nominal loop at low frequencies important for performance.

As a final comment, it is noted in [54] that – internal stability and steady-state performance notwithstanding – the design of the nominal controller $k_0(s)$ is important for closed-loop performance for $\omega > 0$ where $|\Delta_G(j\omega)| \neq 0$ in (3.8). Incautious designs of $k_0(s)$ that disregard the delay in $g_P(s)$ in (3.7) will not lead to good performance of the Smith predictor system in Figure 3.7.

3.5.3 Recycle Compensator

Recycle streams in chemical industries are used to feed back some of the process output for further processing [43]. For economical and environmental reasons (e.g. saving energy and materials), plants with recycle streams are becoming more common [57]. It has been shown in [55] that the overall dynamics of such plants can be very different from those of plants having no recycle streams and should be taken into account in the controller design procedure.

A chemical process with a recycle stream can be described in terms of a plant model with an inverse additive perturbation given in Figure 3.2b, where $g_0(s)$ and $\Delta_g(s)$ are the

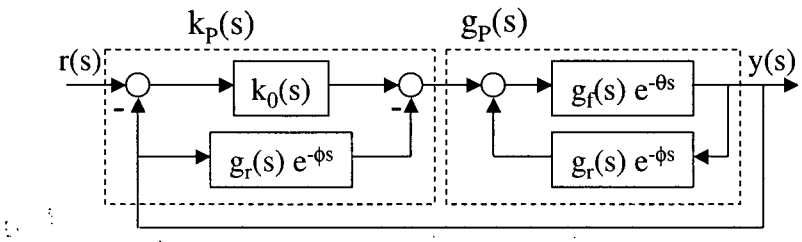

Figure 3.8: Recycle compensator for plants with recycle dynamics (compare with Figure 3.3b).

models of the process forward path and recycle path respectively,

$$g_0(s) = g_f(s)e^{-\theta s}, \quad \text{and} \quad \Delta_g(s) = g_r(s)e^{-\phi s} \tag{3.10}$$

and $g_f(s)$ where $g_r(s)$ are stable (often first-order) transfer functions. One of the controller design procedures for the processes with recycle streams, explained in [43, 55, 57], can be presented in terms of the results given in Section 3.3. First one synthesizes a stabilizing controller $k_0(s)$ for the forward path $g_0(s)$ in (3.10) (possibly using the Smith predictor of Section 3.5.2 above). Since $\Delta_g(s)$, as defined in (3.10), is a stable transfer function, the controller modification procedure outlined in Theorem 1 (case (b)) and illustrated in Figure 3.3b is used in the second step. A block diagram of the closed-loop control system with a recycle compensator is illustrated in Figure 3.8.

As in the case of Smith predictor, the controller modification is $\Delta_k = \Delta_g$ (as opposed to $\Delta_k = -\Delta_g$ in Theorem 1) due to the negative feedback being used in the recycle compensation in Figure 3.8.

As with the Smith predictor, the recycle compensator will typically be used as illustrated in Figure 3.8 without further modification due to the fact that for this particular configuration the complementary sensitivity function is unchanged by the perturbations,

$$[1 + g_P k_P]^{-1} g_P k_P = [1 + g_0 k_0]^{-1} g_0 k_0 \tag{3.11}$$

and thus the nominal performance is recovered.

3.6 Summary

A novel and straightforward modification technique with which a controller that stabilizes one plant may be modified so that it stabilizes a second (related) plant has been presented in this chapter. In addition to paper machine CD control, the presented technique can also be implemented on a broad class of multivariable linear time-invariant control systems.

Some of the well-known industrial controller design methods have been shown to be special cases of the presented technique.

Although the technique guarantees only the resulting system closed-loop stability, in certain industrial applications (e.g. Smith predictor and recycle compensator), it does achieve a successful design in terms of closed-loop performance as well.

In terms of CD controllers initially designed under the (idealized) spatial-invariance assumption, a developed technique is guaranteed to stabilize a true (spatially-variant) process models in a straightforward and efficient manner. However, the other requirements (closed-loop performance and robustness), specified in Chapter 2, are not directly considered with this approach.

Chapter 4

Open-Loop Approach to CD Controller Modifications

The effects that arise in paper machine CD control systems near spatial domain boundaries (see Figure 1.9 in Introduction) have qualitative similarities with the Gibbs phenomenon encountered in Fourier analysis. The Gibbs effect is a well-known consequence of approximating a discontinuous function with a truncated Fourier series. Unavoidably, this reconstruction exhibits overshoots and undershoots around the point(s) of discontinuity. Even though a truncated Fourier series is equivalent to filtering a signal with an ideal low-pass filter, overshoot and undershoot near discontinuities are evident in all forms of signal filtering. As described in Chapter 2, the paper machine CD controllers are essentially spatial and temporal low-pass filters. Also, the paper sheet edges are process spatial domain discontinuities.

Considering the above similarities, the methods used for reducing the Gibbs phenomenon [41] are used as an inspiration for the CD control modifications proposed in this chapter. An overview of Gibbs phenomenon and its relation to paper machine cross-directional control near the sheet edges is presented in Section 4.1. Proposed CD controller modifications are given in Section 4.2, and a closed-loop simulation example in Section 4.3.

The proposed modifications meet the first requirement in Section 2.3 (the requirement for static modifications of the existing industrial CD control law). The second requirement (closed-loop stability) is subsequently checked and confirmed. The last two requirements from Section 2.3 are not addressed with the approach presented in this chapter.

4.1 Gibbs Phenomenon and Spatial Filtering

The Gibbs phenomenon is an effect of a special case of discontinuous signal filtering that has been very well studied. It occurs when a discontinuous input signal is filtered with the ideal low-pass filter, which has an impulse response in the original domain (e.g. 1-D spatial domain x) as: $sinc(x) = \frac{\sin(x)}{x}$. The ideal low-pass filters cannot be implemented in practice as they are infinite order filters. The infinite order constraint would be impossible to satisfy for either temporal or spatial filters.

To illustrate the Gibbs phenomenon, consider the original signal given as a function

$f(x)$, which is defined as:

$$f(x) = \begin{cases} 1 & \text{for } 0.25 < x < 0.75 \\ 0 & \text{otherwise} \end{cases} \tag{4.1}$$

The function $f(x)$ (shown in Figures 4.1a and 4.1b with dotted lines) obviously has two points of discontinuity, at $x = 0.25$ and $x = 0.75$. After modifying the Fourier coefficients of the original signal $f(x)$ by setting high frequency coefficients to zero while keeping the low frequency coefficients unchanged (which is equivalent to filtering $f(x)$ with the ideal low-pass filter) and doing inverse Fourier transform with such modified Fourier coefficients, the modified signal $f_1(x)$ is obtained. The signal $f_1(x)$ is shown in Figure 4.1a with full line. The oscillating error effects of the original signal discontinuities, at points $x = 0.25$ and $x = 0.75$, are clearly seen in Figure 4.1a. This error is called Gibbs phenomenon.

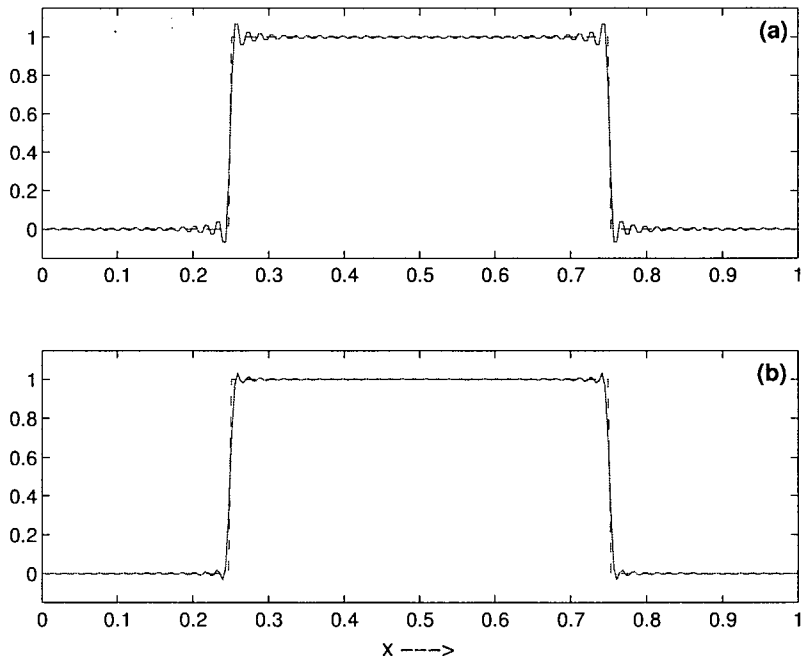

Figure 4.1: Traditional illustration of Gibbs effect in Fourier analysis (a) and its reduction achieved by using Lanczos filter (b).

Various methods for reducing and eliminating the Gibbs phenomenon are presented in [41] and its references. One of the proposed methods is based on the Lanczos filtering. In this method, the modified signal $f_1(x)$ (a signal obtained by setting high frequency Fourier coefficients of the original discontinuous signal $f(x)$ to zero) is further filtered with a Lanczos filter. The Lanczos filter is a low-pass filter whose frequency response is

defined by the $sinc(\omega)$ function in frequency domain. More details on Lanczos filter, shape of its magnitude response, and its use in this work are given in Section 4.3. The original signal $f(x)$ and modified signal filtered with Lanczos filter $\tilde{f}_1(x)$ are given in Figure 4.1b. By comparing the signals $f_1(x)$ and $\tilde{f}_1(x)$ given in Figures 4.1a and 4.1b respectively, it can clearly be seen that Lanczos filter has substantially reduced overshoots and undershoots around points of discontinuity $x = 0.25$ and $x = 0.75$.

Paper machine CD controllers act as spatial and temporal low-pass filters and the paper sheet edges can be understood as the points of discontinuity. Taking this into account, the analogy between the Gibbs phenomenon (briefly illustrated above) and spatial filtering as realized by CD controllers around the edges can be observed. As mentioned earlier, paper machine CD control systems exhibit overshoots and undershoots when implemented near the sheet edges, which is also in accordance with the Gibbs phenomenon.

4.2 CD Control Modifications Near the Boundaries

As pointed out in Section 2.2, two-dimensional loop shaping technique [62, 66] typically produces a controller $K(z)$ in (2.12) with the periodic boundary conditions (2.18) and coefficients $\overline{d} > 0$. Theorem 2 states that, in such a case, replacing the periodic boundary conditions with the corresponding Dirichlet boundary conditions, will not destabilize the controller.

Theorem 2 *The controller $K(z)$ given with (2.12)-(2.15) is stable with $C_d = \mathcal{T}(\overline{c}, n)$ and $D_d = \mathcal{T}(\overline{d}, n)$ if $K(z)$ is stable with $C_c = \mathcal{C}(\overline{c}, n)$ and $D_c = \mathcal{C}(\overline{d}, n)$ and $\overline{d} \geq 0$ with $d_{-j} = d_j$ for $j = 1, \cdots, l_d$.*

Proof. A necessary and sufficient condition for controller stability (marginal stability) is that all the eigenvalues of D in (2.12) are in the open (closed) unit circle. The spectral radius of the matrix corresponding to periodic BCs is given as [36]: $\rho(D_c) = d_0 + \sum_{p=1}^{l_d} 2d_p \leq 1$. The eigenvalues of the equivalent Toeplitz symmetric matrix D_d (corresponding to Dirichlet BCs) are bounded [36] by a function:

$$f(\lambda) = d_0 + \sum_{p=1}^{l_d} 2d_p \cos(p\lambda), \qquad \lambda \in [0, 2\pi)$$

Finally, $\rho(D_d) \leq d_0 + \sum_{p=1}^{l_d} 2d_p = \rho(D_c) \leq 1.\Diamond$

Consider further modifying the boundary conditions of D_d in Theorem 2 by multiplying it by a real $n \times n$ matrix,

$$D_f = F \cdot D_d \quad , \quad F = \begin{bmatrix} f_1 & & \\ & I & \\ & & f_2 \end{bmatrix} \tag{4.2}$$

where f_1 and f_2 are each $n_f \times n_f$ real constant matrices and I is the identity matrix of order $n - 2 \cdot n_f$. Note that each of the matrices D_f, D_d, and D_c has elements defined by (2.14), the only difference being those elements δd_{ij} in the first and last $n_{D1} = n_f$ rows that define the implicit boundary layer.

The proposed design of the matrices f_1 and f_2 in (4.2) is inspired by research on the Gibbs phenomenon. To mitigate the effect of the Gibbs ripples, a straightforward technique is to locally filter the jump discontinuities for smoothness.

Approximating a function by a truncated Fourier series is equivalent to performing a convolution of the function with an ideal low pass filter (usually referred to as a *'sinc'* function). However, overshoot and undershoot are not limited to *sinc* functions and may occur in other types of non-ideal filtering.

Thus we propose to design the matrices f_1 and f_2 in (4.2) to provide local low-pass filtering that mitigates the effect of the transition induced by the implicit boundary conditions. The following Theorem provides a conservative result for directing the design of the matrices f_1 and f_2 in (4.2) such that controller stability is preserved.

Theorem 3 *If the controller $K(z)$ given with (2.12)-(2.15) is stable with $C_d = \mathcal{T}(\bar{c}, n)$ and $D_d = \mathcal{T}(\bar{d}, n)$ (with $d_{-j} = d_j$ for $j = 1, \cdots, l_d$) then it is stable with $D_f = F \cdot D_d$, if $\overline{\sigma}(F) \leq 1$, where $\overline{\sigma}(F)$ is the maximum singular value of F.*

Proof. For the symmetric matrix D_d we have

$$\rho(FD_d) \leq \overline{\sigma}(FD_d) \leq \overline{\sigma}(F)\overline{\sigma}(D_d) = \overline{\sigma}(F)\rho(D_d) \leq 1$$

where the final inequality is implied by stability of $K(z)$ with $D = D_d$.$\diamondsuit$

Note that for the block-diagonal matrix F in (4.2), we need only to ensure that $\overline{\sigma}(f_1) \leq 1$ and $\overline{\sigma}(f_2) \leq 1$ for the $n_f \times n_f$ matrices to satisfy Theorem 3. This can lead to a much easier calculation if $n_f \ll n$. This is fortunate since the number of actuators is potentially as large as $n = 300$ for some cross-directional control systems.

It is not difficult to see from (4.2) and (2.20) that the above proposed modifications can be represented with the controller matrices' additive perturbations δC and δD in

(2.21)–(2.22) defined as,

$$\begin{aligned} \delta C &= -\Delta C, \\ \delta D &= -\Delta D + (F - I) \cdot D_d, \end{aligned} \tag{4.3}$$

where ΔC and ΔD are the 'ears' of the controller circulant symmetric matrices, defined in (2.20), matrix $F \in \Re^{n \times n}$ as given in (4.2), and D_d a controller's matrix (spatial filter) D in (2.12), corresponding to Dirichlet boundary conditions.

The next section contains an example where a standard finite impulse response (FIR) filter is used in the design of f_1 and f_2 in (4.2) to modify the spatial boundary conditions of a cross-directional controller $K(z)$ in (2.12).

4.3 Simulation Example

4.3.1 Edge Filter Design

Based on the techniques used for the reduction and elimination of the Gibbs phenomenon presented in [41], and the theorems given in Section 4.2, a modification of CD controller boundary conditions is proposed. Modifying the control law includes smoothing the control signal around paper machine edges with a low-pass filter computed based on the techniques presented in [41]. As will be shown below, the proposed control law modifications preserve controller stability while also maintaining closed-loop stability. Controller stability is proved using Theorem 3 in Section 4.2, and closed loop stability is checked and confirmed. It will also be shown that in contrast to the original (unmodified) control law (computed implementing reflection edge padding, as defined in Section 2.1), the actuator array obtained with a modified control law does not contain high spatial frequency content. The gradual development and buildup of the high spatial frequency content in the actuator array often leads to control system instability in CD control applications.

The smoothing filter, proposed here, is based on the Lanczos filters [41], used for the reduction of Gibbs phenomenon exhibited in truncated Fourier series. The original Fourier series of a signal $f(x)$, with discontinuities, is given as:

$$f_n(x) = a_0 + \sum_{k=1}^{n} [a_k \cos(kx) + b_k \sin(kx)], \tag{4.4}$$

where a_k and b_k are the Fourier coefficients of the signal, and is modified as:

$$\tilde{f}_n(x) = a_0 + \sum_{k=1}^{n} \frac{\sin(k\pi/n)}{k\pi/n} [a_k \cos(kx) + b_k \sin(kx)] \tag{4.5}$$

The factor $\zeta_k = \frac{\sin(k\pi/n)}{k\pi/n}$ in (4.5) has a smoothing influence on the Fourier series representation [41] and reduces the Gibbs effect exhibited at signal discontinuities. This was illustrated in Section 4.1 with the example shown in Figures 4.1a and 4.1b. It is also interesting to notice that the filter ζ_k can be cascaded for even better convergence of the series (i.e. smaller overshoots and undershoots around discontinuities). However, in that case, the transition of such a representation from one level to the other around discontinuity is less sharp [41]. Using this factor m times simply means using ζ_k^m instead of ζ_k in (4.5). In the example shown in Figures 4.1a and 4.1b, in Section 4.1, ζ_k^2 was used.

A finite impulse response (FIR) digital filter that is equivalent to the above Lanczos filter with a smoothing factor ζ_k, has been designed using MATLAB function *firls* [47]. Based on the Lanczos filter used for the Fourier series in [41] and shown in (4.5), the target and achieved (using the above mentioned MATLAB function) frequency responses are shown in Figure 4.2. The frequency response, shown in Figure 4.2 with

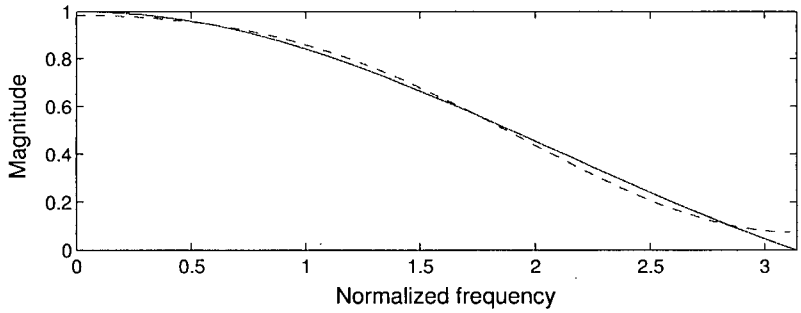

Figure 4.2: Desired (full line) and achieved (dotted line) frequency responses

dotted line, is the least square approximation to the Lanczos filter and has been obtained with a symmetric fourth order FIR filter whose impulse response coefficients are $[h_0, h_1, h_2, h_3, h_4] = [h_0, h_1, h_2, h_1, h_0] = [-0.0306, 0.2149, 0.6148, 0.2149, -0.0306]$. Based

on this, the edge filtering matrix H is defined as follows:

$$\begin{bmatrix}
h_2 & h_1 & h_0 & 0 & 0 & 0 & 0 & \dots & 0 & & & \dots & & & 0 \\
h_1 & h_2 & h_1 & h_0 & 0 & 0 & 0 & \dots & 0 & & & \dots & & & 0 \\
h_0 & h_1 & h_2 & h_1 & h_0 & 0 & 0 & \dots & 0 & & & \dots & & & 0 \\
0 & h_0 & h_1 & h_2 & h_1 & h_0 & 0 & \dots & 0 & & & \dots & & & 0 \\
0 & 0 & 0 & 0 & 1 & 0 & 0 & \dots & 0 & & & \dots & & & 0 \\
0 & 0 & 0 & 0 & 0 & 1 & 0 & \dots & 0 & & & \dots & & & 0 \\
0 & 0 & 0 & 0 & 0 & 0 & 1 & \dots & 0 & & & \dots & & & 0 \\
\vdots & & & & & & \vdots & \ddots & \vdots & & & & & & \vdots \\
0 & & & \dots & & & 0 & \dots & 1 & 0 & 0 & 0 & 0 & 0 & 0 \\
0 & & & \dots & & & 0 & \dots & 0 & 1 & 0 & 0 & 0 & 0 & 0 \\
0 & & & \dots & & & 0 & \dots & 0 & 0 & 1 & 0 & 0 & 0 & 0 \\
0 & & & \dots & & & 0 & \dots & 0 & h_0 & h_1 & h_2 & h_1 & h_0 & 0 \\
0 & & & \dots & & & 0 & \dots & 0 & 0 & h_0 & h_1 & h_2 & h_1 & h_0 \\
0 & & & \dots & & & 0 & \dots & 0 & 0 & 0 & h_0 & h_1 & h_2 & h_1 \\
0 & & & \dots & & & 0 & \dots & 0 & 0 & 0 & 0 & h_0 & h_1 & h_2
\end{bmatrix} = \begin{bmatrix} H_1 & & \\ & I & \\ & & H_2 \end{bmatrix} \quad (4.6)$$

which can be written in a block diagonal form as $H = diag(H_1, I, H_2)$. It is important to notice that in order to obtain a block-diagonal structure, in addition to the matrix rows on which edge filtering is being implemented, two additional rows (because there are two non-zero off-diagonal elements in H_1 and H_2) are being included in blocks H_1 and H_2. Also, the block H_2 is obtained just by flipping the block H_1 twice, first its rows and then its columns.

4.3.2 Closed-Loop Simulations

The process model and feedback controller, used in this chapter, were obtained from an industrial paper machine. This particular system was described in detail in [64]. An array of $n = 54$ slice lip actuators is used to control the basis weight profile of a sheet of light weight 'telephone directory grade' paper. The parameters of the process model in (2.10)–(2.11) were identified using software described in [30, 32] as $l_b = 7$ and

$$\begin{aligned} \{b_0, b_1, ..., b_7\} &= \{0.0713, 0.0337, -0.0167, -0.0200, -0.0050, 0.0006, 0.0005, 0.0001\} \\ a_0 &= 0.8311 \quad , \quad d = 3 \end{aligned}$$

The feedback controller $K(z)$ in (2.12)–(2.15) is designed using the two-dimensional loop shaping technique [62, 66]. We first replace the Dirichlet boundary conditions of the

Coeffs. δd_{ij} in (2.14) with $n_d = 3$ and reflective BCs		
$\delta d_{11} = d_0 + 2(d_1 + d_2 + d_3)$	$\delta d_{12} = 0$	$\delta d_{13} = 0$
$\delta d_{21} = d_1 + 2(d_2 + d_3)$	$\delta d_{22} = d_0 - d_2$	$\delta d_{23} = d_1 - d_3$
$\delta d_{31} = d_2 + 2d_3$	$\delta d_{32} = d_1 - d_3$	$\delta d_{33} = 0$

Table 4.1: Boundary layer coefficients of the controller matrix D in case of reflective boundary conditions and $\overline{d} = [d_0, \cdots, d_3]$, $d_{-j} = d_j$ for $j = 1, 2, 3$.

process $B_d = \mathcal{T}(\overline{b}, 54)$, with a model using periodic boundary conditions $B_c = \mathcal{C}(\overline{b}, 54)$, then the controller matrices $C_c = \mathcal{C}(\overline{c}, 54)$ and $D_c = \mathcal{C}(\overline{d}, 54)$ with $l_c = 5$ and $l_d = 3$ with

$$\begin{aligned} \{c_0, c_1, ..., c_5\} &= \{-10.4708, -3.5297, 1.4841, -0.0042, 0.0017, 0.0006\} \\ \{d_0, d_1, d_2, d_3\} &= \{0.9860, 0.0046, 0.0020, 0.0004\} \end{aligned}$$

The parameters of the Dahlin controller $c(z)$ in (2.12) are also produced by the design, but are not central to the spatial boundary condition issue and may be found in [64].

The current industrial practice for modifying the controller coefficients is to replace the periodic boundary conditions with reflection conditions as given in Table 4.1.

The proposed design technique involves first replacing the periodic boundary conditions with Dirichlet conditions $D = \mathcal{T}(\overline{d}, 54)$, according to Theorem 2. Next, a matrix F in (4.2) is designed for further modification of the control near the sheet edges. As discussed earlier, the submatrices f_1 and f_2 in (4.2) are synthesized based on a finite impulse response (FIR) digital filter, computed as an approximation to the Lanczos filter. The resulting symmetric fourth order FIR filter has impulse response coefficients $[\delta f_2, \delta f_1, \delta f_0, \delta f_1, \delta f_2] = [-0.0306, 0.2149, 0.6148, 0.2149, -0.0306]$. The matrices f_1 and f_2 with $n_f = 5$, in (4.2), are then given by:

$$f_1 = 0.9595 \cdot \begin{bmatrix} \delta f_0 & \delta f_1 & \delta f_2 & 0 & 0 \\ \delta f_1 & \delta f_0 & \delta f_1 & \delta f_2 & 0 \\ \delta f_2 & \delta f_1 & \delta f_0 & \delta f_1 & \delta f_2 \\ 0 & 0 & 0 & 1 & 0 \\ 0 & 0 & 0 & 0 & 1 \end{bmatrix}, \quad f_2 = 0.9595 \cdot \begin{bmatrix} 1 & 0 & 0 & 0 & 0 \\ 0 & 1 & 0 & 0 & 0 \\ \delta f_2 & \delta f_1 & \delta f_0 & \delta f_1 & \delta f_2 \\ 0 & \delta f_2 & \delta f_1 & \delta f_0 & \delta f_1 \\ 0 & 0 & \delta f_2 & \delta f_1 & \delta f_0 \end{bmatrix} \tag{4.7}$$

The coefficient 0.9595 in (4.7) has been introduced in order to satisfy the requirement of Theorem 3 ($\overline{\sigma}(F) \leq 1$). As a result, the stability of the controller with the matrix D_f as defined in (4.2)–(4.7) is guaranteed by Theorem 3.

Although the proposed design is mainly concerned with stability of the controller, we will present simulation results of the closed-loop behaviour. In order to compare the

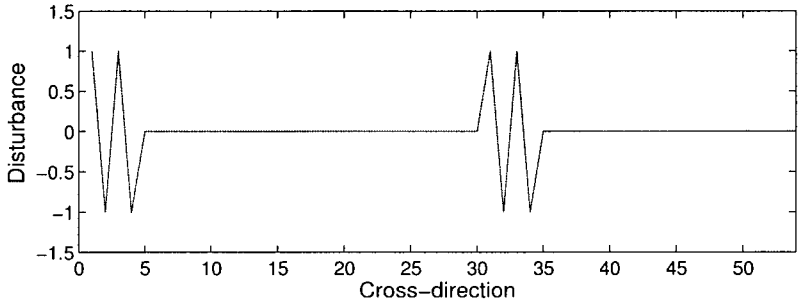

Figure 4.3: Process output disturbance (at zero temporal frequency $\omega = 0$).

standard industrial approach with the proposed design, closed-loop simulations have been performed with the steady state process output disturbance, $d(z)$ in (2.9), as shown in Figure 4.3. The disturbance has been constructed to allow comparison of the closed-loop performance at the sheet edges and also away from the spatial boundaries. The same localized disturbance is introduced at the edge and also near the middle of the sheet, as illustrated in Figure 4.3.

The closed loop simulation results are shown in Figures 4.4 and 4.5. Figure 4.4 illustrates the closed-loop steady state process output and actuator profiles obtained with controller $K(z)$ using the reflection boundary conditions given in Table 4.1. It can be seen that control signal at the edges has significant high frequency content with maximum and minimum values varying between -4.85 and 4.4. At the same time, the control signal away from the edges has significantly smaller high frequency component with the maximum and minimum values varying between -2.1 and 2.1. Such actuator profile at the edges would be unacceptable in real life paper machine CD control systems.

In Figure 4.5, the steady state values of the process output and control signal are shown in case when the controller using D_f matrix, in (4.2)–(4.7), is used. Compared with the results achieved using reflective boundary conditions, the control is significantly less active at the sheet edges while, as expected, the performance away from the edges is unchanged. From Figure 4.5, it can be seen that the proposed control modifications at the edges result in the less active (more conservative) control than the control away from the edges. Figure 4.4 illustrates that the control designed with reflective boundary conditions is more active at the sheet edges, indicating a reduced robust stability margin compared to the original design. However, the obtained control signal at the edges is significantly more acceptable than the signal obtained using the current industrial practice (see Table 4.2 below). At the end of this chapter, the approach to modifying CD control law near spatial domain boundaries developed in Chapter 3 is briefly revisited. As pointed out earlier, the approach to modifying CD control developed in Chapter 3 (detailed in Section 3.4) guarantees only the resulting system closed-loop stability. However, for comparison

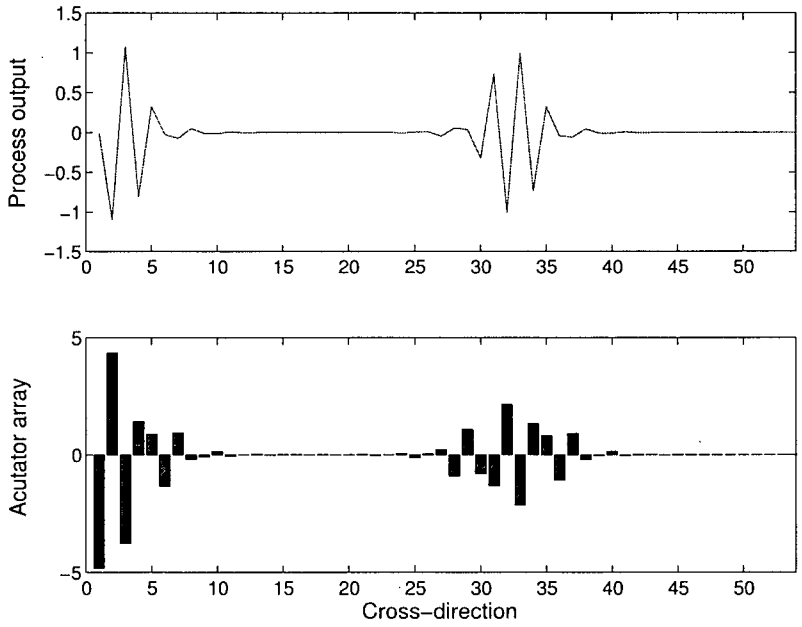

Figure 4.4: Steady state process output and actuator array in case of the reflective boundary conditions in Table 4.1.

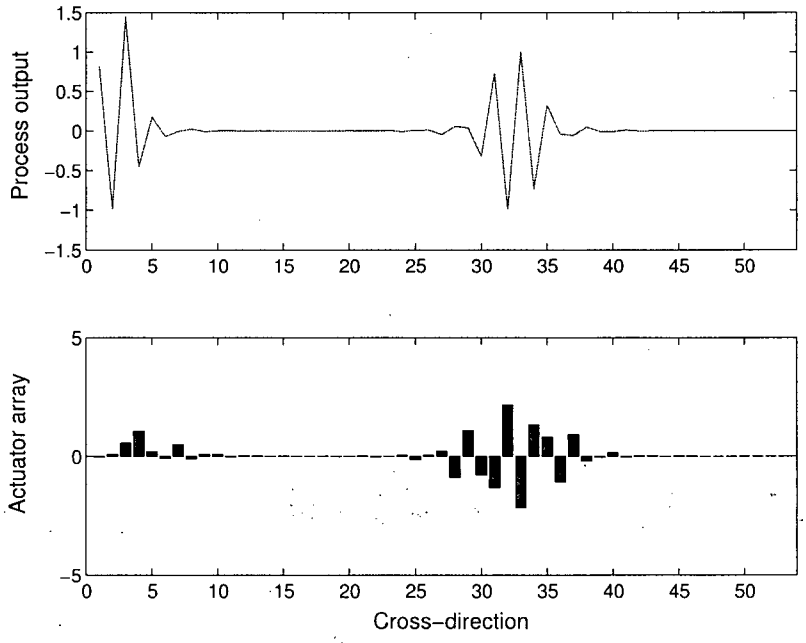

Figure 4.5: Steady state process output and actuator array when the controller with matrix D_f, given with (4.2) and (4.7), is used.

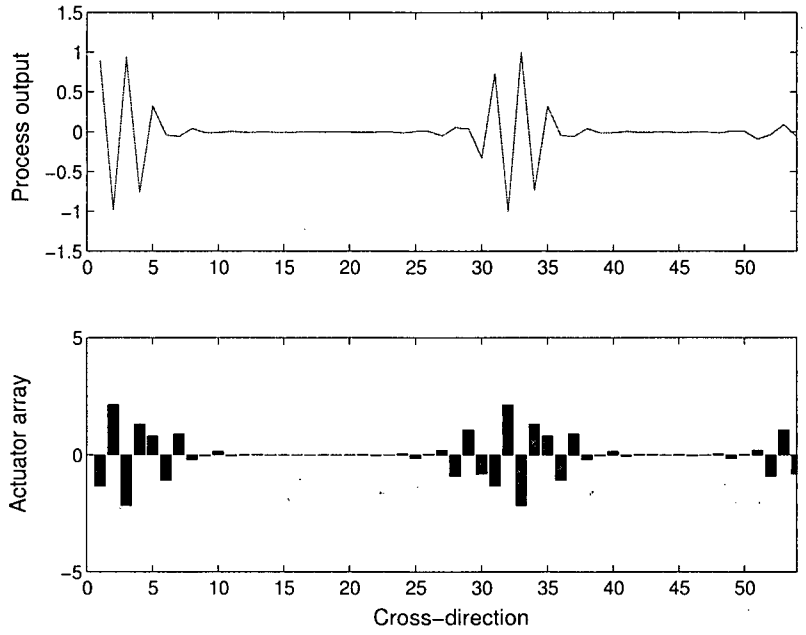

Figure 4.6: Steady state process output and actuator array when the approach presented in Chapter 3 (controller with the structure illustrated in Figure 3.5) is used.

reasons, closed-loop simulations with the process and controller parameters given above and the controller structure illustrated in Figure 3.5 (based on Theorem 1) are shown in Figure 4.6. As expected, given controller's circulant symmetric matrices C_c and D_c, a non-zero disturbance near only one edge (Figure 4.3), results in non-zero control signal at the both edges. This would, of course, be unacceptable in the industrial setting.

Finally, the results obtained with all three approaches (current industrial practice and the approaches from Chapters 3 and this chapter) are summarized in Table 4.2.

	Current technique (Reflection padding)	**STT approach** (Chapter 3)	**Open-loop approach** (Chapter 4)
Process output $\|\|y\|\|_2$	2.5297	2.5772	2.6928
Actuator array $\|\|u\|\|_2$	8.9678	6.0388	4.47
Output y and control signal u near left edge			
$\|\|y(1:10)\|\|_2$	1.7629	1.8244	1.9899
$\|\|u(1:10)\|\|_2$	7.8876	3.9402	1.3327

Table 4.2: 2-norms of the steady-state process output and control signal profiles shown in Figures 4.4 – 4.6.

4.4 Summary

In this chapter, a novel technique for modifying CD controllers near spatial domain boundaries, based on the method for mitigating the well-known Gibbs effect, has been developed. A closed-loop simulation example has also been presented at the end of the chapter, where the new approaches (developed in Chapters 3 and 4) to modifying CD control law near the sheet edges have been compared against the existing industrial practice.

Considering that CD controllers are spatial (and temporal) low-pass filters and that paper sheet edges represent clear spatial domain discontinuities, the observed similarities between the effects occurring in CD control systems near the edges and the well-studied Gibbs phenomenon are no surprise. Based on a Lanczos filter, used for mitigating the Gibbs effect, a CD controller stability-guaranteeing modification technique has been developed. While, the proposed technique does not alter the structure/complexity of the industrial CD controller (the first requirement in Chapter 2), the closed-loop performance and robustness requirements are not directly considered with this approach.

Chapter 5

Closed-Loop Approach to CD Controller Modifications

In this chapter, a method for modifying the existing industrial paper machine CD control law is presented directly taking into account all of the requirements from Section 2.3. The proposed modifications to the existing controller's static matrices (requirement 1 in Section 2.3), and the resulting closed-loop system stability, performance, and robustness (requirements 2–4 in Section 2.3) are directly and systematically considered with this approach.

There are a few important observations that should be made about the problem defined in Section 2.3 and illustrated in Figure 2.7. Since the desired compensator E is a (block-diagonal) static matrix, the problem is a static output feedback (SOF) design problem. While such a problem is very easy to state, a wide variety of SOF problems are still unsolved and represent a significant design challenge (see [69] and references therein). In this work the design of δD and δC in Figure 2.7 will be performed sequentially as it is very difficult to design a static output feedback compensator E with the additional block-diagonal structure constraint. A low-bandwidth static output feedback controller design algorithm, used for computing δD and δC, is outlined in Section 5.1.

The generalized plant $P(z)$, in Figure 2.7, consists of the CD control system closed-loop transfer functions. Considering the CD control system size (the number of actuators $30 \leq n \leq 300$), and high-order dynamics introduced by the process delay d in (2.10) and Dahlin compensator $c(z)$ in (2.12), the number of states included in these closed-loop functions can easily be of the order $\sim 10^3$. This renders implementation of most of the existing controller design algorithms, including the efficient one presented in Section 5.1, practically intractable. However, knowing that the desired controller modifications (2.21)–(2.22) are localized to a small fraction of the total matrices, the order of the resulting generalized plants used for computing modifications δC and δD can be reduced significantly, as detailed in Section 5.2.

Implementation of the low-bandwidth static output feedback (SOF) compensator design algorithm, to be presented in Section 5.1, presumes stable systems. Based on numerous simulation and industrial data, replacing the process and controller circulant symmetric matrices with the corresponding Toeplitz symmetric matrices (which is the first step of the computation of CD controller modifications procedure, presented in Section 5.2)

typically results in closed-loop stable systems. This is not surprising considering that the original (spatially-invariant) controllers are obtained by the two-dimensional loop shaping technique, in which system robustness, with respect to the unstructured process additive perturbations, is a requirement [65, 66]. However, if the closed-loop system, with process and controller Toeplitz symmetric matrices, happens to be unstable (very rarely), a stabilization algorithm, outlined in Section 5.4, has to be implemented.

In preparation for an industrial trial, the simulation studies, presented in Section 5.3, were carried out using the Honeywell hardware-in-the-loop paper machine simulator and the industrial identification and controller tuning software detailed in [32, 65]. Newly developed Matlab prototype software, based on the approach presented in this chapter, was used for computing CD control law modifications δD and δC in Figure 2.7. The results obtained with the new approach are subsequently compared against the existing industrial practice.

A novel static output feedback compensator design algorithm, used for computing CD controllers modifications in Sections 5.2–5.4, is detailed in Section 5.1. The algorithm is presented in full generality, independent of CD control problem. However, in order to address performance and robustness conditions (requirements (3) and (4) in Section 2.3), a generalized plant $N(z)$ with two exogenous outputs, $w_a(z)$ for performance and $w_b(z)$ for robustness, is considered in Section 5.1, as illustrated in Figure 5.1. Transfer functions that make up the generalized plant $N(z)$ will be made explicit in Sections 5.2–5.4.

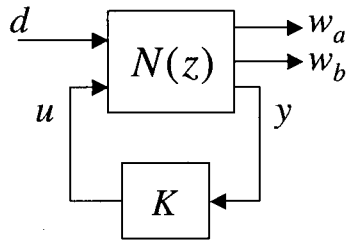

Figure 5.1: Diagram of the lower linear fractional transformation $\mathcal{F}_l(N, K)$.

5.1 Static Output Feedback (SOF) Controller Synthesis

The static output feedback problem considers the linear, time-invariant plant

$$x(k+1) = A_0 x(k) + B_0 u(k), \quad y(k) = C_0 x(k) + D_0 u(k) \tag{5.1}$$

with the controller

$$u(k) = K_0 y(k) \tag{5.2}$$

where K_0 is a constant matrix of appropriate dimensions. In general, the SOF problem is concerned with designing K_0 such that various closed-loop properties of the control system given by (5.1)–(5.2) are satisfied [69].

In this work, we are concerned with a stable, finite-dimensional generalized plant $N(z)$:

$$N(z) = \begin{bmatrix} N_{11}(z) & N_{12}(z) \\ N_{21}(z) & N_{22}(z) \\ N_{31}(z) & N_{32}(z) \end{bmatrix}, \tag{5.3}$$

illustrated in Figure 5.1. The signal $d(z)$ represents the exogenous input into the control system, $w_a(z)$ and $w_b(z)$ represent the exogenous outputs, $y(z)$ represents the feedback signal, and $u(z)$ represents the control signal.

Let the generalized plants $N_a(z)$ and $N_b(z)$ be defined as,

$$N_a(z) = \begin{bmatrix} N_{11}(z) & N_{12}(z) \\ N_{31}(z) & N_{32}(z) \end{bmatrix}, \quad N_b(z) = \begin{bmatrix} N_{21}(z) & N_{22}(z) \\ N_{31}(z) & N_{32}(z) \end{bmatrix}, \tag{5.4}$$

then the input-output transfer functions, $d(z) \rightarrow w_a(z)$ and $d(z) \rightarrow w_b(z)$, are given by lower linear fractional transformations (LFTs):

$$\begin{aligned} \mathcal{F}_l(N_a(z), K(z)) &= N_{11}(z) + N_{12}(z)K(z)(I - N_{32}(z)K(z))^{-1}N_{31}(z) \\ \mathcal{F}_l(N_b(z), K(z)) &= N_{21}(z) + N_{22}(z)K(z)(I - N_{32}(z)K(z))^{-1}N_{31}(z) \end{aligned} \tag{5.5}$$

Our objective is to design a compensator such that:

(a) the controller $K(z) = K_0$ is a static matrix,

(b) the feedback system in Figure 5.1, with $K(z) = K_0$ is stable,

(c) the compensator improves the closed-loop performance as measured by the Frobenius norm,

$$\|\mathcal{F}_l(N_a(e^{j\omega}), K_0)\|_F < \|\mathcal{F}_l(N_a(e^{j\omega}), 0)\|_F, \quad \forall\, |\omega| < \omega_b, \tag{5.6}$$

for some $\omega_b > 0$,

(d) the performance at higher frequencies is not overly degraded. In other words, a constraint,

$$\|\mathcal{F}_l(N_b(z), K_0)\|_\infty < 1, \tag{5.7}$$

is satisfied.

It can be seen that the above requirements (a)–(b) completely correspond to the requirements (1)–(2) in Section 2.3. Also, the requirement (c) above is closely related to the requirement (3), as the Frobenius norm is equal to the sum of all singular values [5, 58]:

$$\|H\|_F = \sqrt{\sum_{i,j} |h_{ij}|^2} = \sqrt{\sum_k \sigma_k^2(H)}, \tag{5.8}$$

where h_{ij} indicates the element in the i^{th} row and j^{th} column, and $\sigma_k(\cdot)$ denotes the k^{th} singular value.

Since $N(z)$ in (5.3) is stable, the internal stability of the closed-loop system in Figure 5.1 is equivalent to the input-output stability of $K(z)(I - N_{32}(z)K(z))^{-1}$ in (5.5). We can then write down the familiar parametrization of stabilizing controllers $K(z)$ for the feedback system in Figure 5.1,

$$K(z) = Q(z)(I + N_{32}(z)Q(z))^{-1} \tag{5.9}$$

for stable $Q(z)$ (see for example [76]), leading to the convenient form of the LFTs in (5.5),

$$\mathcal{F}_l(N_a(z), K(z)) = N_{11}(z) + N_{12}(z)Q(z)N_{31}(z) \tag{5.10}$$

$$\mathcal{F}_l(N_b(z), K(z)) = N_{21}(z) + N_{22}(z)Q(z)N_{31}(z) \tag{5.11}$$

Consider the low-frequency requirement on the Frobenius norm in (5.6). Using (5.10) we can write the LFT at steady-state ($\omega = 0$),

$$\mathcal{F}_l(N_a(e^{j0}), K(e^{j0})) = N_{11}(e^{j0}) + N_{12}(e^{j0}) \cdot Q(e^{j0}) \cdot N_{31}(e^{j0}) \tag{5.12}$$

Now consider the following optimization problem motivated by (5.12),

$$\begin{aligned} Q_0 &= \arg\min_{Q \in \mathcal{R}} J(N_a(e^{j0}), \rho, Q) \\ J(N_a(e^{j0}), \rho, Q) &= \left\| N_{11}(e^{j0}) + N_{12}(e^{j0}) \cdot Q \cdot N_{31}(e^{j0}) \right\|_F^2 + \rho \|Q\|_F^2 \end{aligned} \tag{5.13}$$

A closed-form solution to this optimization problem for a real static matrix Q_0 is given in Appendix B. Subsequently, the resulting Q_0 from (5.13) is used to form the static controller K_0 (requirement (a) above),

$$K_0 = Q_0(I + N_{32}(e^{j0})Q_0)^{-1} \tag{5.14}$$

The first term in optimization (5.13) is intended to address the above specified performance requirement (5.6), while the second term is intended to limit the magnitude of the

synthesized matrix Q_0. Allowing the optimization weight $\rho \to 0$ in (5.13) would produce the static matrix K_0 in (5.14) such that the matrix norm $\|\mathcal{F}_l(N_a(e^{j0}), K_0)\|_F$ is globally minimized.

The conditions on ρ and generalized plant $N(z)$, such that the stability condition (b) and the dynamical condition (d) above are satisfied, are determined by Theorem 4 below.

Theorem 4 (Stability and Full Bandwidth Performance Limit) *If $N(z)$ in (5.3) is stable, $\bar{\sigma}(\mathcal{F}_l(N_b(e^{j\omega}), 0)) < 1$ for all ω, and $\rho > \beta$ in (5.13) where*

$$\beta = \sqrt{r_{12} r_{31}} \cdot \bar{\sigma}(N_{12}(e^{j0}))\, \bar{\sigma}(N_{31}(e^{j0}))\, \bar{\sigma}(N_{11}(e^{j0})) \cdot \left\{ \left\| N_{32}(z) - N_{32}(e^{j0}) \right\|_\infty + \frac{\|N_{22}(z)\|_\infty \cdot \|N_{31}(z)\|_\infty}{1 - \|N_{21}(z)\|_\infty} \right\} \tag{5.15}$$

with the integers r_{12} and r_{31} denoting the number of nonzero singular values of $N_{12}(e^{j0})$ and $N_{31}(e^{j0})$, respectively. Then K_0 synthesized from (5.13)–(5.14) stabilizes the feedback system in Figure 5.1 and

$$\bar{\sigma}\big(\mathcal{F}_l(N_b(e^{j\omega}), K_0)\big) < 1, \qquad \text{for all } \omega \tag{5.16}$$

where $\bar{\sigma}(\cdot)$ denotes the maximum singular value.

Proof: Given in Appendix C.

Note that since $1 > \|\mathcal{F}_l(N_b(z), 0)\|_\infty = \|N_{21}(z)\|_\infty$ in Theorem 4, the denominator in (5.15) is always greater than 0.

The closed-loop performance improvement, as defined in (5.6), with the CD controller designed using the above outlined algorithm is guaranteed by Theorem 5.

Theorem 5 (Low Frequency Performance Improvement) *If $N(z)$ in (5.3) is stable, then for any $K_0 \neq 0$ constructed from (5.13)-(5.14) that stabilizes the system in Figure 5.1, there exists a frequency $\omega_b > 0$ such that*

$$\left\| \mathcal{F}_l(N_a(e^{j\omega}), K_0) \right\|_F < \left\| \mathcal{F}_l(N_a(e^{j\omega}), 0) \right\|_F \tag{5.17}$$

for all $|\omega| < \omega_b$.

Proof: Given in Appendix C.

The value for the weight ρ in (5.13) is determined through bisection on ρ to produce a K_0 in (5.14) such that the requirements (b)–(d) are successfully traded off, and is initialized with the value computed based on Theorem 4. Subsequently, the bisection continues as long as the stability and full bandwidth requirements are satisfied, and until the difference

between the two consecutive values of the weight ρ in (5.13) is smaller than some specified value of the tolerance $\epsilon > 0$. A more detailed outline of the static compensator synthesis algorithm is given in Section 5.1.1 below.

5.1.1 Synthesis Algorithm

The overall algorithm for **determining the weight** ρ in the optimization (5.13) and computing the corresponding **static compensator** K_0, satisfying all the requirements (a)–(d) above, is given as follows:

1. INITIALIZATION
   Set $\rho_l = 0$ and specify tolerance $\epsilon > 0$. Based on Theorem 4, find $\rho_h > 0$ that is guaranteed to satisfy the stability condition (b) and the performance condition (d).

2. Set $\rho = \rho_h$ and compute the corresponding Q_0 and K_0 based on (5.13) and (5.14) respectively. (Theorems 4 and 5 guarantee that so computed compensator K_0 satisfies all the requirements (a)–(d) above.)

3. IF $\rho_h - \rho_l \leq \epsilon$ GOTO STEP 7.

4. Find $\rho = \frac{\rho_h + \rho_l}{2}$ and compute the corresponding Q^* and K^* based on (5.13) and (5.14) respectively.

5. (Verifying conditions (b) and (d) for the system with the above computed compensator K^*).
   IF either one of the requirements (b) and (d) **is not** satisfied THEN set $\rho_l = \rho$ and GOTO STEP 3.

6. Set $K_0 = K^*$ and $\rho_h = \rho$.
   GOTO STEP 3.

7. END

The above algorithm converges to a non-zero K_0 satisfying all the requirements (a)–(d) above, for every tolerance $\epsilon > 0$.

5.2 Computation of CD Controller Modifications

The process spatial invariance assumption, given with (2.17), significantly facilitates CD controller design and is central to the two-dimensional loop shaping technique [66]. However, the implementation of the controller with circulant symmetric matrices in (2.18) would mean a computation of the control signal near one paper machine edge based on

the measurements and previous control signal near the other edge (for a typical paper machine that is between 3 and 11 metres away). This is clearly unwarranted considering that the actual process model (2.10) is characterized by actuators with a localized response on the paper sheet. As a result, the first step in the proposed CD controller modification is a replacement of the initially computed spatially-invariant (circulant) controller matrices C_c and D_c in (2.18) with their corresponding Toeplitz symmetric matrices. Next, the final controller modifications are computed using the SOF algorithm, presented in Section 5.1, in turn on the δD and δC matrices in Figures 2.6 and 2.7. Since the SOF algorithm presumes stable systems, the closed-loop stability of the system with Toeplitz symmetric process and controller models, is assumed. Based on numerous industrial data, as well as simulation studies, this is not a restrictive assumption and is only violated in certain pathological examples. However, if the system with Toeplitz symmetric process and controller models is not stable, then a stabilization procedure is required. Such a stabilization procedure is presented in Section 5.4.

Based on the above, the **overall algorithm for computing CD controller modifications δC and δD** is given as follows:

1. Replace the controller circulant symmetric matrices C_c and D_c in (2.18) with their corresponding Toeplitz symmetric matrices C_d and D_d respectively, and check stability of the resulting closed-loop system.

2. IF Toeplitz system is stable GOTO 4.

3. (Rarely required) Use the stabilization procedure given in Section 5.4.

4. Compute δC and δD modifications (for performance) as detailed in Sections 5.2.1–5.2.2.

5. END.

Since the two edges of the paper machine are modelled to be identical, it is enough to retune the controller at one edge only, e.g. upper left corners of the matrices δC and δD. Subsequently, the corresponding modifications at the other edge can easily be found by symmetry arguments.

5.2.1 Modifications Near One Sheet Edge (C_e and D_e)

Factoring out of the control system inputs and outputs near one edge, based on the closed-loop system in Figure 2.7, is performed with rectangular weights W_i, $i = 1, 2, \ldots, 7$, as illustrated in Figure 5.2.

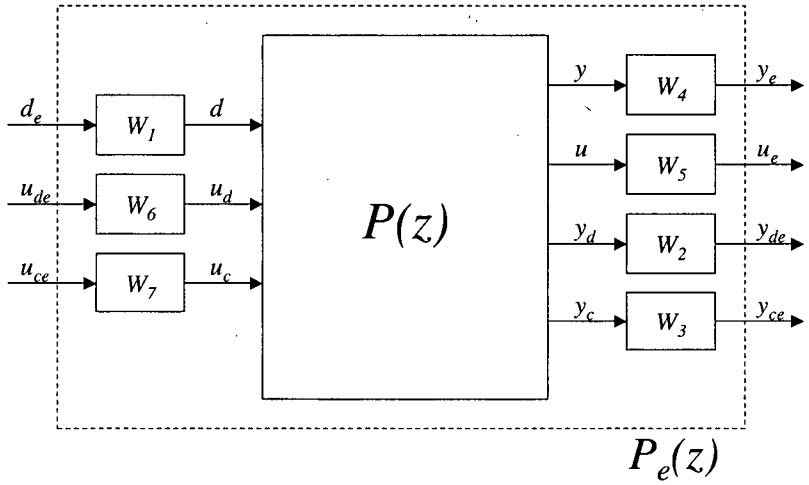

Figure 5.2: Isolating system inputs/outputs near one edge.

The rectangular weighting matrices W_i, $i = 2, 3, 4, 5$ are defined as:

$$W_2 = \underbrace{[\mathrm{I}_{n_{D1}} \quad 0_{n_{D1}\times(n-n_{D1})}]}_{n_{D1}\times n}, \qquad W_3 = \underbrace{[\mathrm{I}_{n_{C1}} \quad 0_{n_{C1}\times(n-n_{C1})}]}_{n_{C1}\times n},$$
$$W_4 = \underbrace{[\mathrm{I}_{n_y} \quad 0_{n_y\times(n-n_y)}]}_{n_y\times n}, \qquad W_5 = \underbrace{[\mathrm{I}_{n_u} \quad 0_{n_u\times(n-n_u)}]}_{n_u\times n}, \tag{5.18}$$

and the rectangular weighting matrices W_i, $i = 1, 6, 7$:

$$W_1 = \underbrace{\begin{bmatrix} I_{n_d} \\ 0_{(n-n_d)\times n_d} \end{bmatrix}}_{n\times n_d}, \quad W_6 = \underbrace{\begin{bmatrix} I_{n_{D2}} \\ 0_{(n-n_{D2})\times n_{D2}} \end{bmatrix}}_{n\times n_{D2}}, \quad W_7 = \underbrace{\begin{bmatrix} I_{n_{C2}} \\ 0_{(n-n_{C2})\times n_{C2}} \end{bmatrix}}_{n\times n_{C2}} \tag{5.19}$$

The matrices W_2, W_3, W_6, W_7 are used to convert the matrix sub-block design into a full-block design problem, as illustrated in Figure 5.3. From (5.18)–(5.19) and Figure 5.3, it can be seen that the elements are given by:

$$\begin{aligned} [D_e]_{ij} &= \delta d_{ij}, \quad 1 \le i \le n_{D1} \text{ and } 1 \le j \le n_{D2}, \\ [C_e]_{ij} &= \delta c_{ij}, \quad 1 \le i \le n_{C1} \text{ and } 1 \le j \le n_{C2}, \end{aligned} \tag{5.20}$$

where δc_{ij} and δd_{ij} are the same as those elements in (2.21)–(2.22). In other words, $C_e \in \mathcal{R}^{n_{C1}\times n_{C2}}$ and $D_e \in \mathcal{R}^{n_{D1}\times n_{D2}}$ are the non-zero, upper-left elements of the matrices δC and δD in (2.21)–(2.22), respectively.

The matrices W_1, W_4, W_5, on the other hand, are used to isolate the sheet edges for

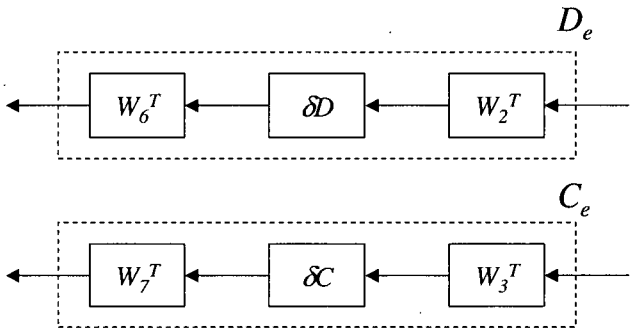

Figure 5.3: Transforming a sub-block into a full-block design problem.

consideration in the performance design. All the closed-loop transfer functions that define $P_e(z)$ in Figure 5.2 are given in Appendix D.

However, elimination of inputs/outputs with the matrices $W_i, i = 1, 2, \ldots, 7$ does not necessarily reduce the number of states of the corresponding closed-loop transfer functions. As a result, the order of the transfer matrix $P_e(z)$ in Figure 5.2, in typical CD control systems, can easily reach into the thousands. Fortunately, most of these states have very little impact on input/output behavior of the corresponding closed-loop transfer functions. This is the case because many of the states are mainly related to the inputs/outputs located in the middle of the sheet and other machine edge, i.e. those inputs/outputs that were eliminated with the rectangular weights W_i.

The (in)significance of the states, in terms of the corresponding transfer function input/output behavior, can be quantified using Hankel singular values [2, 5, 26, 58, 76]. For example, in the case of the system to be presented in Section 5.3, out of 144 Hankel singular values of the closed-loop transfer function $P_1 : d_e \rightarrow y_e$, 80 are smaller than $2.2 \cdot 10^{-16}$, 105 smaller than 10^{-9}, and 125 smaller than 10^{-3} (as illustrated in Figure 5.4). Such a rapid decrease of the Hankel singular values is quite representative of these systems and not surprising, considering the localized nature of the CD processes and controllers.

The order reduction procedure, based on Hankel singular values, has two important characteristics [4, 5]:

1. Stability preservation (stability of $P_e(z)$ implies stability of $P_r(z)$),

2. An apriori computable upper bound of the approximation error $\mathcal{H}_\infty$ norm:

$$\|P_e(z) - P_r(z)\|_\infty \leq 2 * \sum(\textit{discarded Hankel singular values}) \qquad (5.21)$$

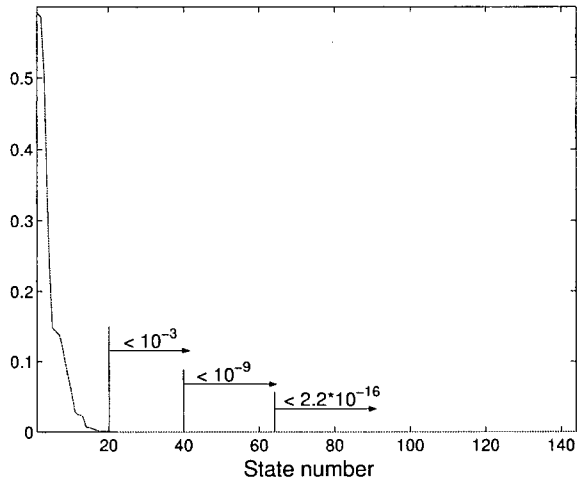

Figure 5.4: Illustration of the rapid decrease of the Hankel singular values of the closed-loop transfer functions that define a generalized plant $P_e(z)$ in Figure 5.2: Hankel singular values of $P_1 : d_e \rightarrow y_e$ for the CD control system presented in Section 5.3.

5.2.2 Computation of C_e and D_e

Based on the diagram given in Figure 5.2, the linear fractional transformations (LFT's) for computing modifications C_e and D_e in Figure 5.3 can be defined. They are presented in Figures 5.5a and 5.5b. The design of C_e and D_e is performed by alternately synthesizing one matrix component while holding the other fixed, as detailed below. The synthesis procedure is the low-bandwidth procedure of Section 5.1.

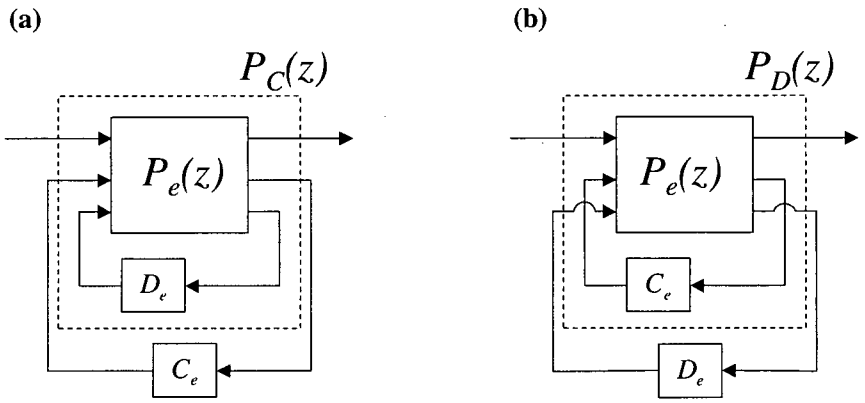

Figure 5.5: Linear fractional transformations for computing (a) C_e and (b) D_e modifications.

The **algorithm for computing C_e and D_e** is given as follows:

1. Compute D_e by the use of the static compensator synthesis procedure in Section 5.1.1, based on the linear fractional transformation given in Figure 5.5b.

2. Based on (5.20), find the corresponding controller modification δD in (2.22) and update the controller matrix D.

3. Compute C_e by the use of the static compensator synthesis procedure in Section 5.1.1, based on the linear fractional transformation given in Figure 5.5a.

4. Based on (5.20), find the corresponding controller modification δC in (2.21) and update the controller matrix C.

5. END.

It should be noticed here that this sequential static output feedback (SOF) controller design procedure does not increase the order of the resulting system $P_e(z)$, unlike conventional sequential decentralized control (see discussion and references in [39]). This is, of course, a consequence of the designed compensator being a static matrix at each iteration of the design and so does not contribute to the number of states.

5.3 Hardware-In-The-Loop Simulator Example

In preparation for testing the new technique on a real paper machine, the simulation studies presented in this section were carried out using the industrial identification and controller tuning software detailed in [32, 65] (residing on one computer), and a hardware-in-the-loop simulator (residing on another computer), as illustrated in Figure 5.6.

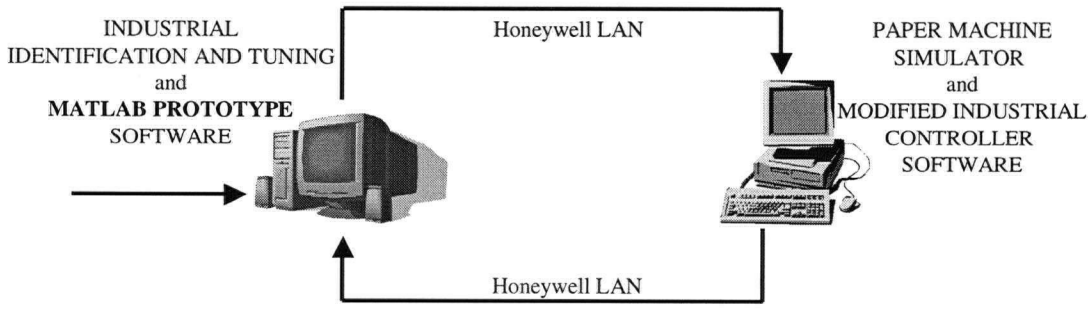

Figure 5.6: Schematic of the simulator trial setup.

The industrial controller algorithm, implemented in the simulator, was modified to accommodate the control law changes according to Figure 2.6. The process simulator was set up with parameters to correspond to those of the actual paper machine on which the

real testing was afterwards carried out (Chapter 6). The simulator testing procedure was as follows. The open-loop 'bump test', with three actuators stepped up (down) for 150 *microns*, was carried out for identification purposes. Process identification and controller tuning were performed using the industrial software presented in [32, 65]. Next, the design for various controller modifications D_e and C_e in Figure 5.5 was completed, and these parameters were transferred over the LAN into the correct database location for use by the industrial controller (the information flow between the Matlab prototype software and the industrial software packages is given in Figure 6.4 in Chapter 6). Finally, the performance of the resulting closed-loop systems was observed, recorded, and is presented below. This is the same procedure that was followed in a working paper mill (Chapter 6).

5.3.1 Process and Controller Parameters

The CD control system, presented below, describes an array of $n = 36$ slice lip actuators being used to control the paper sheet basis weight profile. More details about basis weight control using slice lip actuators were given in the Introduction. The parameters of the process model in (2.10)–(2.11) were identified using software described in [32] with the size of the matrix B band $l_b = 6$ in (2.11) and

$$\begin{aligned} \{b_0, b_1, \ldots, b_6\} &= 10^{-3} \cdot \{0.1652, 0.2044, 0.0789, -0.0382, -0.0169, -0.0009, 0.0001\} \\ a_0 &= 0.855, \quad d = 2 \end{aligned} \tag{5.22}$$

The feedback controller $K(z)$ in (2.12) was designed using the standard two-dimensional loop shaping technique [65, 66]. First, the process Toeplitz symmetric matrix B_d in (2.11) is replaced with the corresponding circulant symmetric matrix B_c in (2.17), resulting in a (spatially-invariant) controller with circulant symmetric matrices (2.18). The controller parameters obtained had matrix band sizes $l_c = 4, l_d = 1$, with:

$$\begin{aligned} \{c_0, c_1, c_2, c_3, c_4\} &= \{-0.2089, -0.2129, -0.0487, 0.0856, 0.0481\} \\ \{d_0, d_1\} &= \{0.9878, 0.0061\} \end{aligned} \tag{5.23}$$

The tuning parameter α of the Dahlin controller $c(z)$ in (2.12) was also produced by the two-dimensional loop shaping design, $\alpha = 0.8506$.

Subsequently, the initially computed circulant-symmetric controller matrices are replaced with the corresponding Toeplitz symmetric matrices. After confirming stability of the system with the process and controller Toeplitz symmetric matrices, the procedure for modifying CD control near the edges, presented in Section 5.2, can be implemented.

5.3.2 Controller Modifications and Closed-Loop Simulations

The closed-loop simulations have been performed with the steady-state process output disturbance, $d(z)$ in (2.9), as shown in Figure 5.7. Near one edge (left side), the disturbance has a significant high spatial frequency content, and near the other (right side), has a smoother appearance. The first type of disturbance very often leads to system instabilities in real life CD systems as the actuator array is trying to remove the uncontrollable (high frequency) modes of the process output disturbance. The second type of disturbance (introduced near the right edge) is usually successfully attenuated by the control systems.

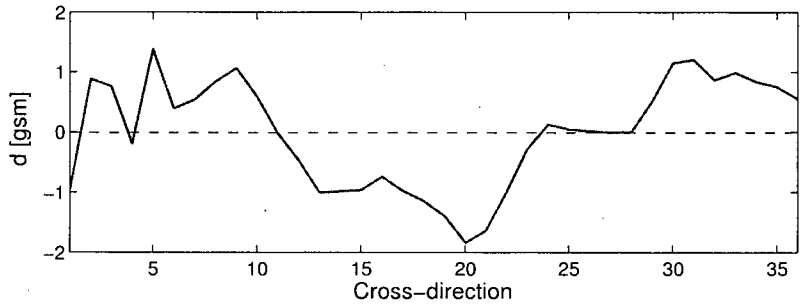

Figure 5.7: Process output disturbance d (at zero temporal frequency $\omega = 0$).

The closed-loop simulation results are shown in Figures 5.8–5.11, and summarized in Table 5.1. Figure 5.8 illustrates the closed-loop steady-state process output and actuator profile using the reflection padding (one of the techniques currently used in industry). It can be seen that, in spite of excessive control action near left edge, the process output profile is not particularly good, with maximum and minimum varying between 1.176 and -1.235.

Simulation results, with the controller tuned in turn conservatively, balanced, and aggressively using the new approach presented in Sections 5.1 and 5.2, are given in Figures 5.9 – 5.11.

In all three cases, the sizes of the rectangular weights $W_i, i = 1, \ldots, 7$ in (5.18)–(5.19) were chosen as, $n_{C1} = 5, n_{C2} = 8, n_{D1} = 3, n_{D2} = 8, n_u = 8, n_d = 8, n_y = 8$. The output vectors $w_a(z)$ and $w_b(z)$ in Figure 5.1 were chosen as:

$$w_a(z) = [k_P \cdot y(z) \;\; u(z)]^T, \qquad w_b(z) = \frac{1}{1 + k_R} \cdot u(z), \tag{5.24}$$

where $y(z)$ and $u(z)$ are the process output and control signal respectively, and coefficients $\mathbf{k_P}$ and $\mathbf{k_R}$ are the **tuning variables**.

Parameter k_P is a closed-loop performance tuning variable, as it affects the generalized plant N_a in (5.6). The point of reference for k_P is the inverse of the process maximum singular value at steady-state. For the CD process model given with (5.22), $\frac{1}{\overline{\sigma}(G(e^{j0}))} = \frac{1}{0.0043} = 232.56$, where $\overline{\sigma}(\cdot)$ denotes the maximum singular value. Variable k_R, on the other hand, is a closed-loop robustness tuning variable, since it affects the generalized plant N_b in (5.7). Parameter k_R is determined considering a maximum allowed performance degradation at higher frequencies (requirement (d) in Section 5.1). For example, a maximum allowed degradation of 10% corresponds to $k_R = 0.1$.

In the case of **conservative tuning** (Figure 5.9), the tuning variables k_P and k_R in (5.24) were chosen as $\mathbf{k_P = 300}$, $\mathbf{k_R = 0.2}$. The computed controller modifications δC and δD are given with (5.25)–(5.26) respectively[1].

$$\delta C = \begin{bmatrix} 0.01284 & 0.01139 & -0.02907 & -0.03857 & 0.01151 & 0.03860 & 0.07592 & 0.06971 \\ -0.02690 & 0.02531 & 0.06664 & 0.02755 & -0.00872 & -0.05851 & -0.07427 & -0.02425 \\ -0.05871 & 0.02930 & 0.11821 & 0.05045 & -0.03373 & -0.11619 & -0.15091 & -0.05849 \\ -0.07497 & 0.06390 & 0.22949 & 0.20296 & 0.11884 & -0.05596 & -0.17865 & -0.10772 \\ -0.04865 & -0.07756 & 0.04778 & 0.19367 & 0.19066 & 0.17263 & 0.03482 & -0.07492 \end{bmatrix} \tag{5.25}$$

$$\delta D = \begin{bmatrix} -0.08934 & -0.00653 & 0.01573 & 0.00946 & -0.02752 & -0.00943 & 0.01168 & 0.00885 \\ -0.05200 & -0.04448 & 0.00710 & 0.02074 & -0.01803 & -0.01664 & 0.00547 & 0.00188 \\ 0.00926 & -0.01185 & -0.06767 & 0.02585 & 0.01692 & -0.01097 & -0.01788 & -0.00230 \end{bmatrix} \tag{5.26}$$

The resulting upper left sections of the resulting control law matrices $C_d+\delta C$ and $D_d+\delta D$, in the case of conservative tuning, are given in (5.27)-(5.28).

$$C_d(1:n_{C1}, 1:n_{C2}) + \delta C = \begin{bmatrix} -0.19606 & -0.20151 & -0.07777 & 0.04703 & 0.05961 & 0.03860 & 0.07592 & 0.06971 \\ -0.23980 & -0.18359 & -0.14626 & -0.02115 & 0.07688 & -0.01041 & -0.07427 & -0.02425 \\ -0.10741 & -0.18360 & -0.09069 & -0.16245 & -0.08243 & -0.03059 & -0.10281 & -0.05849 \\ 0.01063 & 0.01520 & 0.01659 & -0.00594 & -0.09406 & -0.10466 & -0.09305 & -0.05962 \\ -0.00055 & 0.00804 & -0.00092 & -0.01923 & -0.01824 & -0.04027 & -0.01388 & 0.01068 \end{bmatrix} \tag{5.27}$$

[1]All the computed matrix modifications in this Chapter and Chapter 6 are given with the precision 10^{-5}, as that level of accuracy has been achieved in the communication link between the Matlab prototype software and the industrial software packages.

$$D_d(1:n_{D1}, 1:n_{D2}) + \delta D =$$

$$\begin{bmatrix} 0.89846 & -0.00043 & 0.01573 & 0.00946 & -0.02752 & -0.00943 & 0.01168 & 0.00885 \\ -0.04590 & 0.94332 & 0.01320 & 0.02074 & -0.01803 & -0.01664 & 0.00547 & 0.00188 \\ 0.00926 & -0.00575 & 0.92013 & 0.03195 & 0.01692 & -0.01097 & -0.01788 & -0.00230 \end{bmatrix} \tag{5.28}$$

In the case of **balanced tuning** (Figure 5.10), the tuning variables k_P and k_R in (5.24) were chosen as $\mathbf{k_P = 1600}$, $\mathbf{k_R = 0.2}$, and the computed controller modifications are given with (5.29)–(5.30).

$$\delta C =$$

$$\begin{bmatrix} 0.01067 & -0.02047 & 0.01566 & 0.00062 & -0.00071 & -0.00375 & -0.00422 & 0.01422 \\ -0.01959 & 0.03168 & -0.02330 & 0.00434 & -0.00675 & 0.00885 & 0.00482 & -0.01655 \\ 0.01019 & -0.02143 & 0.02107 & -0.00808 & 0.00353 & -0.00198 & 0.00041 & 0.00169 \\ 0.02468 & -0.00089 & -0.05615 & 0.05064 & -0.02132 & -0.00315 & 0.00791 & -0.00904 \\ -0.01064 & 0.01550 & 0.01087 & -0.03997 & 0.04554 & -0.02272 & -0.00035 & 0.00431 \end{bmatrix} \tag{5.29}$$

$$\delta D =$$

$$\begin{bmatrix} 0.00605 & -0.00394 & -0.00041 & 0.00139 & -0.00233 & 0.00171 & 0.00080 & -0.00154 \\ -0.00448 & 0.00721 & -0.00421 & -0.00348 & 0.00467 & 0.00016 & -0.00390 & -0.00085 \\ 0.00050 & -0.00497 & 0.00906 & -0.00781 & 0.00025 & 0.00459 & -0.00274 & -0.00299 \end{bmatrix} \tag{5.30}$$

The upper left sections of the resulting control law matrices $C_d + \delta C$ and $D_d + \delta D$, in the case of balanced tuning, are given in (5.31)-(5.32).

$$C_d(1:n_{C1}, 1:n_{C2}) + \delta C =$$

$$\begin{bmatrix} -0.19823 & -0.23337 & -0.03304 & 0.08622 & 0.04739 & -0.00375 & -0.00422 & 0.01422 \\ -0.23249 & -0.17722 & -0.23620 & -0.04436 & 0.07885 & 0.05695 & 0.00482 & -0.01655 \\ -0.03851 & -0.23433 & -0.18783 & -0.22098 & -0.04517 & 0.08362 & 0.04851 & 0.00169 \\ 0.11028 & -0.04959 & -0.26905 & -0.15826 & -0.23422 & -0.05185 & 0.09351 & 0.03906 \\ 0.03746 & 0.10110 & -0.03783 & -0.25287 & -0.16336 & -0.23562 & -0.04905 & 0.08991 \end{bmatrix} \tag{5.31}$$

$$D_d(1:n_{D1}, 1:n_{D2}) + \delta D =$$

$$\begin{bmatrix} 0.99385 & 0.00216 & -0.00041 & 0.00139 & -0.00233 & 0.00171 & 0.00080 & -0.00154 \\ 0.00162 & 0.99501 & 0.00189 & -0.00348 & 0.00467 & 0.00016 & -0.00390 & -0.00085 \\ 0.00050 & 0.00113 & 0.99686 & -0.00171 & 0.00025 & 0.00459 & -0.00274 & -0.00299 \end{bmatrix} \tag{5.32}$$

Finally in the case of **aggressive tuning**, the tuning parameters k_P and k_R in (5.24) were chosen as $\mathbf{k_P = 2400}$, $\mathbf{k_R = 0.5}$, and the computed controller modifications δC and δD are given with (5.33)–(5.34).

$$\delta C =$$

$$\begin{bmatrix} 0.00139 & -0.09556 & 0.12427 & -0.04591 & 0.01286 & 0.02910 & 0.00224 & 0.07400 \\ 0.09924 & -0.06312 & -0.26003 & 0.32070 & -0.21818 & 0.07590 & 0.07775 & -0.21568 \\ 0.14139 & -0.08458 & -0.14097 & 0.12526 & -0.09832 & 0.02563 & 0.10160 & -0.06081 \\ 0.36969 & -0.09298 & -0.65551 & 0.56045 & -0.37441 & 0.00775 & 0.29926 & -0.18947 \\ -0.22865 & 0.36187 & 0.15454 & -0.50466 & 0.44304 & -0.25590 & -0.10725 & 0.28026 \end{bmatrix} \tag{5.33}$$

$$\delta D =$$

$$\begin{bmatrix} 0.00854 & -0.00446 & -0.00089 & 0.00142 & -0.00233 & 0.00238 & 0.00097 & -0.00290 \\ -0.00493 & 0.00907 & -0.00418 & -0.00462 & 0.00518 & 0.00051 & -0.00436 & -0.00067 \\ 0.00013 & -0.00532 & 0.01133 & -0.00892 & -0.00022 & 0.00504 & -0.00275 & -0.00288 \end{bmatrix} \tag{5.34}$$

The upper left sections of the resulting control law matrices $C_d + \delta C$ and $D_d + \delta D$, in the case of aggressive tuning, are given in (5.35)-(5.36).

$$C_d(1:n_{C1}, 1:n_{C2}) + \delta C =$$

$$\begin{bmatrix} -0.20751 & -0.30846 & 0.07557 & 0.03969 & 0.06096 & 0.02910 & 0.00224 & 0.07400 \\ -0.11366 & -0.27202 & -0.47293 & 0.27200 & -0.13258 & 0.12400 & 0.07775 & -0.21568 \\ 0.09269 & -0.29748 & -0.34987 & -0.08764 & -0.14702 & 0.11123 & 0.14970 & -0.06081 \\ 0.45529 & -0.14168 & -0.86841 & 0.35155 & -0.58731 & -0.04095 & 0.38486 & -0.14137 \\ -0.18055 & 0.44747 & 0.10584 & -0.71756 & 0.23414 & -0.46880 & -0.15595 & 0.36586 \end{bmatrix} \tag{5.35}$$

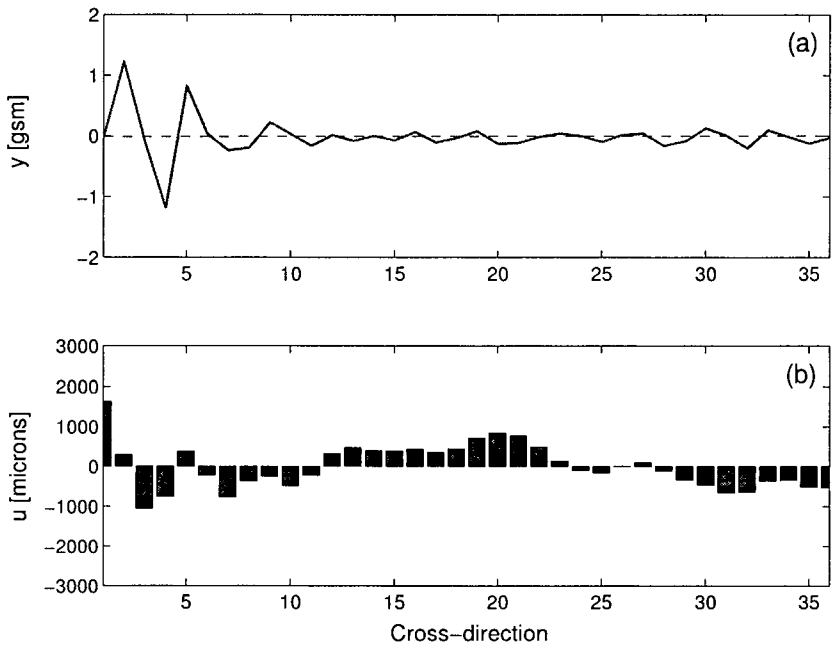

Figure 5.8: Steady-state process output (a) and control signal (b), using the current industrial technique - reflection padding.

$$D_d(1:n_{D1}, 1:n_{D2}) + \delta D =$$

$$\begin{bmatrix} 0.99634 & 0.00164 & -0.00089 & 0.00142 & -0.00233 & 0.00238 & 0.00097 & -0.00290 \\ 0.00117 & 0.99687 & 0.00192 & -0.00462 & 0.00518 & 0.00051 & -0.00436 & -0.00067 \\ 0.00013 & 0.00078 & 0.99913 & -0.00282 & -0.00022 & 0.00504 & -0.00275 & -0.00288 \end{bmatrix} \tag{5.36}$$

It can be seen from Figures 5.9 – 5.11 and Table 5.1 that, by using the approach presented in Sections 5.1 and 5.2, a successful trade-off between performance (a flat CD profile) and the corresponding control signal magnitude, can be achieved. From Table 5.1, it can be noticed that in case of all three tunings based on the new approach, the output profile has been improved in comparison to the result achieved with the current industrial technique. Also, in the cases of conservative and balanced tunings, such a result has been achieved with less actuator usage.

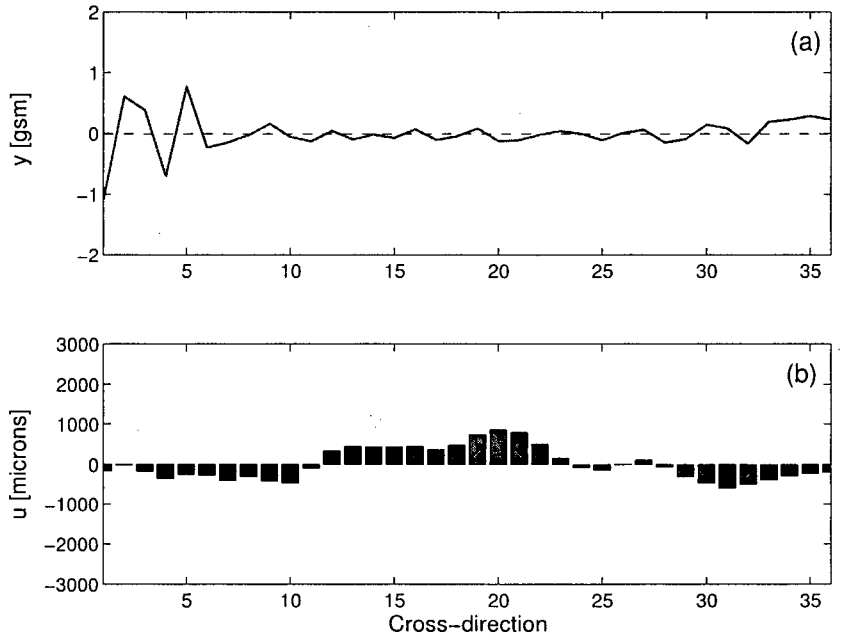

Figure 5.9: Steady-state process output (a) and control signal (b), using the new technique - conservative tuning ($k_P = 300$ and $k_R = 0.2$ in (5.24)).

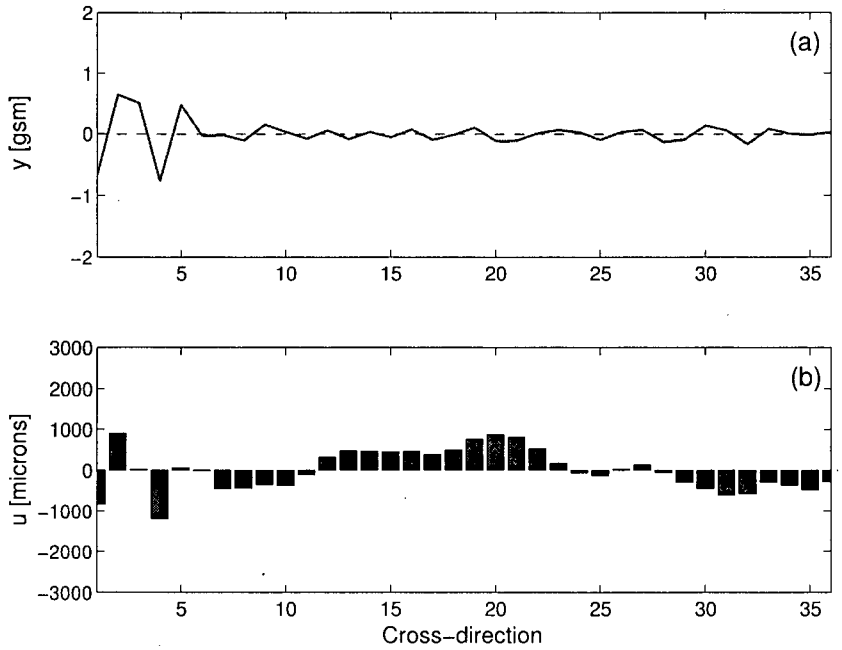

Figure 5.10: Steady-state process output (a) and control signal (b), using the new technique - balanced tuning ($k_P = 1600$ and $k_R = 0.2$ in (5.24)).

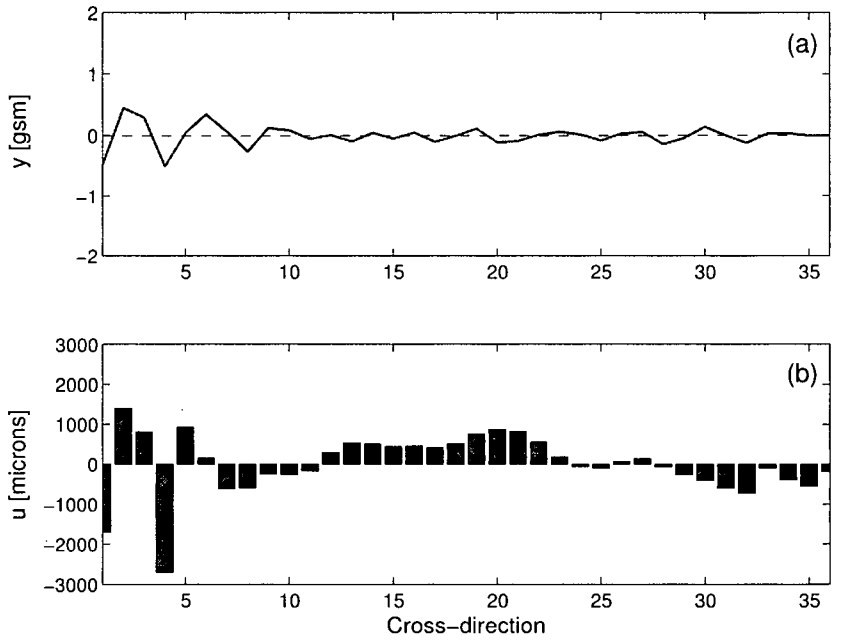

Figure 5.11: Steady-state process output (a) and control signal (b), using the new technique - aggressive tuning ($k_P = 2400$ and $k_R = 0.5$ in (5.24)).

	Current industrial technique	**New technique**		
	Reflection padding	Conservative tuning: $k_P = 300$ $k_R = 0.2$	Balanced tuning: $k_P = 1600$ $k_R = 0.2$	Aggressive tuning: $k_P = 2400$ $k_R = 0.5$
Process output [gsm]	1.9913	1.8305	1.4467	1.0577
Control signal [microns]	3307	2376	2974	4436

Table 5.1: 2-norm of the process output and control signal steady-state profiles shown in Figures 5.8 – 5.11.

5.4 Stabilization Procedure (Rarely Required)

Modification of process and controller matrices from circulant into Toeplitz symmetric, as proposed in the overall algorithm presented in Section 5.2, clearly represents a one-step elimination of the corresponding circulant matrices' 'ears' ΔC and ΔD in (2.20). As pointed out earlier, it has been established (based on numerous industrial and simulation data analyzed) that, except in some pathological cases, the resulting closed-loop systems with Toeplitz symmetric process and controller matrices are nominally stable. However, if that is not the case, a gradual elimination of the circulant symmetric matrices' 'ears' $\Delta G_c(z), \Delta C$, and ΔD in (2.19)–(2.20) is proposed. This is illustrated in Figure 5.12 with the parameter $\lambda \in [0, 1]$: $\lambda = 0$ corresponds to periodic boundary conditions (circulant symmetric process and controller models), and $\lambda = 1$ corresponds to Dirichlet boundary conditions (Toeplitz symmetric process and controller models). Further controller modifications δC and δD in Figure 5.12, to be computed in accordance with the algorithm below, are defined with (2.21)–(2.22).

The overall **stabilization algorithm** is given as follows:

1. Find the maximum value of $\lambda \in [0, 1]$ for which the system is closed-loop stable.
   IF $\lambda = 1$ GOTO STEP 6.

2. Based on the diagram in Figure 5.2, with W_i, $i = 1, 2, 3, 5, 6, 7$ given with (5.18)–(5.19) and $W_4 = 0_{n_y \times n}$, define linear fractional transformations (LFT's) for computing modifications C_e and D_e in Figure 5.3
   (Note: $W_4 = 0$, i.e. process output y is not a part of the LFT's exogenous output vector, as in the stabilization procedure we are exclusively interested in reducing the gain $d \rightarrow u$).

3. Using the algorithm from Section 5.2.2, compute modifications D_e and C_e and find the corresponding controller modifications δC and δD in (2.21)–(2.22).

4. Update the controller matrices C and D with the above obtained δC and δD - as illustrated in Figure 5.12.

5. GOTO STEP 1.

6. END.

At the end of the above algorithm, the process and controller 'ears' $\Delta G(z)$, ΔC and ΔD in (2.19)–(2.20) are eliminated, and further controller modifications, that optimize the gain from the process output disturbance d to process output y and control signal u, as detailed in Section 5.2, can be carried out.

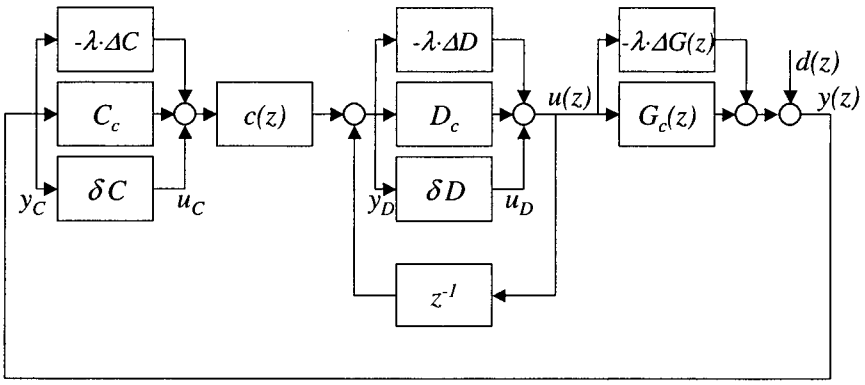

Figure 5.12: A gradual elimination of the process and controller circulant symmetric matrices' 'ears' with the parameter $\lambda \in [0, 1]$.

5.4.1 Example

As pointed out above, the stabilization procedure, when going from periodic to Dirichlet boundary conditions, is very rarely (practically never) required for the actual CD control systems designed with the two-dimensional loop shaping technique. However, after extensive simulation studies, one CD control system, destabilized by the change of the boundary conditions from periodic to Dirichlet (as defined in Section 2.1), was found. The simulated system had 36 actuators, with the fabricated but realistic process parameters resulting in a very wide bi-modal spatial response, illustrated in Figure 5.13. The specific parameters of the process model in (2.10)–(2.11) are given as,

$$\begin{aligned} \{b_0, b_1, \ldots, b_{12}\} &= 10^{-3} \cdot \{0.56966, 0.85783, 0.8600, 0.010764, -0.63285, -0.47079, \\ &\quad -0.091566, 0.047077, 0.029923, 0.0053444, -0.00039524, -0.00027924, \\ &\quad -0.00001078\} \\ a_0 &= 0.916, \quad d = 3 \end{aligned} \tag{5.37}$$

Next, the corresponding feedback controller $K(z)$ in (2.12) was intentionally designed with (unacceptably) small stability margins,

$$\begin{aligned} \{c_0, c_1, c_2, c_3, c_4, c_5\} &= \{-0.14168, -0.15141, -0.11392, 0.0046317, 0.090511, 0.068683\} \\ \{d_0, d_1\} &= \{0.9998, 0.00010119\}, \end{aligned} \tag{5.38}$$

and the tuning parameter α of the Dahlin controller $c(z)$ in (2.12), $\alpha = 0.88959$. The resulting circulant (spatially-invariant) closed-loop system (corresponding to $\lambda = 0, \delta C =$

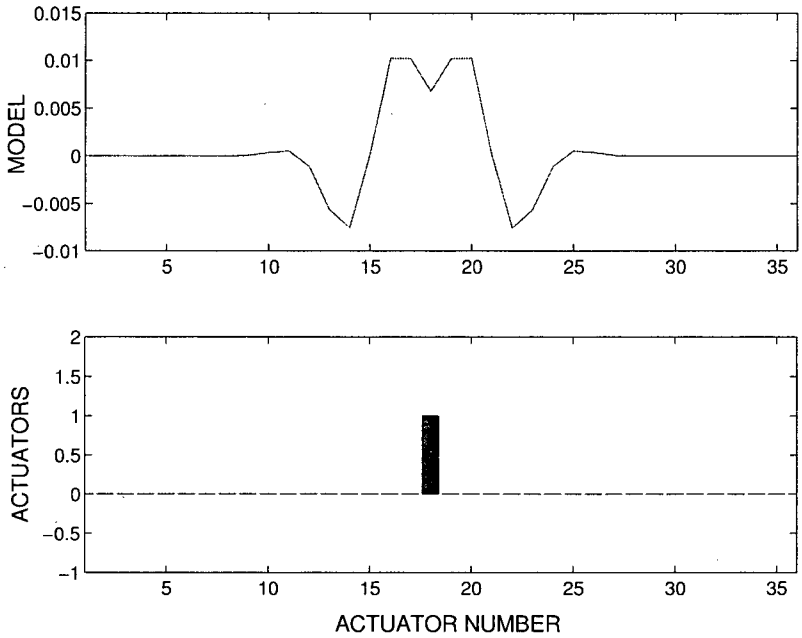

Figure 5.13: Actuator array shape (upper figure) and the corresponding process steady-state response (lower figure) for the process model given with (5.37).

$0, \delta D = 0$ in Figure 5.12) is (barely) stable[1] with the maximum closed-loop pole magnitude equal to 0.99997.

However, the system with the same parameters (5.37)–(5.38), and Dirichlet boundary conditions (i.e. process and controller Toeplitz symmetric matrices, corresponding to $\lambda = 1, \delta C = 0, \delta D = 0$ in Figure 5.12) is unstable - the maximum pole magnitude equal to 1.0004.

Using the stabilization algorithm in Section 5.4, it was possible to stabilize the above system.

First (following **Step 1** of the stabilization algorithm), the maximum value of $\lambda \in [0, 1]$ for which the system remains stable was found to be $\lambda = 0.46$ (resulting in a maximum closed-loop pole magnitude: 0.9999). Next, following **Steps 2–4**, the sizes of the rectangular weights $W_i, i = 1, 2, 3, 5, 6, 7$ in (5.18)–(5.19) were chosen as, $n_{C1} = 5, n_{C2} = 8, n_{D1} = 3, n_{D2} = 8, n_u = 8, n_d = 8$, and the output vector $\omega_b(z)$ in Figure 5.2 as $\omega_b(z) = 0.5u(z)$.

[1]The controller (5.38) should certainly never be implemented on a real paper machine having CD process parameters (5.37) as the stability margins are unacceptably small for industrial implementation.

Subsequently, the controller modifications δC and δD were computed[1],

$$\delta C(1:n_{C1}, 1:n_{C2}) =$$
$$\begin{bmatrix} 0.03229 & -0.04907 & 0.01572 & -0.01601 & -0.00609 & 0.02133 & -0.00397 & -0.01116 \\ 0.00116 & -0.00029 & 0.00011 & -0.00013 & -0.00088 & 0.00062 & 0.00072 & 0.00018 \\ -0.01859 & 0.02756 & -0.00887 & 0.00905 & 0.00379 & -0.01221 & 0.00192 & 0.00615 \\ 0.24680 & -0.05612 & -0.06934 & -0.01706 & -0.01454 & 0.02257 & 0.09182 & 0.09304 \\ 0.10920 & -0.03441 & -0.04335 & -0.02383 & -0.01608 & 0.02055 & 0.06249 & 0.05152 \end{bmatrix} \tag{5.39}$$

$$\delta D(1:n_{D1}, 1:n_{D2}) =$$
$$\begin{bmatrix} -1.00632 & 0.11875 & -0.26057 & 1.07935 & -1.12241 & 0.35009 & 0.11752 & -0.89432 \\ 0.00024 & -0.81129 & -0.49785 & 1.90570 & -1.58477 & 0.22826 & 0.94664 & -1.75554 \\ 0.00020 & 0.10728 & -1.28327 & 1.75901 & -0.94426 & -0.25715 & 0.98224 & -1.00001 \end{bmatrix} \tag{5.40}$$

The resulting upper left sections of the controller matrices $C_c+\delta C$ and $D_c+\delta D$, in Figure 5.12, are given with (5.41)-(5.42).

$$C_c(1:n_{C1}, 1:n_{C2}) + \delta C =$$
$$\begin{bmatrix} -0.10939 & -0.20048 & -0.09820 & -0.01138 & 0.08442 & 0.09001 & -0.00397 & -0.01116 \\ -0.15025 & -0.14197 & -0.15130 & -0.11405 & 0.00375 & 0.09113 & 0.06940 & 0.00018 \\ -0.13251 & -0.12385 & -0.15055 & -0.14236 & -0.11013 & -0.00758 & 0.09243 & 0.07483 \\ 0.25143 & -0.17004 & -0.22075 & -0.15874 & -0.16595 & -0.09135 & 0.09645 & 0.18355 \\ 0.19971 & -0.02978 & -0.15727 & -0.17524 & -0.15776 & -0.13086 & -0.05143 & 0.05616 \end{bmatrix} \tag{5.41}$$

$$D_c(1:n_{D1}, 1:n_{D2}) + \delta D =$$
$$\begin{bmatrix} -0.00652 & 0.11885 & -0.26057 & 1.07935 & -1.12241 & 0.35009 & 0.11752 & -0.89432 \\ 0.00034 & 0.18851 & -0.49775 & 1.90570 & -1.58477 & 0.22826 & 0.94664 & -1.75554 \\ 0.00020 & 0.10738 & -0.28347 & 1.75911 & -0.94426 & -0.25715 & 0.98224 & -1.00001 \end{bmatrix} \tag{5.42}$$

Finally, following **Step 5** of the stabilization algorithm, it can be found that a complete elimination of the 'ears' of the matrices C_c, D_c, and $G_c(z)$ can be done (i.e. λ set to 1), without destabilizing the system, as the resulting maximum closed-loop pole magnitude

[1]Note the magnitude of δD being significantly larger in this case of modification for stabilization than in the cases of modifications for performance illustrated in Section 5.3.2.

is 0.99978. In other words, with the above stabilization algorithm, the maximum closed-loop pole magnitude has been reduced from 1.0004 (unstable system) to 0.99978 (stable system). However, it should be stressed again that the above stabilization procedure is practically never needed for the practical CD control systems, designed with the reasonable (practically acceptable) stability margin.

5.5 Summary

A novel method for modifying a CD control law near spatial domain boundaries that systematically takes into account all the requirements from Chapter 2 has been developed in this chapter. A simulation example, with the use of Honeywell hardware-in-the-loop paper machine simulator, comparing the newly proposed technique with the current industrial practice has also been presented.

The objective of modifying the industrial CD controller near spatial domain boundaries has been posed, in this chapter, in terms of a block-diagonal static output feedback (SOF) compensator design problem. The problem has been solved and the control law modifications computed by implementing a novel low-bandwidth SOF controller design algorithm. The algorithm is implemented sequentially on the existing industrial controller's two constant matrix components. The newly proposed approach systematically takes into account all the closed-loop requirements (stability, performance, and robustness) specified in Chapter 2.

Chapter 6

Industrial Trial

The method for designing CD edge controllers presented in Chapter 5 has been evaluated in an industrial setting. Three different control law modifications (conservative, balanced, and aggressive), δC and δD in Figure 2.7 were computed and implemented during the trial. The mill was producing the paper grade on which the tests were carried out for about 15 hours on the day of the trial. During this period, the trial setup was arranged and the controller testing carried out.

The newly developed approach provides a systematic way of modifying the existing, industrial, CD control law near the sheet edges, guaranteeing the resulting closed-loop system stability, robustness margins, and performance improvement. Considering that the resulting closed-loop system robustness margins near the sheet edges are directly taken into account, the possibility of CD control instability originating from the edges (as illustrated in Figure 1.9) and 'creeping' into the rest of the system is eliminated with the new approach. The new technique has a clear economic benefit for the papermakers, since with a stable, robust, and performance improving control law, the quality of the paper sheet near the edges can be significantly improved. In some papermaking situations, the 'trim squirts' (Figure 1.2) can be moved outward, thus resulting in less paper being trimmed off and more on-spec paper is being produced from which the papermaker can extract his orders.

Two photos of the author taken in the mill where the trial was completed are given in Figure 6.1.

Details regarding the paper machine used for testing, as well as the mill's existing CD control setup, are given in Section 6.1. The overall trial procedure and setup are detailed in Section 6.2. In Section 6.3, the results obtained during the industrial trial are presented.

6.1 CD Control Setup in the Mill

The inaugural test site for the Matlab prototype tuning tool was selected to be a Canadian mill producing a wide variety of paper grades. During the site visit, the mill was producing a 66$[lbs/ream]$ grade paper[1]. The particular paper machine, on which the testing was done, uses slice lip actuators to reduce the variations of the paper sheet cross-directional

[1] 1 $[lbs/ream] = 1.6289\ [gr/m^2]$

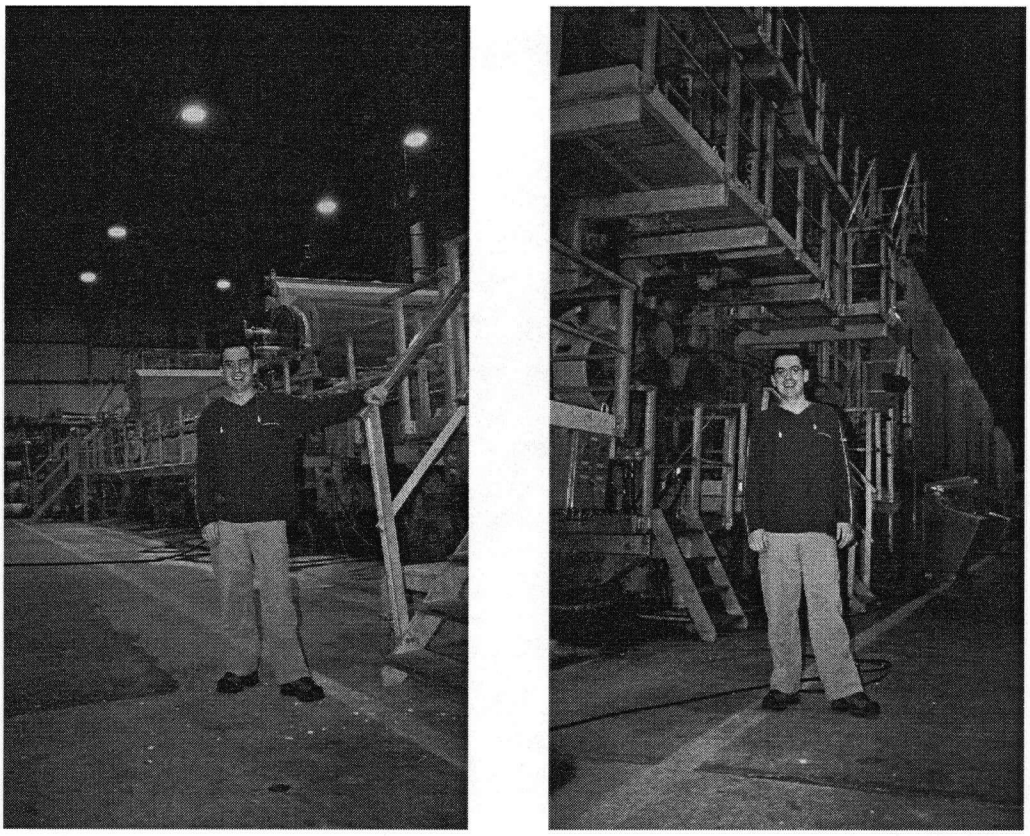

Figure 6.1: Stevo Mijanovic near machine on which the industrial trial was carried out. In the background: machine's forming section (left photo), and the press and dryer sections (right photo).

dry weight[1] profile, as discussed in the Introduction. The machine has 36 actuators spaced on $x_a = 95.6mm$ centres and distributed across the machine width of $3.44m$. The total number of scanner measurement points was 216. High-pressure water jets ('trim squirts' - illustrated in Figure 1.2 in Section 1.1), in the sheet-forming section of the paper machine, were located approximately two actuator zones (or 12 measurement points or $191.2mm$) from the machine edges. As a result of this trimming in the sheet-forming section, of $191.2mm$ wide sheet strips, on both sides of the machine, only the measurement points 13-205 were actual paper sheet measurements (so called 'on-sheet' measurements). Accordingly the actuators 3-34, corresponding to the 'on-sheet' measurements, are called 'on-sheet' actuators. The 'off-sheet' actuators (actuators 1-2 and 35-36) were in open-loop (at constant values) throughout the whole trial. The exact setpoint values for the 'off-sheet' actuators are given in Section 6.3 below. (An illustration of the 'on-sheet' and

[1]Paper sheet dry weight is defined as the sheet basis weight reduced by the water (moisture) content.

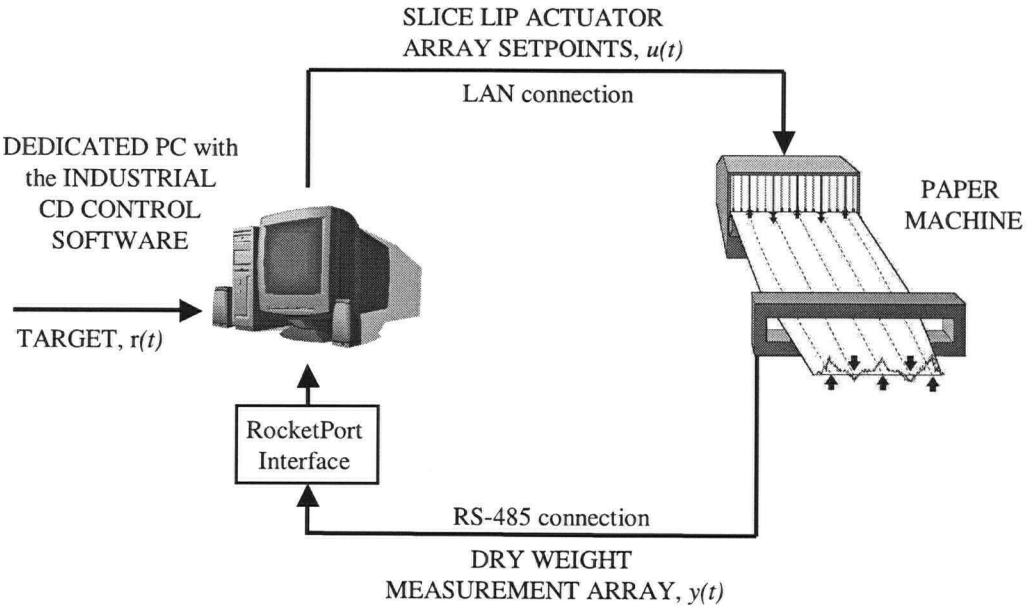

Figure 6.2: A simplified schematic of the mill's CD control setup.

'off-sheet' actuators locations is also given in Figure 1.2.)

The period over which the scanner was making one set of measurements (the control system sampling time) was $T_s = 30s$. A simplified schematic of the mill's CD control system is shown in Figure 6.2 (compare with Figure 1.7 given in Introduction). Slice lip actuators are connected via local LAN connection to a PC with the industrial CD controller software, while the scanning sensor is serially connected via RS-485 connection through a RocketPort interface to a RS-232 connection to computer.

6.2 Trial Setup and Procedure

A simplified schematic of the industrial trial setup is given in Figure 6.3. The mill's existing PC with the industrial CD controller software had to be replaced with the laptop on which the modified industrial controller software had been loaded (Laptop 1 in Figure 6.3). The industrial controller software was modified in order to accommodate the control law changes according to Figure 2.6. The existing control law modifications were computed, based on the approach presented in Chapter 5, using a newly developed Matlab prototype tuning tool. Proper dataflow between the Matlab prototype tuning tool and the industrial software packages (outlined in Figure 6.4), as well as correct implementation of the computed modifications by the industrial control software had previously been thoroughly tested and verified [48].

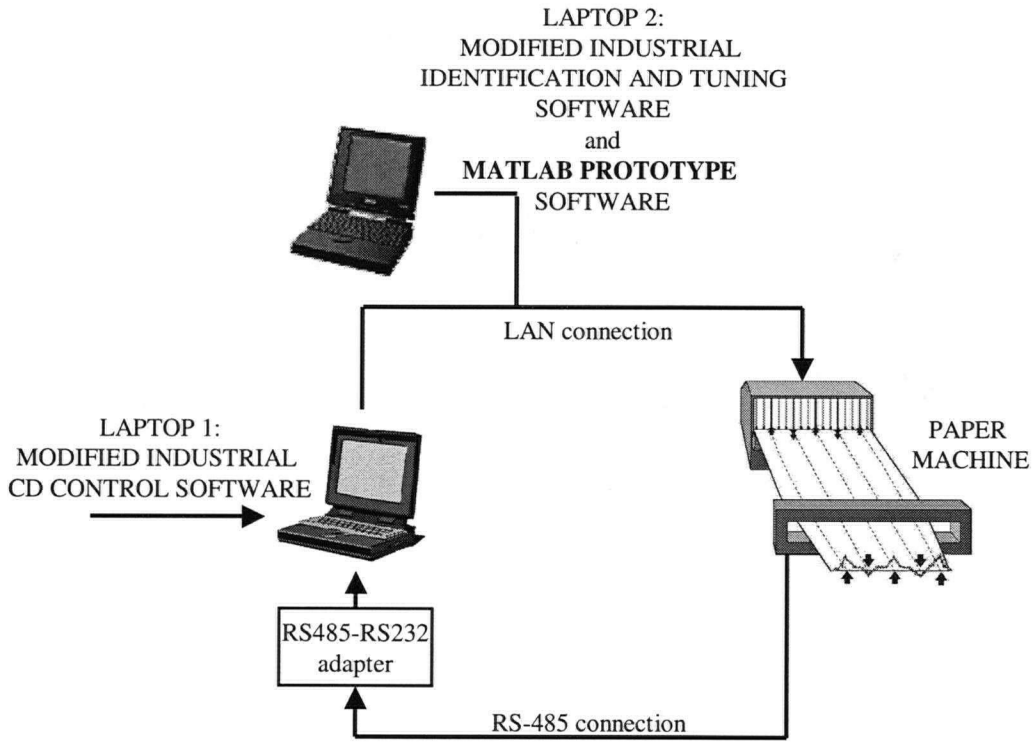

Figure 6.3: A simplified schematic of the industrial trial setup.

The overall procedure followed for the field trial is outlined as follows:

1. All the system parameters, for the particular paper grade being tested, were copied from the mill's PC with the industrial CD controller algorithm (PC in Figure 6.2) onto the laptop computer (Laptop 1 in Figure 6.3) with the specially modified controller algorithm.

2. The control system actuators were placed in open-loop and left at the positions assumed just before taking them out of the closed-loop.

3. The scanner was disconnected from the mill's PC and connected (through a RS485-RS232 adapter) to Laptop 1. It was subsequently confirmed that the communication link between the paper machine scanner and Laptop 1 was working properly and that controller on Laptop 1 was receiving the scanner measurements.

4. The actuator array of the controller on Laptop 1 was verified to be in Manual mode so that a smooth transition from the mill's existing PC to Laptop 1 control software could be ensured. The mill's PC was disconnected from the mill's LAN, thus detaching the paper machine's actuator array from the existing control software

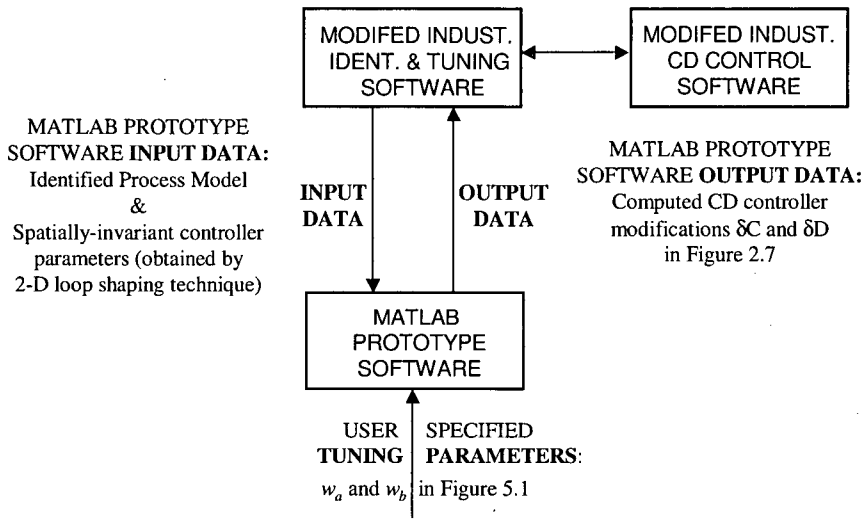

Figure 6.4: The dataflow diagram between the Matlab prototype software and the industrial software packages.

residing on the PC. Afterwards, Laptop 1 (previously having been assigned the same TCP-IP address as the above mentioned PC) was connected onto the local LAN.

5. The communication link between the paper machine actuator array and Laptop 1 control software was checked and confirmed to be working properly. The modified industrial controller software on Laptop 1 was receiving the actuators' current position information.

6. The actuator array was put on control (i.e. in closed-loop) with Laptop 1 controller settings the same as on the mill's industrial controller PC (the setting had been previously copied as outlined in Step 1 above). The control system was left in closed-loop for about an hour, to ensure it operated correctly with Laptop 1 controller software.

7. A local TCP-IP address was assigned to the second laptop computer (Laptop 2 in Figure 6.3) with the industrial CD process identification and controller tuning software [32, 65], as well as the Matlab prototype software for computing controller modifications near the paper sheet edges, as detailed in Chapter 5. Laptop 2 was successfully connected onto the local LAN.

8. The control system actuator array was put in open-loop (off control), and the standard process identification procedure [32] was initiated from Laptop 2. The open-loop 'bump test', with three actuators stepped up (down) for 200 *microns*, was

carried out and process identification and controller tuning completed using the industrial software presented in [32, 65] (see Figure 6.5).

9. The design for various modifications D_e and C_e in Figure 5.5 was completed according to the algorithm outlined in Section 5.2.2, and these parameters were transferred by the modified identification and tuning software on Laptop 2 over the LAN into the correct database location, for use by the modified industrial controller software on Laptop 1. (The dataflow between the Matlab prototype software and the industrial software packages is outlined in Figure 6.4.)

10. The trial control system was put on closed-loop with one of the existing industrial techniques for CD control near the paper sheet edges - average padding. The resulting closed-loop data were logged over the course of about an hour.

11. The three sets of controller modifications (referred to as conservative, balanced, and aggressive), computed in Step 9 above, were implemented in turn (each one over the course of about an hour).
    The data logged in Step 10, with the current industrial technique, and in this step with the three sets of tuning numbers obtained with the new technique are called Data Set 1 in Section 6.3 below.

12. The steps 10-11 above were repeated once more. This logged data are called Data Set 2 (Section 6.3).

13. The control system actuators were put back in open-loop so that a smooth transition back to the mill's existing industrial controller system on the PC could be carried out.

14. The scanner was disconnected from Laptop 1 and connected back to the mill's PC with the industrial CD controller software. Subsequently, Laptop 1 was also disconnected from the local LAN, and the mill's PC connected back thus enabling the communication between the paper machine actuators and the PC with the industrial controller software.

15. After it was confirmed that the communication link between the paper machine and PC was working properly, the control system was put back in closed-loop with the original settings found upon arrival at the mill.

The closed-loop data obtained during the trial procedure, outlined above, are presented and analyzed in Section 6.3.

6.3 Trial Results

In Section 6.3.1, the process and controller parameters, as obtained by the industrial identification and tuning software [32, 65], are presented. The subsequently computed controller modifications δC and δD in (2.21)–(2.22), based on the approach outlined in Chapter 5, are given in Section 6.3.2. Finally, the closed-loop control data obtained during the trial are presented and analyzed in Sections 6.3.3 and 6.3.4.

6.3.1 Process and Controller Parameters

As detailed in Step 8 of the field test trial procedure in Section 6.2, an open-loop 'bump test' with three actuators stepped up (down) for 200 *microns* was carried out. The system scan time (sampling period), as pointed out in Section 6.2, was $T_s = 30s$. The parameters of the process model in (2.10)–(2.11) were identified using software described in [32] with the size of the matrix B in (2.11) band $l_b = 8$ and

$$\begin{aligned} \{b_0, b_1, \ldots, b_8\} &= 10^{-2} \cdot \{0.1362, 0.1033, 0.0216, -0.0364, -0.0302, \\ &\quad -0.0073, 0.0005, 0.0005, 0.0001\} \\ a_0 &= 0.759, \quad d = 2 \end{aligned} \tag{6.1}$$

The process model spatial response identification results are illustrated in Figure 6.5.

Subsequently, the feedback controller $K(z)$ in (2.12) was designed using the standard two-dimensional loop shaping technique [65, 66]. The controller parameters obtained had matrix band sizes $l_c = 4, l_d = 1$, with:

$$\begin{aligned} \{c_0, c_1, c_2, c_3, c_4\} &= \{-0.338689, -0.232651, -0.024331, 0.070768, -0.002905\} \\ \{d_0, d_1\} &= \{0.991399, 0.004301\} \end{aligned} \tag{6.2}$$

The tuning parameter α of the Dahlin controller $c(z)$ in (2.16) was also produced by the two-dimensional loop shaping design: $\alpha = 0.8506$.

6.3.2 Computed Controller Modifications δC and δD

Next, the design for various controller modifications (conservative, balanced, and aggressive tuning) D_e and C_e in Figure 5.5 and described by the algorithm in Section 5.2.2 was completed and these were transferred over the LAN into the correct database location for use by the industrial controller software on Laptop 1 (see Figures 6.3 and 6.4).

In all three cases (conservative, balanced, and aggressive tuning), the sizes of the rectangular weights $W_i, i = 1, \ldots, 7$ in (5.18)–(5.19) were chosen as, $n_{C1} = 5, n_{C2} =$

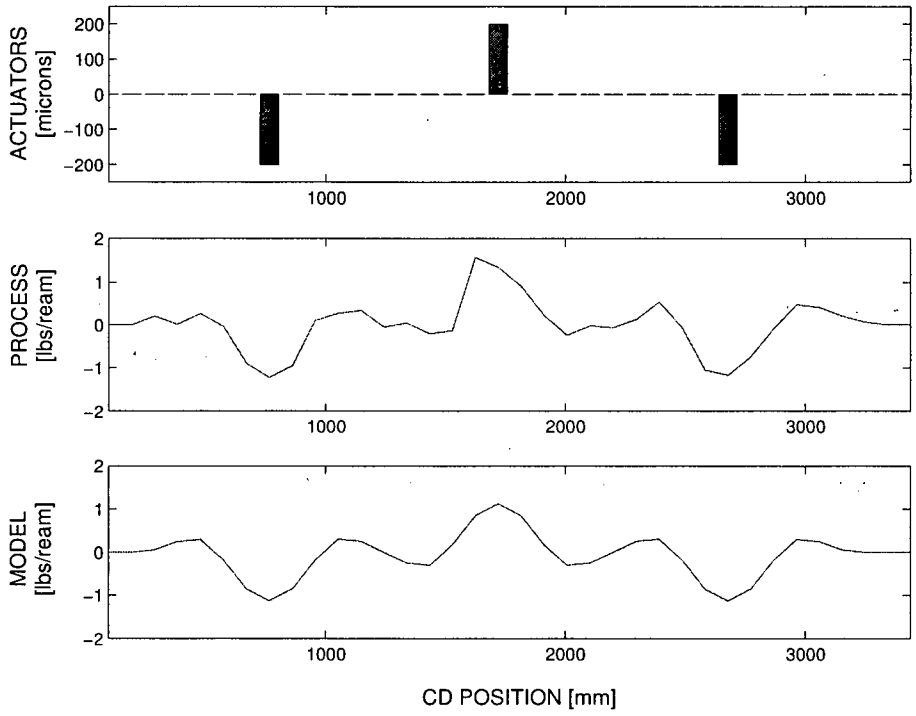

Figure 6.5: Model identification: The upper plot illustrates the shape of the actuator array used for process excitation. The middle plot shows the measured process output profile. The bottom plot illustrates the identified model, as given by the parameters b_j, $j = 0, 1, 2, ..., 8$ in (6.1).

$8, n_{D1} = 3, n_{D2} = 8, n_u = 8, n_d = 8, n_y = 8$. Also, the output vectors $w_a(z)$ and $w_b(z)$ in Figure 5.1 were chosen as:

$$w_a(z) = [k_P \cdot y(z) \;\; u(z)]^T, \qquad w_b(z) = \frac{1}{1 + k_R} \cdot u(z), \tag{6.3}$$

where $y(z)$ and $u(z)$ are the process output and control signal respectively, and coefficients $\mathbf{k_P}$ and $\mathbf{k_R}$ are the **tuning variables**. As explained in more detail in Section 5.3.2, k_P is a closed-loop performance tuning variable, and k_R is a a closed-loop robustness tuning variable. For the CD process model given with (6.1), inverse of the process' maximum singular value at steady-state (i.e. the point of reference for choosing k_P) is $\frac{1}{\bar{\sigma}(G(e^{j0}))} = \frac{1}{0.01674} = 59.74$.

In the case of **conservative tuning**, the tuning variables k_P and k_R in (6.3) were chosen as $\mathbf{k_P = 180}$, $\mathbf{k_R = 0.2}$. Subsequently, using Matlab prototype software, the industrial

controller modifications δC and δD given with (6.4)–(6.5) respectively were obtained.

$$\delta C = \begin{bmatrix} 0.03849 & 0.03452 & 0.00158 & -0.00733 & 0.00579 & 0.00955 & -0.00287 & -0.01349 \\ -0.15373 & -0.00357 & 0.10040 & 0.01442 & -0.08664 & -0.03759 & 0.08151 & 0.11252 \\ 0.01922 & -0.03630 & -0.00537 & 0.02771 & -0.00198 & -0.03342 & 0.00068 & 0.05602 \\ -0.03055 & -0.02833 & 0.11562 & 0.15004 & 0.00179 & -0.11406 & -0.04143 & 0.09988 \\ 0.03328 & -0.08007 & -0.03483 & 0.08597 & 0.08674 & -0.03174 & -0.10293 & -0.05167 \end{bmatrix} \tag{6.4}$$

$$\delta D = \begin{bmatrix} -0.04205 & 0.03983 & -0.03423 & 0.00459 & -0.00329 & 0.00521 & -0.00765 & 0.00119 \\ 0.00652 & -0.05617 & 0.05445 & -0.02583 & 0.00602 & -0.01773 & 0.02016 & -0.00059 \\ 0.01487 & -0.00503 & -0.04141 & 0.03139 & -0.00380 & -0.00736 & -0.01085 & 0.01548 \end{bmatrix} \tag{6.5}$$

The upper left sections of the resulting control law matrices $C_d + \delta C$ and $D_d + \delta D$, in the case of conservative tuning, are given in (6.6)-(6.7).

$$C_d(1 : n_{C1}, 1 : n_{C2}) + \delta C = \begin{bmatrix} -0.30020 & -0.19813 & -0.02275 & 0.06343 & 0.00288 & 0.00955 & -0.00287 & -0.01349 \\ -0.38639 & -0.34226 & -0.13226 & -0.00992 & -0.01588 & -0.04049 & 0.08151 & 0.11252 \\ -0.00511 & -0.26895 & -0.34406 & -0.20494 & -0.02631 & 0.03735 & -0.00223 & 0.05602 \\ 0.04021 & -0.05266 & -0.11703 & -0.18865 & -0.23086 & -0.13839 & 0.02934 & 0.09697 \\ 0.03038 & -0.00930 & -0.05916 & -0.14668 & -0.25195 & -0.26439 & -0.12726 & 0.01910 \end{bmatrix} \tag{6.6}$$

$$D_d(1 : n_{D1}, 1 : n_{D2}) + \delta D = \begin{bmatrix} 0.94935 & 0.04413 & -0.03423 & 0.00459 & -0.00329 & 0.00521 & -0.00765 & 0.00119 \\ 0.01083 & 0.93523 & 0.05875 & -0.02583 & 0.00602 & -0.01773 & 0.02016 & -0.00059 \\ 0.01487 & -0.00073 & 0.94999 & 0.03569 & -0.00380 & -0.00736 & -0.01085 & 0.01548 \end{bmatrix} \tag{6.7}$$

In the case of **balanced tuning**, the tuning variables k_P and k_R in (6.3) were chosen as $\mathbf{k_P = 480}$, $\mathbf{k_R = 0.2}$. Subsequently computed modifications δC and δD are given in

(6.8)–(6.9), respectively.

$$\delta C = \begin{bmatrix} -0.02680 & 0.01935 & 0.00090 & -0.03639 & 0.02692 & 0.01608 & -0.02549 & -0.01109 \\ 0.04499 & -0.09894 & 0.01944 & 0.13122 & -0.12908 & -0.04844 & 0.11027 & 0.04539 \\ 0.03625 & 0.02275 & -0.02307 & -0.00725 & 0.03103 & -0.00458 & -0.01791 & -0.00541 \\ 0.10985 & 0.02207 & -0.00882 & 0.07469 & 0.01370 & -0.02780 & 0.01941 & 0.01187 \\ 0.05526 & 0.07139 & -0.01473 & -0.01478 & 0.08206 & 0.00500 & -0.04921 & -0.01843 \end{bmatrix} \tag{6.8}$$

$$\delta D = \begin{bmatrix} 0.00116 & 0.00256 & -0.00724 & 0.00569 & -0.00653 & 0.00641 & -0.00604 & 0.00284 \\ -0.00272 & -0.00109 & 0.00979 & -0.02097 & 0.02342 & -0.02121 & 0.01315 & 0.00105 \\ 0.00228 & -0.00449 & 0.00189 & 0.00140 & -0.00597 & 0.00740 & -0.00971 & 0.00802 \end{bmatrix} \tag{6.9}$$

The upper left sections of the resulting control law matrices $C_d + \delta C$ and $D_d + \delta D$, in the case of balanced tuning, are given in (6.10)-(6.11).

$$C_d(1 : n_{C1}, 1 : n_{C2}) + \delta C = \begin{bmatrix} -0.36549 & -0.21330 & -0.02343 & 0.03438 & 0.02402 & 0.01608 & -0.02549 & -0.01109 \\ -0.18767 & -0.43763 & -0.21321 & 0.10689 & -0.05831 & -0.05134 & 0.11027 & 0.04539 \\ 0.01192 & -0.20990 & -0.36176 & -0.23990 & 0.00669 & 0.06619 & -0.02081 & -0.00541 \\ 0.18062 & -0.00226 & -0.24147 & -0.26400 & -0.21895 & -0.05213 & 0.09018 & 0.00897 \\ 0.05235 & 0.14216 & -0.03906 & -0.24743 & -0.25663 & -0.22765 & -0.07355 & 0.05234 \end{bmatrix} \tag{6.10}$$

$$D_d(1 : n_{D1}, 1 : n_{D2}) + \delta D = \begin{bmatrix} 0.99256 & 0.00687 & -0.00724 & 0.00569 & -0.00653 & 0.00641 & -0.00604 & 0.00284 \\ 0.00158 & 0.99031 & 0.01409 & -0.02097 & 0.02342 & -0.02121 & 0.01315 & 0.00105 \\ 0.00228 & -0.00019 & 0.99329 & 0.00570 & -0.00597 & 0.00740 & -0.00971 & 0.00802 \end{bmatrix} \tag{6.11}$$

Finally, in the case of **aggressive tuning**, the tuning variables k_P and k_R in (6.3) were chosen as $\mathbf{k_P = 720}$, $\mathbf{k_R = 0.4}$, and the resulting controller modifications δC and

δD are given in (6.12)–(6.13), respectively.

$$\delta C = \begin{bmatrix} -0.09772 & 0.05064 & 0.05991 & -0.06116 & 0.02286 & -0.00860 & -0.04174 & 0.04844 \\ 0.29758 & -0.24731 & -0.16736 & 0.27843 & -0.08941 & 0.01597 & 0.09766 & -0.21222 \\ 0.01688 & 0.06060 & -0.02607 & -0.05450 & 0.01129 & 0.00495 & 0.03017 & 0.03833 \\ 0.20798 & 0.02322 & -0.13026 & 0.02426 & -0.02241 & 0.02265 & 0.11865 & -0.02289 \\ -0.00883 & 0.15726 & 0.00132 & -0.13232 & 0.02982 & 0.00226 & 0.02909 & 0.09746 \end{bmatrix} \tag{6.12}$$

$$\delta D = \begin{bmatrix} 0.00528 & -0.00122 & -0.00434 & 0.00568 & -0.00692 & 0.00658 & -0.00586 & 0.00297 \\ -0.00359 & 0.00428 & 0.00522 & -0.02034 & 0.02512 & -0.02162 & 0.01246 & 0.00124 \\ 0.00102 & -0.00439 & 0.00599 & -0.00146 & -0.00618 & 0.00881 & -0.00960 & 0.00731 \end{bmatrix} \tag{6.13}$$

The upper left sections of the resulting control law matrices $C_d + \delta C$ and $D_d + \delta D$, in the case of aggressive tuning, are given in (6.14)-(6.15).

$$C_d(1 : n_{C1}, 1 : n_{C2}) + \delta C = \begin{bmatrix} -0.43641 & -0.18201 & 0.03558 & 0.00961 & 0.01995 & -0.00860 & -0.04174 & 0.04844 \\ 0.06493 & -0.58600 & -0.40001 & 0.25409 & -0.01864 & 0.01307 & 0.09766 & -0.21222 \\ -0.00745 & -0.17205 & -0.36476 & -0.28715 & -0.01304 & 0.07572 & 0.02726 & 0.03833 \\ 0.27875 & -0.00111 & -0.36291 & -0.31443 & -0.25507 & -0.00169 & 0.18941 & -0.02580 \\ -0.01173 & 0.22803 & -0.02301 & -0.36497 & -0.30886 & -0.23039 & 0.00476 & 0.16822 \end{bmatrix} \tag{6.14}$$

$$D_d(1 : n_{D1}, 1 : n_{D2}) + \delta D = \begin{bmatrix} 0.99668 & 0.00308 & -0.00434 & 0.00568 & -0.00692 & 0.00658 & -0.00586 & 0.00297 \\ 0.00071 & 0.99567 & 0.00952 & -0.02034 & 0.02512 & -0.02162 & 0.01246 & 0.00124 \\ 0.00102 & -0.00009 & 0.99738 & 0.00284 & -0.00618 & 0.00881 & -0.00960 & 0.00731 \end{bmatrix} \tag{6.15}$$

6.3.3 Closed-Loop Control Results: Data Set 1

The Data Set 1 results (Steps 10-11 in the procedure outlined in Section 6.2) are illustrated in Figures 6.6–6.9 and Table 6.1. The closed-loop results obtained using the current industrial practice (with average padding) are shown in Figure 6.6, and the results obtained

with the new technique (conservative, balanced, and aggressive tuning in turn) in Figures 6.7–6.9.

All the plots in Figures 6.6–6.9 were obtained using Honeywell software for paper machine cross-directional control systems data analysis. As detailed in Section 6.2, the closed-loop data was logged over the course of 40-60 *min* for each set of tuning numbers (the existing industrial technique - average padding and the three sets of tuning numbers obtained with the new technique). In other words, between 80-120 scans (as the system sampling time was $T_s = 30s$ as specified in Section 6.3.1) of the closed-loop data in each case. In order to avoid transient effects in changing controller tuning, the data analysis software was used to average the last 20 scans in each case. In each figure, in addition to maximum, minimum, and average signal value, the 2-norm of the corresponding signal is given. Note that in the case of the actuator array profile, only the 2-norm of the on-sheet actuators is given as the off-sheet actuators (2 on each side $u(1:2)$ and $u(35:36)$) were in open-loop and at constant positions throughout the trial: $[u(1); u(2); u(35); u(36)] = [-444.2; -296.4; -271.2; -370.8]$.

From Figures 6.6–6.9 and Table 6.1, it can be seen that in the cases of the balanced and aggressive tunings with the new technique, the paper sheet variations are smaller than with the existing industrial technique and this improvement was achieved with smaller control signals (i.e. actuator usage). For example, in the case of balanced tuning, the paper sheet **dry weight variations** are **reduced by 5.8%** with the **overall control signal magnitude reduced by 9.4%**. The difference between the control signal magnitudes is even more dramatic if only the first (and last) 5 on-sheet actuators are compared ($u(3:7)$ and $u(30:34)$ respectively in Table 6.1) since these are the actuators directly modified with the new technique[1]. In the case of conservative tuning, as expected, the sheet variations are larger than those obtained with the existing technique. This is not surprising since a significantly smaller actuator usage is invoked, particularly near the left edge (see $u(3:7)$ in Table 6.1). It can also be noticed that, in the case of aggressive tuning, the sheet variations are the same as those obtained with the balanced tuning. Obviously for the particular process model and process output disturbance encountered during the trial, making the CD controller modifications near the sheet edges more aggressive than those obtained with the balanced tuning (given with (6.8)–(6.9)) is not warranted.

[1]Partitioning the process output in the same way would not be appropriate since considering the identified process model given with (6.1), 5 edge actuators on each side directly influence the process output across 13 zones on the corresponding side. As a result, a total of 26 (out of 32) zones are directly affected by the modified actuator zones.

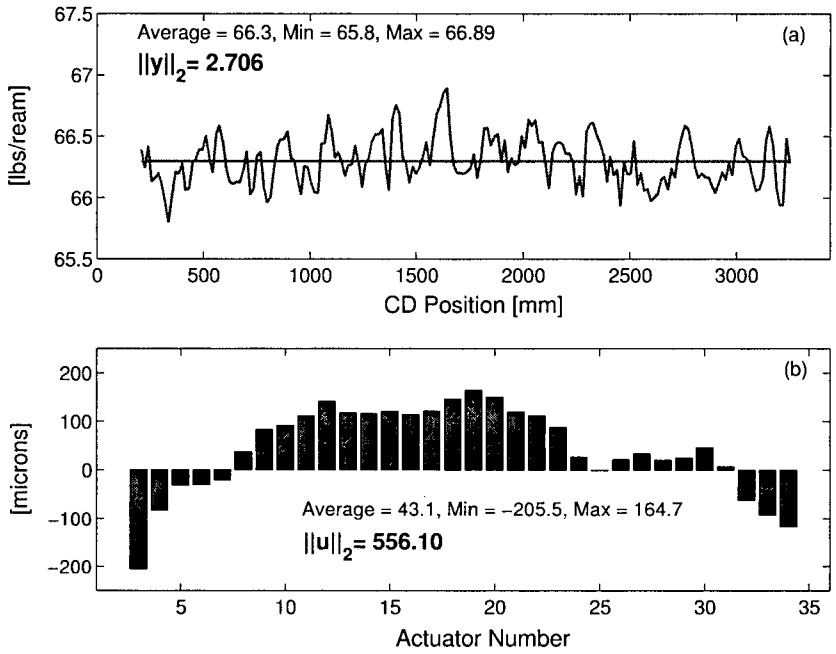

Figure 6.6: Data set 1 process output (a) and control signal (b), using the current industrial technique - average padding.

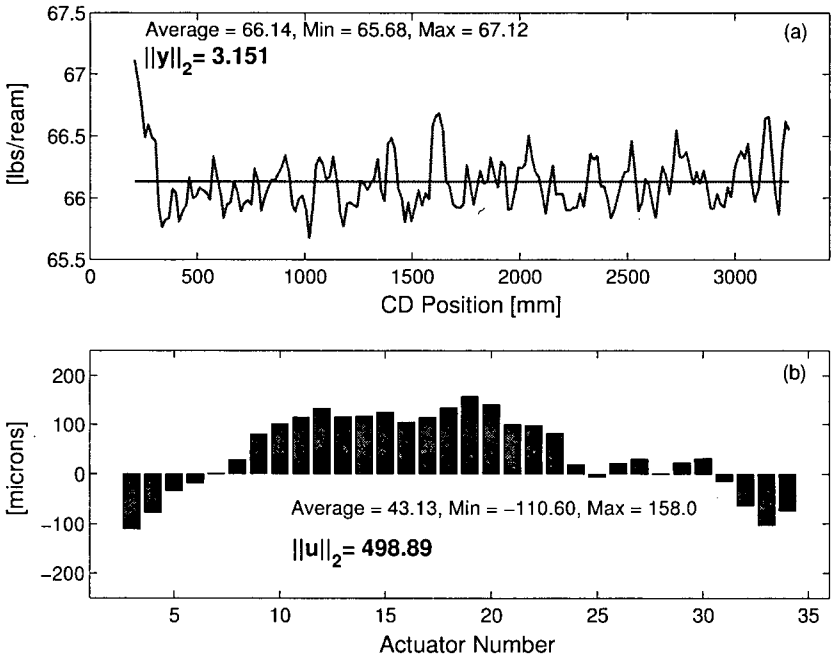

Figure 6.7: Data Set 1 process output (a) and control signal (b), using the new technique - conservative tuning ($k_P = 180$ and $k_R = 0.2$ in (6.3)).

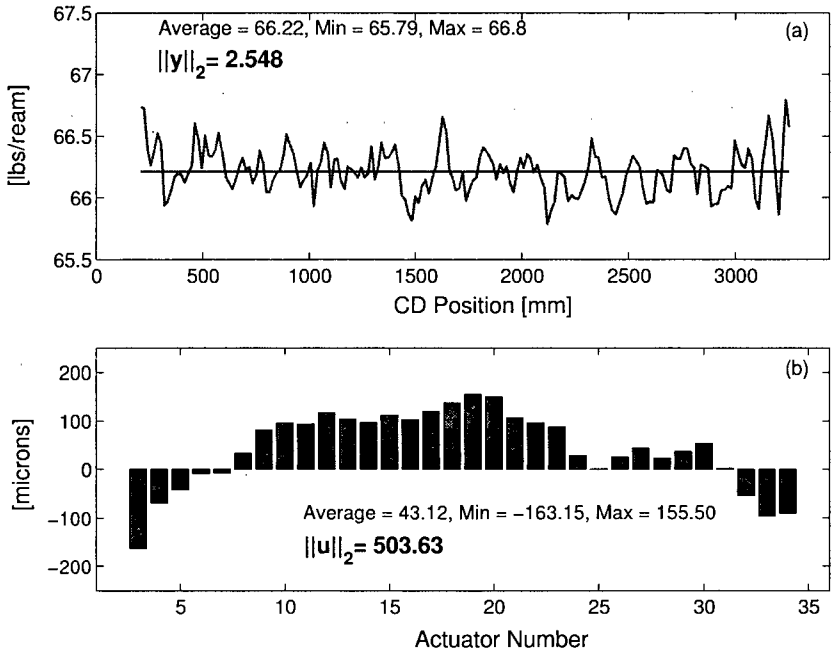

Figure 6.8: Data Set 1 process output (a) and control signal (b), using the new technique - balanced tuning ($k_P = 480$ and $k_R = 0.2$ in (6.3)).

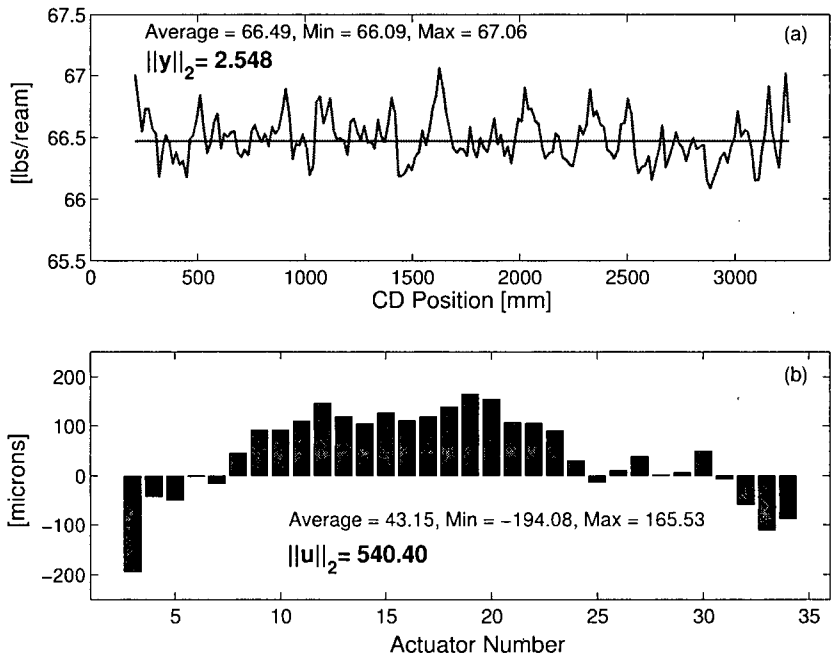

Figure 6.9: Data Set 1 process output (a) and control signal (b), using the new technique - aggressive tuning ($k_P = 720$ and $k_R = 0.4$ in (6.3)).

	Current technique	**New approach**		
	Average padding	Conservative tuning: $k_P = 180$ $k_R = 0.2$	Balanced tuning: $k_P = 480$ $k_R = 0.2$	Aggressive tuning: $k_P = 720$ $k_R = 0.4$
$\|\|y\|\|_2$ [lbs/ream]	**2.706**	**3.151**	**2.548**	**2.548**
$\|\|u(3:34)\|\|_2$ [microns]	**556.10**	**498.89**	**503.63**	**540.40**
On-sheet actuator array sections				
$\|\|u(3:7)\|\|_2$ [microns]	**226.91**	**140.38**	**182.44**	**205.42**
$\|\|u(8:29)\|\|_2$ [microns]	478.16	456.06	444.26	473.00
$\|\|u(30:34)\|\|_2$ [microns]	**169.22**	**145.61**	**151.64**	**161.58**

Table 6.1: 2-norms of the process output and control signal profiles shown in Figures 6.6 – 6.9 (Data Set 1).

6.3.4 Closed-Loop Control Results: Data Set 2

The Data Set 2 results (Step 12 in the procedure outlined in Section 6.2) are illustrated in Figures 6.10–6.13 and Table 6.2. The closed-loop results obtained using the current industrial practice (with average padding) are illustrated in Figure 6.10, and the results obtained with the new technique (conservative, balanced, and aggressive tuning in turn) in Figures 6.11–6.13.

The data is analyzed in the same way (using the Honeywell cross-directional control data analysis software) as Data Set 1 (Section 6.3.3). The off-sheet actuators were again in open-loop and at the constant positions: $[u(1); u(2); u(35); u(36)] =$ $[-444.2; -296.4; -271.2; -370.8]$.

From Figures 6.10–6.13 and Table 6.2, it can be noticed that the results are similar to those from Data Set 1, presented in Section 6.3.3. The paper sheet dry weight variations are again reduced by using the new technique with balanced and aggressive tunings in comparison to the existing industrial practice. In this data set, the **sheet variations are reduced by 8.7% with a reduction of the control signal magnitude by 5.5%** by using the balanced tuning in comparison to the existing industrial practice (see Table 6.2). However, while smaller than the variations resulting from the use of the existing industrial technique, the variations obtained with the aggressive tuning are larger than those obtained with the balanced tuning. This confirms as has been stated in Section 6.3.3, that for the particular process and disturbance characteristics encountered on the day of trial, making the CD control law modifications near the sheet edges more aggressive than those obtained with the balanced tuning (given with (6.8)–(6.9)) is not warranted. Also, as expected, in the case of conservative tuning, the sheet dry weight variations are larger

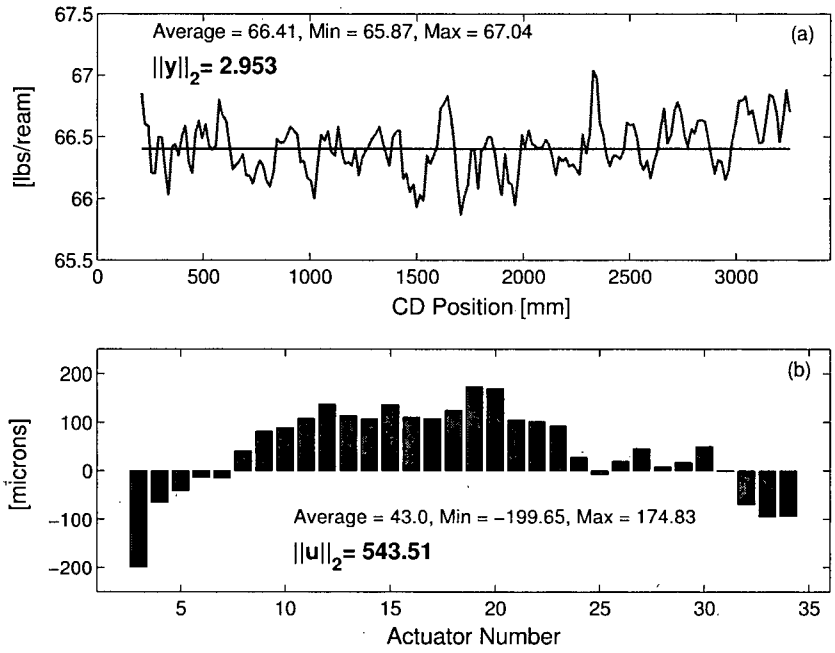

Figure 6.10: Data Set 2 process output (a) and control signal (b), using the current industrial technique - average padding.

in comparison to the existing technique, although the actuator usage level is significantly lower (Table 6.2).

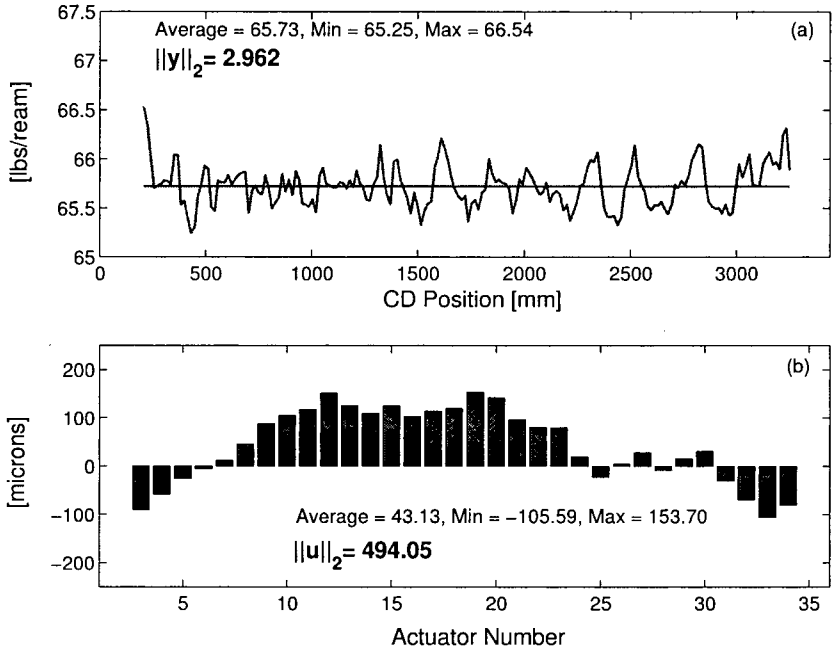

Figure 6.11: Data Set 2 process output (a) and control signal (b), using the new technique - conservative tuning ($k_P = 180$ and $k_R = 0.2$ in (6.3)).

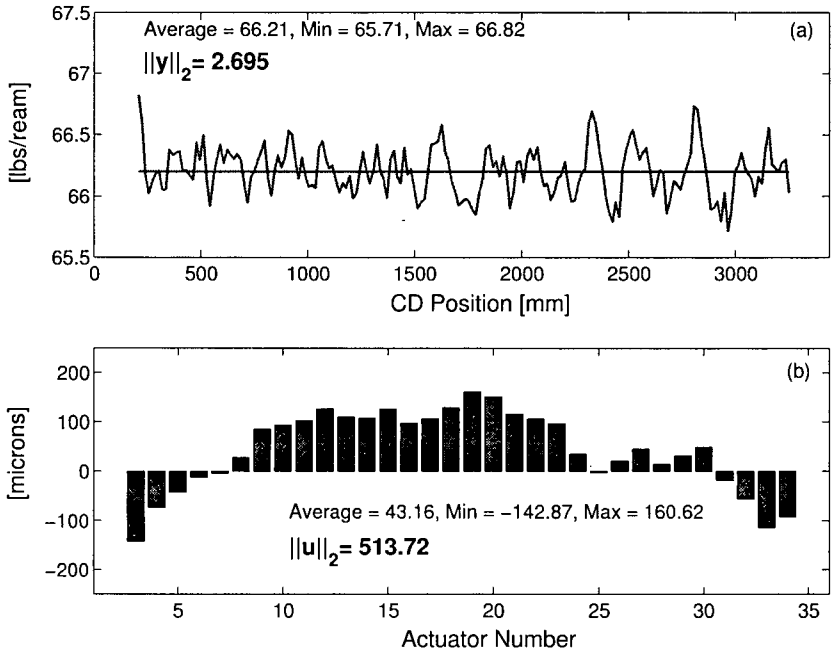

Figure 6.12: Data Set 2 process output (a) and control signal (b), using the new technique - balanced tuning ($k_P = 480$ and $k_R = 0.2$ in (6.3)).

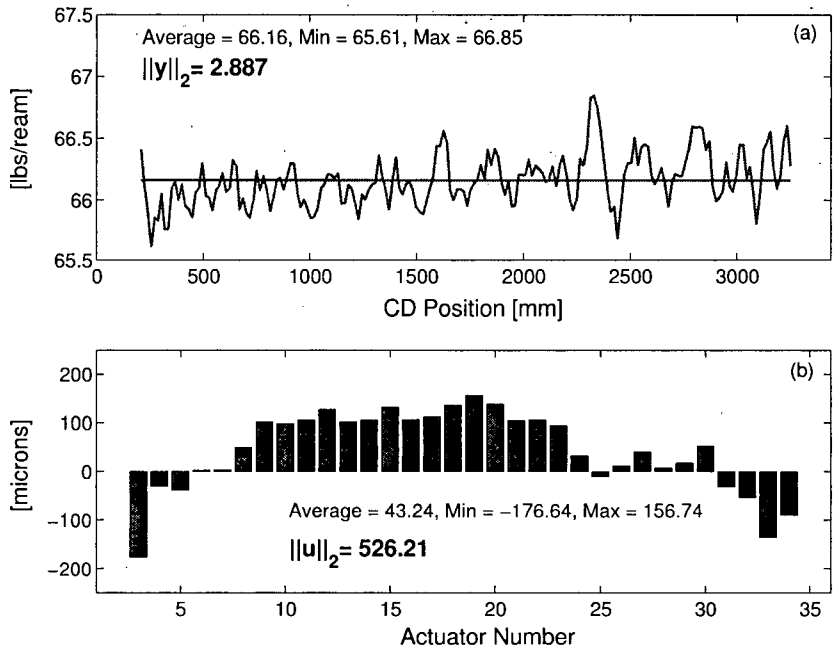

Figure 6.13: Data Set 2 process output (a) and control signal (b), using the new technique - aggressive tuning ($k_P = 720$ and $k_R = 0.4$ in (6.3)).

	Current technique	**New approach**		
	Average padding	Conservative tuning: $k_P = 180$ $k_R = 0.2$	Balanced tuning: $k_P = 480$ $k_R = 0.2$	Aggressive tuning: $k_P = 720$ $k_R = 0.4$
$\|\|y\|\|_2$ [lbs/ream]	**2.953**	**2.962**	**2.695**	**2.887**
$\|\|u(3:34)\|\|_2$ [microns]	**543.51**	**494.05**	**513.72**	**526.21**
On-sheet actuator array sections				
$\|\|u(3:7)\|\|_2$ [microns]	**214.79**	**111.12**	**166.98**	**183.46**
$\|\|u(8:29)\|\|_2$ [microns]	473.39	455.90	456.7	458.29
$\|\|u(30:34)\|\|_2$ [microns]	**158.65**	**155.34**	**165.67**	**182.24**

Table 6.2: 2-norms of the process output and control signal profiles shown in Figures 6.10 – 6.13 (Data Set 2).

6.4 Summary

A novel technique for modifying the industrial CD controllers near spatial domain boundaries, developed in Chapter 5, has been successfully tested in a working paper mill and the results are presented in this chapter. The trial was carried out on a paper machine CD control system with slice lip actuators controlling the paper sheet dry weight profile.

This trial demonstrates that with the new approach it is possible to achieve a successful trade-off between the CD control system closed-loop performance and the required control signal magnitude. In other words, the level of the resulting CD control law 'aggressiveness' near the sheet edges can be chosen with the new approach.

The new technique was also compared with the existing industrial practice, and a better performance with smaller control signal magnitude was achieved by implementing the newly developed technique.

Paper sheet quality improvement, achieved with a stable and robust control law near the sheet edges (as provided with the newly developed technique), has a clear economic benefit for the papermakers. In some papermaking situations, the 'trim squirts' (Figure 1.2) can be moved outward, thus resulting in less paper being trimmed off and more on-spec paper is being produced from which the papermaker can extract his orders.

Chapter 7

Concluding Remarks

This work has focused on modifying an existing industrial paper machine cross-directional control law near spatial domain boundaries (paper sheet edges). As the process spatial-invariance assumption (i.e. neglecting of paper sheet edges) is central to the current industrial controller tuning technique, thus computed CD control laws have to be modified near spatial domain boundaries before implementation on a paper machine. A brief review of the motivation, objectives, approaches, and results presented in this thesis is given below.

7.1 Summary of the Thesis

It is illustrated in Chapter 1, that paper machine CD control systems belong to a set of large, multivariable, spatially-distributed control systems. The task of a particular cross-directional actuator array, on a paper machine, is to reduce the variations of the corresponding paper sheet property (weight, moisture content, or caliper) as much as possible in the cross-direction. Depending on the installation, the number of CD actuators (inputs) in an array is between 30–300 and the number of measurement points (outputs) 200–2000. The most frequently used types of CD actuators, various CD control techniques, and the problems encountered near the sheet edges are illustrated in Chapter 1.

In Chapter 2, it is shown that the CD process and industrial controller models can be viewed as two dimensional (spatio-temporal) filters, causal in temporal and non-causal in spatial (cross-direction) domain. The two-dimensional loop shaping technique (briefly outlined in this Chapter 2), being used for tuning the industrial CD control systems, assumes idealized spatially-invariant CD process characteristics. As a result, the computed CD control law is also spatially-invariant. Indeed the spatial-invariance assumption is common to many of the recently developed techniques for the analysis and controller synthesis of spatially-distributed systems. The controllers obtained by the implementation of these techniques are generally spatially-invariant. In the case of paper machine CD control, spatial invariance is equivalent to assuming that a paper machine produces a tube rather than a sheet of paper. Since the paper machine edges represent a clear disruption of the assumed spatial-invariance, the control laws obtained by the two-dimensional loop shaping technique must be modified near the sheet edges before being implemented on the paper machine. Current industrial practice addressing these issues is based on techniques

for extending finite-width signals, that have been borrowed from signal processing. Such methods very often result in poor control near the edges. The object of this work, discussed in Chapter 2, is a modification of the existing industrial CD control law near spatial domain boundaries, considering relevant control engineering criteria (closed-loop stability, performance, and robustness), without a change in the controller structure and/or complexity.

In Chapter 3, a straightforward perturbation technique with which a controller stabilizing one plant may be modified so that it stabilizes a second, related, plant is presented. The technique is based on the known difference between the two plants, and it is shown that various application examples (other than CD control) can be viewed in terms of this result. While the implementation of the proposed technique, in the case of the initially designed spatially-invariant CD control law, is very simple, and the resulting closed-loop stability guaranteed, it does not, however, address other important requirements - performance, robustness, and the desired preservation of the existing CD controller structure.

Considering that CD controllers are essentially two dimensional low-pass filters and the paper sheet edges are clear spatial domain discontinuities, a similarity between the effects occurring near the sheet edges in the industrial CD control systems and the well-known Gibbs effect, is observed in Chapter 4. Subsequently, a CD control law modification technique, based on methods for reducing the Gibbs effect, is presented. The technique, which does not change the structure of the CD controller, guarantees the resulting CD controller stability. As illustrated in a simulation example in Chapter 4, the approach eliminates the 'actuator picketing' near the sheet edges. However, the resulting closed-loop performance and robustness are not systematically considered with this approach, and closed-loop stability has to be verified after the modifications have been carried out.

Modification of the CD control law, while taking into account relevant control engineering criteria (closed-loop stability, performance, and robustness), and without changing the controller structure or complexity, is presented in Chapter 5. All the requirements from Chapter 2, have thus been taken into account with this approach. Modifications to the two constant controller matrices are computed by the sequential implementation of a novel low-bandwidth static output feedback design algorithm. It is demonstrated, using the Honeywell hardware-in-the-loop simulator example, that a successful trade-off between the performance and the corresponding actuator array signal magnitude can be achieved using the newly proposed approach.

The technique presented in Chapter 5 was successfully tested in a paper mill on a paper machine. The trial was carried out at a Canadian mill, with the slice lip actuator array being used for controlling the paper sheet CD weight profile. Based on the algorithm developed in Chapter 5, Matlab prototype software was developed for computing the CD

controller modifications near the sheet edges. The industrial controller algorithm was also modified so that the computed control law modifications could be implemented and tested. The field trial results are given in Chapter 6. As predicted by the hardware-in-the-loop simulator example, it was possible to achieve a trade-off between the performance and the corresponding control signal magnitude during the industrial trial. Also, the final product (paper sheet) quality was improved and the actuator usage reduced, with the new technique in comparison to the results obtained with the industrial state-of-the-art practice. It is also particularly important to notice that, in contrast to the existing industrial techniques, the developed approach provides a systematic way of modifying the existing CD control law near the sheet edges, taking into account important control engineering criteria. The new approach guarantees the resulting closed-loop system stability, as well as robustness margins, as measured by the $\mathcal{H}_\infty$ norm of the gain from the process output disturbance to control signal. The performance improvement, as measured by the Frobenius norm of the gain from the process output disturbance to the process output, at low frequencies, is also guaranteed with the new approach.

7.2 Future Work

Some of the possible research directions directly related to the work presented in this thesis are outlined below.

Modelling of CD processes near the sheet edges with the CD process parameters from the centre of the sheet and Dirichlet boundary conditions is currently accepted industrial practice. Obviously, a more accurate identification of CD processes near spatial domain boundaries would allow for even better CD control. In particular, the use of more accurate process models in conjunction with the closed-loop approach technique presented here should result in a better CD control.

The transfer functions that define linear fractional transformation used in the closed-loop approach initially have a lot of insignificant states (related to the centre of sheet), subsequently eliminated by the use of Hankel singular values. Since state elimination (i.e. dynamical order reduction) could require a considerable computational effort (particularly in the case of very wide paper machines), a better way of eliminating (or even not including in the first place) insignificant states would be of clear benefit.

As pointed out in Chapters 5 and 6, two tuning variables (k_P and k_R) were used in the newly proposed closed-loop approach to modifying industrial CD controller near spatial domain boundaries. This work provided guidelines for choosing the values of these variables. Further analysis of the influence k_P and k_R have on the resulting closed-loop system behavior in case of various industrial CD process and controller parameters

would certainly be beneficial. An interesting question would be, for example, the point of reference for k_P. In this work, the process maximum singular value at steady-state was used as the point of reference. An additional analysis and research in this direction should result in the development of more exact guidelines for choosing the values of tuning variables, which would particularly be useful for non-expert users. This, in turn, would make the new approach (i.e. tuning tool based on it) easily implementable on the existing CD control systems worldwide.

Bibliography

[1] Calculation and partitioning of variance using paper machine scanning sensor measurements. Technical information paper TIP 1101-01, Technical Association of the Pulp and Paper Industry, 1996.

[2] V.M. Adamjan, D.Z. Arov, and M.G. Krein. Infinite block Hankel matrices and related extension. *American Math. Society Transactions*, 111:133–156, 1978.

[3] B.D.O. Anderson. From Youla-Kucera to identification, adaptive and nonlinear control. *Automatica*, 34(12):1485–1506, December 1998.

[4] A.C. Antoulas. Approximation of linear operators in the 2-norm. *Linear Algebra and its Applications*, 278:309–316, 1998.

[5] A.C. Antoulas. Approximation of linear dynamical systems. *Wiley Encyclopedia of Electrical and Electronics Engineering*, 11:403–422, 1999.

[6] J.U. Backstrom, C. Gheorghe, G.E. Stewart, and R. Vyse. Constrained model predictive control for cross-directional multi-array processes. *Pulp & Paper Canada*, 102(5):T128–T131, May 2001.

[7] J.U. Backstrom, B. Henderson, and G.E. Stewart. Identification and multivariable control of supercalenders. In *Proc. of Control Systems*, pages 85–91, Stockholm, Sweden, June 2002.

[8] B. Bamieh, F. Paganini, and M. Dahleh. Distributed control of spatially invariant systems. *IEEE Trans. on Automatic Control*, 47(7):1091–1107, July 2002.

[9] R.D. Braatz and J.G. VanAntwerp. Robust cross-directional control of large scale paper machines. In *Proc. of IEEE Conference on Control Applications*, pages 155–160, Dearborn, September 1996.

[10] K. W. Corscadden and S. R. Duncan. The use of basis function expansions to analyze the robustness of cross-directional control systems. In *Proc. of American Control Conference*, pages 1478–1482, Albuquerque, New Mexico, June 1997.

[11] R. F. Curtain and H. J. Zwart. *An Introduction to Infinite-Dimensional Linear Systems Theory.* Springer-Verlag, New York, 1995.

[12] K. Cutshall. Cross-direction control. In *Paper Machine Operations, Pulp and Paper Manufacture, 3rd ed., vol.7*, pages 472–506, Atlanta and Montreal, 1991.

[13] R. D'Andrea. A linear matrix inequality approach to decentralized control of distributed parameter systems. In *Proc. of American Control Conf.*, pages 1350–1354, Philadelphia, Pennsylvania, June 1998.

[14] R. D'Andrea. Linear matrix inequalities, multidimensional system optimization, and control of spatially distributed system: An example. In *Proc. of American Control Conf.*, pages 2713–2717, San Diego, CA, USA, June 1999.

[15] R. D'Andrea and G.E. Dullerud. Distributed control design for spatially interconnected systems. *IEEE Trans. on Automatic Control*, 48(9):1478–1495, September 2003.

[16] M.M. Daniel and A.S. Willsky. Efficient implementation of 2-D noncausal IIR filters. *IEEE Trans. Circuits and Systems*, 44(7):549–563, July 1997.

[17] S. R. Duncan and G. F. Bryant. The spatial bandwidth of cross-directional control systems for web processes. *Automatica*, 33(2):139–153, February 1997.

[18] S.R. Duncan. *The cross-directional control of web forming processes.* PhD thesis, University of London, UK, 1989.

[19] S.R. Duncan. The design of robust cross-directional control systems for paper making. In *Proc. of American Control Conference*, Seattle, WA, June 1995.

[20] J. Fan. *Model Predictive Control for Multiple Cross-Directional Processes: Analysis, Tuning, and Implementation.* PhD thesis, University of British Columbia, BC, Canada, 2003.

[21] J. Fan and G. A. Dumont. A novel model reduction method for sheet forming processes using wavelet packets. In *Proc. of IEEE Conference on Decision and Control*, pages 4820–4825, Orlando, FL, USA, December 2001.

[22] J. Fan, G. E. Stewart, and G. A. Dumont. Model predictive cross-directional control using a reduced model. In *Proc. of Control Systems*, pages 65–69, Stockholm, Sweden, June 2002.

[23] A.P. Featherstone, J.G. VanAntwerp, and R.D. Braatz. *Identification and Control of Sheet and Film Processes.* Springer-Verlag, London, 2000.

[24] J. M. Fowler and R. D'Andrea. Distributed control of close formation flight. In *Proc. of IEEE Conference on Decision and Control*, pages 2972–2977, Las Vegas, Nevada, USA, December 2002.

[25] G. Gavelin. *Paper Machine Design and Operation - Descriptions and Explanations.* Angus Wilde Publications, Vancouver and Bellingham, 1998.

[26] K. Glover. All optimal hankel-norm approximations of linear multivariable systems and their L^∞ -error bounds. *International Journal of Control*, 39:1115–1193, 1984.

[27] G.H. Golub and C.F. Van Loan. *Matrix Computations.* Johns Hopkins University Press, Baltimore, Maryland, 3rd edition, 1996.

[28] R.C. Gonzales and P. Wintz. *Digital Image Processing.* Addison-Wesley Publishing Company, second edition, 1987.

[29] G.C. Goodwin, S.F. Graebe, and M.E. Salgado. *Control System Design.* Prentice Hall, Inc., Upper Saddle River, New Jersey, 2001.

[30] D.M. Gorinevsky, M. Heaven C.H. Alexander, M. Kean, and S. Morgan. New algorithms for intelligent identification of paper alignment and nonlinear shrinkage. In *Control Systems 96*, Halifax, NS, Canada, 1996.

[31] D.M. Gorinevsky, S. Boyd, and G. Stein. Optimization-based tuning of low-bandwidth control in spatially distributed systems. In *Proc. of American Control Conference*, pages 2658–2663, Denver, Colorado, USA, June 2003.

[32] D.M. Gorinevsky and C. Gheorghe. Identification tool for cross-directional processes. *IEEE Trans. on Control Systems Technology*, 11(5):629–640, September 2003.

[33] D.M. Gorinevsky, E.M. Heaven, and R.N. Vyse. Performance analysis of cross-directional control using multivariable and spectral models. *IEEE Trans. on Control Systems Technology*, July 2000.

[34] D.M. Gorinevsky, T. Hyde, and C. Cabuz. Distributed shape control of lightweight space reflector structure. In *Proc. of IEEE Conference on Decision and Control*, pages 3850–3855, Orlando, Florida, USA, December 2001.

[35] D.M. Gorinevsky and G. Stein. Structured uncertainty analysis of robust stability for multidimensional array systems. *IEEE Trans. on Automatic Control*, 48(9):1557–1568, September 2003.

[36] R.M. Gray. Toeplitz and circulant matrices: A review. http://www-isl.stanford.edu/ gray/toeplitz.pdf, Department of Electrical Engineering, Stanford University, California, Rev. 2002.

[37] A.N. Gundes. Stabilizing controller design for linear systems with sensor or actuator failure. *IEEE Trans. Automat. Contr.*, 39(6):1224–1230, June 1994.

[38] W. P. Heath. Orthogonal functions for cross-directional control of web forming processes. *Automatica*, 32(2):183–198, 1996.

[39] M. Hovd and S. Skogestad. Sequential design of decentralized controllers. *Automatica*, 30(10):1601–1607, 1994.

[40] R. Iserman, R. Schwarz, and S. Stolzl. Fault-tolerant drive-by-wire systems. *IEEE Control Systems Magazine*, 22(5):64–81, October 2002.

[41] A.J. Jerri. *The Gibbs Phenomenon in Fourier Analysis, Splines, and Wavelet Approximations.* Kluwer Academic Publishers, 1998.

[42] K. Kristinsson and G. A. Dumont. Cross-directional control on paper machines using gram polynomials. *Automatica*, 32(4):533–548, 1996.

[43] K.E. Kwok, M. Chong-Ping, and G.A. Dumont. Seasonal model based control of processes with recycle dynamics. *Industrial & Engineering Chemistry Research*, 40(7):1633–1640, April 2001.

[44] C. Langbort and R. D'Andrea. Imposing boundary conditions for a class of spatially-interconnected systems. In *Proc. of American Control Conference*, pages 107–112, Denver, Colorado, USA, June 2003.

[45] D.L. Laughlin, M. Morari, and R.D. Braatz. Robust performance of cross-directional basis-weight control in paper machines. *Automatica*, 29(6):1395–1410, June 1993.

[46] K. Li, E.B. Kosmatopoulos, P.A. Ioannou, and H. Ryaciotaki-Boussalis. Large segmented telescopes. *Control Systems Magazine*, 20(5):59–72, October 2000.

[47] The MathWorks. *Signal Processing Toolbox.* 2000.

[48] S. Mijanovic. Verification of Performance CD algorithms using IMAP saved parameters. Technical report, Honeywell Process Solutions - North Vancouver, July 2003.

[49] S. Mijanovic, G.E. Stewart, G.A. Dumont, and M.S. Davies. $\mathcal{H}_\infty$ robustification of a paper machine cross-directional control system. In *Proc. of American Control Conference*, pages 2203–2209, Arlington, VA, USA, June 2001.

[50] S. Mijanovic, G.E. Stewart, G.A. Dumont, and M.S. Davies. Stability-preserving modification of paper machine cross-directional control near spatial domain boundaries. In *Proc. of IEEE Conference on Decision and Control*, pages 4113–4119, Las Vegas, Nevada, USA, December 2002.

[51] S. Mijanovic, G.E. Stewart, G.A. Dumont, and M.S. Davies. A controller perturbation technique for transferring closed-loop stability between systems. *Automatica*, 39(10):1783–1791, October 2003.

[52] S. Mijanovic, G.E. Stewart, G.A. Dumont, and M.S. Davies. Design of an industrial distributed controller near spatial domain boundaries. In *American Control Conference*, Boston, MA, USA (to appear), June 2004.

[53] S. Mijanovic, G.E. Stewart, G.A. Dumont, and M.S. Davies. Paper machine cross-directional control near the sheet edges. In *Control Systems*, Quebec City, QC, Canada (to appear), June 2004.

[54] M. Morari and E. Zafiriou. *Robust Process Control.* Prentice-Hall, Inc., New Jersey, 1989.

[55] J. Morud and S. Skogestad. Dynamic behaviour of integrated plants. *Journal of Process Control*, 6(2/3):145–156, 1996.

[56] A.W. Saif, D.W. Gu, D. Kavranoglu, and I. Postlethwaite. Simultaneous stabilization of MIMO systems via robustly stabilizing a central plant. *IEEE Trans. Automat. Contr.*, 47(2):363–369, February 2002.

[57] C. Scali and F. Ferrari. Performance of control systems based on recycle compensators in integrated plants. *Journal of Process Control*, 9(5):425–437, October 1999.

[58] S. Skogestad and I. Postlethwaite. *Multivariable feedback control: analysis and design.* Wiley, New York, 1996.

[59] O.J.M. Smith. Closer control of loops with dead time. *Chemical Engineering Progress*, 53(5):217–219, May 1957.

[60] O.J.M. Smith. *Feedback Control Systems.* McGraw-Hill, New York, 1958.

[61] G.A. Smook. *Handbook for Pulp & Paper Technologists.* Angus Wilde Publications, Vancouver and Bellingham, 2nd. edition, 1994.

[62] G.E. Stewart. *Two dimensional loop shaping controller design for paper machine cross-directional processes.* PhD thesis, University of British Columbia, BC, Canada, 2000.

[63] G.E. Stewart. Analysis and design of boundary conditions for a spatially distributed control system. Technical report, Honeywell, February 2001.

[64] G.E. Stewart, P. Baker, D.M. Gorinevsky, and G.A. Dumont. Experimental demonstration of recent results for spatially distributed control systems. In *Proc. of American Control Conf.*, pages 2216–2221, Arlington, VA, USA, June 2001.

[65] G.E. Stewart, D.M. Gorinevsky, and G.A. Dumont. Feedback controller design for a spatially-distributed system: The paper machine problem. *IEEE Trans. on Control Systems Technology*, 11(5):612–628, September 2003.

[66] G.E. Stewart, D.M. Gorinevsky, and G.A. Dumont. Two-dimensional loop shaping. *Automatica*, 39(5):779–792, May 2003.

[67] G. Strang and T. Nguyen. *Wavelets and Filter Banks.* Wellesley - Cambridge Press, 1996.

[68] W.A. Strauss. *Partial Differential Equations: An Introduction.* Wiley, New York, 1992.

[69] V.L. Syrmos, C.T. Abdallah, P. Dorato, and K. Grigoriadis. Static output feedback - a survey. *Automatica*, 33(2):125–137, February 1997.

[70] O. Taiwo and V. Krebs. Robust control system design for plants with recycle. *The Chemical Engineering Journal*, 61(1):1–6, January 1996.

[71] T.T. Tay, I.Mareels, and J.B. Moore. *High Performance Control.* Birkhauser, Boston, 1998.

[72] T.T. Tay, J.B. Moore, and R. Horowitz. Indirect adaptive techniques for fixed controller performance enhancement. *International Journal of Control*, 50(5):1941–1959, 1989.

[73] J. G. VanAntwerp, A. P. Featherstone, and R. D. Braatz. Robust cross-directional control of large scale sheet and film processes. *Journal of Process Control*, 11(2):149–177, April 2001.

[74] R. N. Vyse, J. King, and M. Heaven. Consistency profiling - a new technique for CD basis weight control. In *Proc. of the 81th Annual Meeting, Technical Section CPPA*, pages A267–A273, 1995.

[75] J.I. Yuz and G.C. Goodwin. Loop performance assessment for decentralized control of stable linear systems. *submitted to European Journal of Control*, 2002.

[76] K. Zhou, J.C. Doyle, and K. Glover. *Robust and Optimal Control.* Prentice Hall, New Jersey, 1996.

[77] K. Zhou and Z. Ren. A new controller architecture for high performance, robust, and fault-tolerant control. *IEEE Trans. Automat. Contr.*, 46(10):1613–1618, October 2001.

Appendix A

Proof of Theorem 1

Internal stability of the perturbed systems is established by the stability of the transfer functions between the disturbance inputs (d_i, $i = 1, 2, 3, 4$) inserted in front of each block in the corresponding block diagram, and the outputs (y_i, $i = 1, 2, 3, 4$) of each of the blocks. The corresponding closed-loop system is stable if and only if all 16 transfer functions from d_i to y_i ($i = 1, 2, 3, 4$) are stable.

In all the cases below, closed-loop transfer functions S_o and S_i are defined as $S_o = [I - GK]^{-1}$, $S_i = [I - KG]^{-1}$, and $[y_1 \;\; y_2 \;\; y_3 \;\; y_4]^T = T \cdot [d_1 \;\; d_2 \;\; d_3 \;\; d_4]^T$. It can easily be confirmed that, subject to the conditions given in Theorem 1, the systems in Figures A.1–A.6 are stable.

A.1 Process Additive Perturbation (Case a)

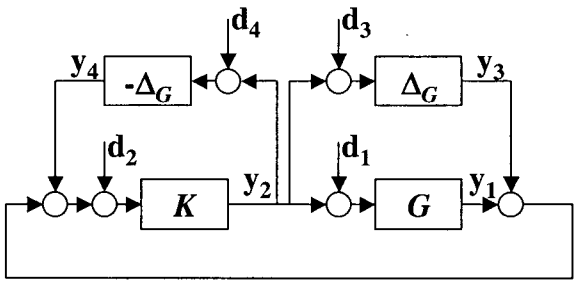

Figure A.1: Diagram used to analyze internal stability for the configuration given in Theorem 1 - case (a).

$$T_a = \begin{bmatrix} S_oG & S_oGK\Delta_G & S_oGK & -S_oGK\Delta_G \\ \Delta_GS_iKG & \Delta_GS_iK\Delta_G + \Delta_G & \Delta_GS_iK & -\Delta_GS_iK\Delta_G \\ S_iKG & S_iK\Delta_G & S_iK & -S_iK\Delta_G \\ -\Delta_GS_iKG & -\Delta_GS_iK\Delta_G & -\Delta_GS_iK & -\Delta_G + \Delta_GS_iK\Delta_G \end{bmatrix} \tag{A.1}$$

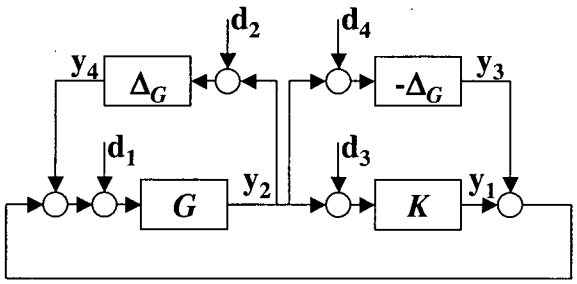

Figure A.2: Diagram used to analyze internal stability for the configuration given in Theorem 1 - case (b).

A.2 Process Inverse Additive Perturbation (Case b)

$$T_b = \begin{bmatrix} S_oG & S_oG\Delta_G & S_oGK & -S_oG\Delta_G \\ \Delta_GS_oG & \Delta_GS_oG\Delta_G + \Delta_G & \Delta_GS_oGK & -\Delta_GS_oG\Delta_G \\ KS_oG & KS_oG\Delta_G & KS_o & -KS_oG\Delta_G \\ -\Delta_GS_oG & -\Delta_GS_oG\Delta_G & \Delta_GS_oGK & \Delta_GS_oG\Delta_G - \Delta_G \end{bmatrix} \tag{A.2}$$

All the closed-loop transfer functions in this case can easily be obtained from (A.1) by simultaneously swapping G and K, and Δ_G and $-\Delta_G$.

A.3 Process Multiplicative Input Perturbation (Case c)

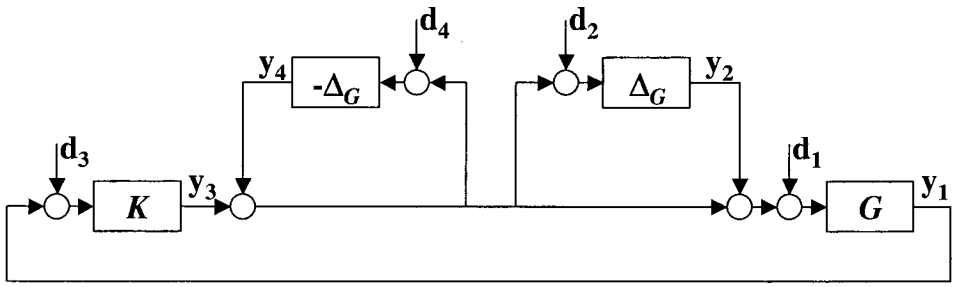

Figure A.3: Diagram used to analyze internal stability for the configuration given in Theorem 1 - case (c).

$$T_c = \begin{bmatrix} S_oG & [I+\Delta_G]^{-1}\Delta_G K S_o G & KS_oG & -[I+\Delta_G]^{-1}\Delta_G K S_o G \\ S_oG\Delta_G & [I+\Delta_G]^{-1}\Delta_G K S_o G\Delta_G + \Delta_G & KS_oG\Delta_G & -[I+\Delta_G]^{-1}\Delta_G K S_o G\Delta_G \\ S_oGK & [I+\Delta_G]^{-1}\Delta_G K S_o & KS_o & -[I+\Delta_G]^{-1}\Delta_G K S_o \\ -S_oG\Delta_G & -[I+\Delta_G]^{-1}\Delta_G(-KS_oG\Delta_G + I) - \Delta_G & -KS_oG\Delta_G & -[I+\Delta_G]^{-1}\Delta_G(-KS_oG\Delta_G + I) \end{bmatrix}^T \tag{A.3}$$

A.4 Process Inverse Multiplicative Input Perturbation (Case d)

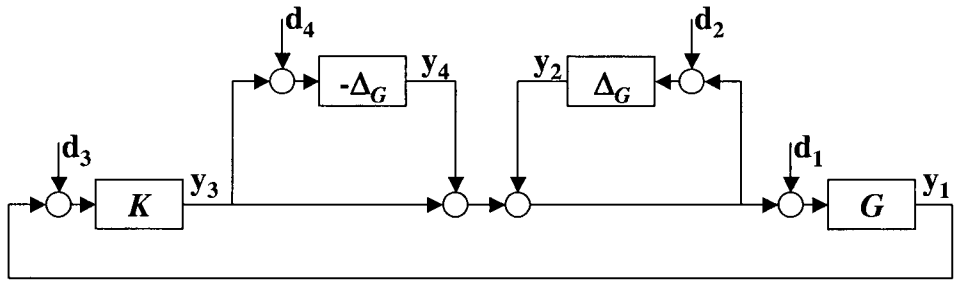

Figure A.4: Diagram used to analyze internal stability for the configuration given in Theorem 1 - case (d).

$$T_d = \begin{bmatrix} S_oG & S_oG[I-\Delta_G]^{-1}G[I-\Delta_G]^{-1}\Delta_G & S_oGK & -S_oG[I-\Delta_G]^{-1}\delta_G \\ \Delta_G K S_o G & (\Delta_G K S_o G + I)[I-\Delta_G]\Delta_G & \Delta_G K S_o & (-\Delta_G K S_o G[I-\Delta_G]^{-1} + I - [I-\Delta_G]^{-1})\Delta_G \\ KS_oG & KS_oG[I-\Delta_G]^{-1}\Delta_G & KS_o & -KS_oG[I-\Delta_G]^{-1}\Delta_G \\ \Delta_G K S_o G & \delta_G K S_o G[I-\Delta_G]\Delta_G & -\Delta_G K S_o & \Delta_G K S_o G[I-\Delta_G]\Delta_G - \Delta_G \end{bmatrix} \tag{A.4}$$

A.5 Process Multiplicative Output Perturbation (Case e)

$$T_e = \begin{bmatrix} S_oG & S_oGK[I+\Delta_G]^{-1}\Delta_G & S_oGK & -S_oGK[I+\Delta_G]^{-1}\Delta_G \\ \Delta_G S_oG & \Delta_G S_oGK[I+\Delta_G]^{-1}\Delta_G + \Delta_G & \Delta_G S_oGK & -\Delta_G S_oGK[I+\Delta_G]^{-1}\Delta_G \\ KS_oG & KS_o[I+\Delta_G]^{-1}\Delta_G & KS_o & -KS_oGK[I+\Delta_G]^{-1}\Delta_G \\ -\Delta_G S_oG & -\Delta_G S_oGK[I+\Delta_G]^{-1}\Delta_G - \Delta_G & \Delta_G S_oGK & \Delta_G S_oGK[I+\Delta_G]^{-1}\Delta_G \end{bmatrix} \tag{A.5}$$

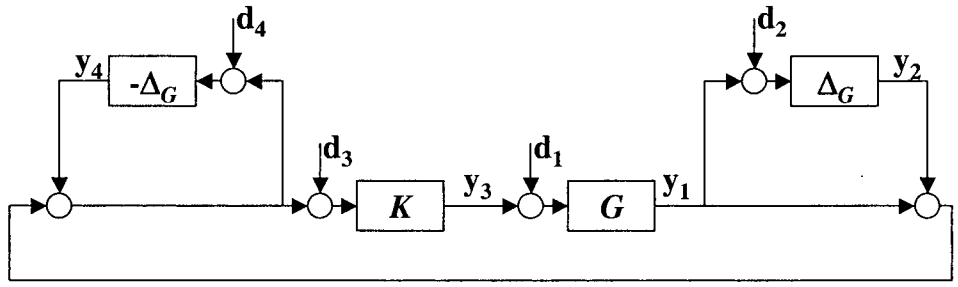

Figure A.5: Diagram used to analyze internal stability for the configuration given in Theorem 1 - case (e).

A.6 Process Multiplicative Output Perturbation (Case f)

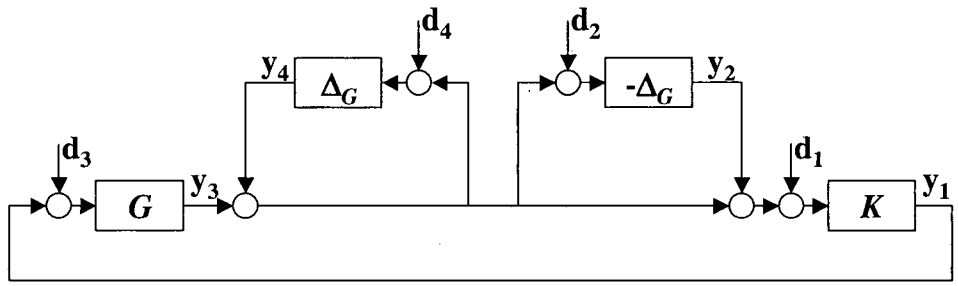

Figure A.6: Diagram used to analyze internal stability for the configuration given in Theorem 1 - case (f).

$$T_f = \begin{bmatrix} S_iK & -[I-\Delta_G]^{-1}\Delta_G GS_iK & GS_iK & [I-\Delta_G]^{-1}\Delta_G GS_iK \\ S_iK\Delta_G & [I-\Delta_G]^{-1}\Delta_G GS_iK\Delta_G - \Delta_G & -GS_iK\Delta_G & -[I-\Delta_G]^{-1}\Delta_G GS_iK\Delta_G \\ S_iKG & -[I-\Delta_G]^{-1}\Delta_G GS_i & GS_i & [I-\Delta_G]^{-1}\Delta_G GS_i \\ S_iK\Delta_G & [I-\Delta_G]^{-1}\Delta_G(GS_iK\Delta_G + I) + \Delta_G & GS_iK\Delta_G & [I-\Delta_G]^{-1}\Delta_G(GS_iK\Delta_G + I) \end{bmatrix}^T \tag{A.6}$$

Appendix B

Matrix Optimization

Given matrices $A \in \mathcal{R}^{m\times n}$, $B \in \mathcal{R}^{k\times l}$, $C \in \mathcal{R}^{m\times l}$, and scalar $\rho \geq 0$. Consider the static matrix optimization problem,

$$Q^* = \arg\min_Q (\|AQB - C\|_F^2 + \rho \|Q\|_F^2) \tag{B.1}$$

with respect to matrix $Q \in \mathcal{R}^{n\times k}$. The Frobenius norm $\|\cdot\|_F$ of a matrix is given in (5.8).

Write the standard singular value decomposition,

$$A = U_A \Sigma_A V_A^T, \quad B = U_B \Sigma_B V_B^T \tag{B.2}$$

where the $m \times m$ matrix U_A and the $n \times n$ matrix V_A are unitary and the $m \times n$ matrix Σ_A is given by,

$$\Sigma_A = \begin{bmatrix} \Sigma_1 \\ 0 \end{bmatrix}, \qquad m \geq n \tag{B.3}$$

$$\Sigma_A = [\Sigma_1 \; 0], \qquad m \leq n \tag{B.4}$$

where

$$\Sigma_1 = \text{diag}\{\sigma_1(A), \ldots, \sigma_p(A)\}, \qquad p = \min(m, n) \tag{B.5}$$

Similar expressions apply to the matrices U_B, Σ_B, and V_B in (B.2).

Now form the new matrices,

$$X = V_A^T Q U_B, \qquad Y = U_A^T C V_B \tag{B.6}$$

then the sum of matrix norms on the right hand side of (B.1) may be rewritten as the equivalent expression,

$$\|AQB - C\|_F^2 + \rho \|Q\|_F^2 = \|\Sigma_A X \Sigma_B - Y\|_F^2 + \rho \|X\|_F^2 \tag{B.7}$$

by substituting (B.6) in (B.1) and due to the fact that multiplication by unitary matrices

does not affect the Frobenius norm [27, 58].

We can expand the Frobenius norms in (B.7) as

$$\|\Sigma_A X \Sigma_B - Y\|_F^2 = \sum_{i=1}^{r_A}\sum_{j=1}^{r_B}(\sigma_i(A)\sigma_j(B)x_{ij} - y_{ij})^2 + \sum_{i=r_A+1}^{m}\sum_{j=1}^{l} y_{ij}^2 + \sum_{i=1}^{m}\sum_{j=r_B+1}^{l} y_{ij}^2 \tag{B.8}$$

and

$$\rho\,\|X\|_F^2 = \sum_{i=1}^{n}\sum_{j=1}^{k}\rho\cdot x_{ij}^2 = \sum_{i=1}^{r_A}\sum_{j=1}^{r_B}\rho\cdot x_{ij}^2 + \sum_{i=r_A+1}^{n}\sum_{j=1}^{k}\rho\cdot x_{ij}^2 + \sum_{i=1}^{n}\sum_{j=r_B+1}^{k}\rho\cdot x_{ij}^2 \tag{B.9}$$

Then the expression in (B.7) can be rewritten as the sum over terms,

$$\begin{aligned}\|\Sigma_A X \Sigma_B - Y\|_F^2 + \rho\,\|X\|_F^2 = &\sum_{i=1}^{r_A}\sum_{j=1}^{r_B}(\sigma_i(A)\sigma_j(B)x_{ij} - y_{ij})^2 + \rho\cdot x_{ij}^2 \\ &+ \sum_{i=r_A+1}^{n}\sum_{j=1}^{k}\rho\cdot x_{ij}^2 + \sum_{i=1}^{n}\sum_{j=r_B+1}^{k}\rho\cdot x_{ij}^2 \\ &+ \sum_{i=r_A+1}^{m}\sum_{j=1}^{l} y_{ij}^2 + \sum_{i=1}^{m}\sum_{j=r_B+1}^{l} y_{ij}^2\end{aligned} \tag{B.10}$$

We can minimize the right hand side of (B.10) by noting that each term in the summation (B.10) contains at most one distinct element x_{ij} of the matrix X in (B.6). This allows the overall optimization to be decoupled in terms of the individual matrix elements. Optimizing term-by-term in (B.10) is straightforward and leads to the solution,

$$x_{ij}^* = \begin{cases} \frac{\sigma_i(A)\sigma_j(B)}{\sigma_i^2(A)\sigma_j^2(B)+\rho}\cdot y_{ij}, & 1 \le i \le r_A \quad \text{and} \quad 1 \le j \le r_B \\ 0, & \text{otherwise} \end{cases} \tag{B.11}$$

so that the $n \times k$ matrix X^* optimizing (B.7) has only $r_A r_B$ nonzero elements, where $r_A \le \min(m, n)$ and $r_B \le \min(k, l)$ are the number of nonzero singular values of matrices A and B respectively.

Finally the $n \times k$ matrix Q^* that minimizes (B.1) can be obtained from the expression

for X in (B.6),

$$Q^* = V_A X^* U_B^T \tag{B.12}$$

So the solution of the optimization problem (B.1) for the matrix Q involves taking the SVD of two matrices in (B.2), computing two matrix products in (B.6), an element-by-element construction in (B.11), and computing a final matrix product in (B.12).

Appendix C

Proofs of Theorems 4–5

First a few supporting relationships, used in proving Theorems 4–5, are given in Section C.1. Next, the proofs are given in Sections C.2–C.3.

C.1 Supporting Relationships

Given a static compensator K_0, the feedback system in Figure 5.1 is internally stable if and only if the dynamic transfer matrix given by,

$$R(z) = K_0(I - N_{32}(z)K_0)^{-1} \tag{C.1}$$

is stable. The stability of $R(z)$ can be computed easily in state-space. First define the factors,

$$R(z) = \left[\begin{array}{c|c} A_r & B_r \\ \hline C_r & D_r \end{array}\right], \quad N_{32}(z) = \left[\begin{array}{c|c} A_{32} & B_{32} \\ \hline C_{32} & D_{32} \end{array}\right] \tag{C.2}$$

then A_r can be written in terms of (C.1) and (C.2) as,

$$A_r = A_{32} + B_{32}K_0(I - D_{32}K_0)^{-1}C_{32} \tag{C.3}$$

and closed-loop stability is equivalent to the stability of all eigenvalues of the matrix A_r in (C.3).

A conservative (sufficient) stability result can be obtained by substituting K_0 from (5.14) into (C.1) to obtain

$$R(z) = Q_0\left[I - (N_{32}(z) - N_{32}(e^{j0}))Q_0\right]^{-1} \tag{C.4}$$

Then since Q_0 is static and $N_{32}(z)$ is stable, small gain arguments lead to the result that $R(z)$ in (C.4) is stable if,

$$\left\|(N_{32}(z) - N_{32}(e^{j0})) \cdot Q_0\right\|_\infty < 1 \tag{C.5}$$

The following relationship indicates that the optimization weight ρ may be used to

govern the size of the resultant matrix Q_0 in (5.13),

$$\bar{\sigma}(Q_0) \leq \|Q_0\|_F \leq \frac{\sqrt{r_{12}r_{31}} \cdot \bar{\sigma}(N_{12}(e^{j0}))\ \bar{\sigma}(N_{31}(e^{j0}))\ \bar{\sigma}(N_{11}(e^{j0}))}{\rho} \tag{C.6}$$

where $\bar{\sigma}(\cdot)$ denotes the maximum singular value, the integers r_{12} and r_{31} denote the number of nonzero singular values in $N_{12}(e^{j0})$ and $N_{31}(e^{j0})$ respectively. The first inequality is standard for any matrix and may be found in, for example [27, 58]. The second inequality in (C.6) holds for Q_0 in (5.13) and may be verified using (5.13) and (B.11)–(B.12).

C.2 Proof of Theorem 4

Let,

$$\Gamma = \sqrt{r_{12}r_{31}} \cdot \bar{\sigma}(N_{12}(e^{j0}))\ \bar{\sigma}(N_{31}(e^{j0}))\ \bar{\sigma}(N_{11}(e^{j0})) \cdot \left\|N_{32}(z) - N_{32}(e^{j0})\right\|_\infty \tag{C.7}$$

Substituting $\rho > \Gamma$ in (C.7) into (C.6) results in Q_0 satisfying (C.5), i.e. the system is stable. Since, by comparing (C.7) and (5.15), $\beta \geq \Gamma$ then $\rho > \beta$ in (5.13) will result in an internally stable system also.

Using K_0 in (5.14) we can write

$$\begin{aligned} \bar{\sigma}\big(\mathcal{F}_l(N_b(e^{j\omega}), K_0)\big) \ &\leq \\ \bar{\sigma}(N_{21}(e^{j\omega})) \ &+ \ \bar{\sigma}(N_{22}(e^{j\omega}))\bar{\sigma}(N_{31}(e^{j\omega}))\frac{\bar{\sigma}(Q_0)}{1-\bar{\sigma}(Q_0)\bar{\sigma}(\Delta(e^{j\omega}))} \end{aligned} \tag{C.8}$$

where $\Delta(e^{j\omega}) = N_{32}(e^{j\omega}) - N_{32}(e^{j0})$. Then substitute (C.6) into (C.8) with $\rho > \beta$ to obtain (5.16). $\diamondsuit$

C.3 Proof of Theorem 5

First prove (5.17) for $\omega = 0$. Note that if Q_0 optimizes $J(N_a(e^{j0}), \rho, Q)$ in (5.13), then $J(N_a(e^{j0}), \rho, Q_0) \leq J(N_a(e^{j0}), \rho, 0) = \|\mathcal{F}_l(N_a(e^{j0}), 0)\|_F^2$ and since $Q_0 \neq 0$ then $\|Q_0\|_F > 0$ and using (5.14) we get $\|\mathcal{F}_l(N_a(e^{j0}), K_0)\|_F^2 < J(N_a(e^{j0}), \rho, Q_0)$ leading to the steady-state result $\|\mathcal{F}_l(N_a(e^{j0}), K_0)\|_F < \|\mathcal{F}_l(N_a(e^{j0}), 0)\|_F$. Then it follows there exists some $\epsilon > 0$ for which $\Big|\ \|\mathcal{F}_l(N_a(e^{j0}), 0)\|_F - \|\mathcal{F}_l(N_a(e^{j0}), K_0)\|_F\ \Big| > \epsilon$, and since $\mathcal{F}_l(N_a(z), K_0)$ is a stable, finite-dimensional transfer matrix, there will exist $\omega_b > 0$ for which $\Big|\ \|\mathcal{F}_l(N_a(e^{j\omega}), K_0)\|_F - \|\mathcal{F}_l(N_a(e^{j0}), K_0)\|_F\ \Big| < \epsilon$ for $-\omega_b < \omega < \omega_b$ and (5.17) follows. $\diamondsuit$

Appendix D

Closed-loop transfer functions used for defining LFTs

D.1 Closed-loop transfer functions that make up $P_e(z)$ in Figure 5.2

Closed-loop transfer functions of interest in case of optimization for performance:

$$
\begin{array}{lcll}
d_e \rightarrow y_e & : & P_1 & = W_4[I - G(z)K(z)]^{-1}W_1 \\
d_e \rightarrow y_{ce} & : & P_{1a} & = W_3[I - G(z)K(z)]^{-1}W_1 \\
d_e \rightarrow u_e & : & P_2 & = W_5K(z)[I - G(z)K(z)]^{-1}W_1 \\
d_e \rightarrow y_{de} & : & P_3 & = W_2[I - Dz^{-1} - c(z)CG(z)D]^{-1}c(z)CW_1 \\
u_{de} \rightarrow u_e & : & P_4 & = W_5[I - Dz^{-1} - c(z)DCG(z)]^{-1}W_6 \\
u_{de} \rightarrow y_e & : & P_5 & = W_4G(z)[I - Dz^{-1} - c(z)DCG(z)]^{-1}W_6 \\
u_{de} \rightarrow y_{ce} & : & P_{5a} & = W_3G(z)[I - Dz^{-1} - c(z)DCG(z)]^{-1}W_6 \\
u_{de} \rightarrow y_{de} & : & P_6 & = W_2[I - Dz^{-1} - c(z)CG(z)D]^{-1}\cdot \\
 & & & \quad [c(z)CG(z) + z^{-1}I]W_6 \\
u_{ce} \rightarrow y_e & : & P_7 & = W_4[I - G(z)[I - Dz^{-1}]^{-1}c(z)C]^{-1}\cdot \\
 & & & \quad G(z)[I - Dz^{-1}]^{-1}c(z)W_7 \\
u_{ce} \rightarrow y_{ce} & : & P_{7a} & = W_3[I - G(z)[I - Dz^{-1}]^{-1}c(z)C]^{-1}\cdot \\
 & & & \quad G(z)[I - Dz^{-1}]^{-1}c(z)W_7 \\
u_{ce} \rightarrow u_e & : & P_8 & = W_5[I - [I - Dz^{-1}]^{-1}c(z)CG(z)]^{-1}\cdot \\
 & & & \quad [I - Dz^{-1}]^{-1}c(z)W_7 \\
u_{ce} \rightarrow y_{de} & : & P_9 & = W_2[I - Dz^{-1} - c(z)CG(z)D]^{-1}W_7
\end{array}
\tag{D.1}
$$

The rectangular matrices W_i, $i = 1, 2, \ldots, 7$ are defined in (5.18)–(5.19).